Department of Chemical Engineering

Study of the Mechanism of Pyrolysis and Gasification of Mallee Biomass

Yanwu Yang

This thesis is presented for the Degree of

Doctor of Philosophy

of

Curtin University

August 2012

Declaration

To the best of my knowledge and belief this thesis contains no material previously published by any other person except where due acknowledgment has been made.

This thesis contains no material which has been accepted for the award of any other degree or diploma in any university.

Signature: ……

Date: ……...…….

To my beloved family

ABSTRACT

Biomass energy has been becoming increasingly important in dealing with the challenges which the world is facing in terms of energy security and sustainable development. It can be considered as concentrated solar energy stored in green plants via photosynthesis hence it is renewable and environmental friendly, depending on its supply chain.

In Australia, as a byproduct of dryland salinity management, mallee biomass is produced at a large scale, small carbon and energy footprints. Therefore it is a true second-generation feedstock for the production of energy, chemicals and other value-added products such as biochar and/or activated carbon (AC).

There are several attractive options for biochar utilization. Biochar can be returned to soil as carbon sequestration and soil amendment. Biochar can also be directly used as a solid fuel for energy supply. Additionally, biochar can also be further activated to produce AC, which has wide applications worldwide. For all of these applications, good properties of biochars are desired so that necessary treatment of biochars may realize such goals. For mallee biomass, while there have been substantial research on producing bio-oil via pyrolysis, there are still significant scope for research into using partial gasification for improving biochar properties and producing high quality AC.

The present study carries out a systematic experimental approach to investigate the pyrolysis/gasification behaviour of mallee biomass (wood, leaf, and bark components). It focuses on understanding the evolution of gas products and biochar structure, particularly at low conversions which are relevant to improving biochar quality and AC production. The specific objectives of this study are to: (1) investigate the effect of key parameters on the characterisctics of biochar such as

temperature, holding time, and heating rate; (2) probe the behavior of biochar steam or CO_2 gasification and the transformation of inherent inorganic species; (3) understand biochar steam gasification pathway at low carbon conversion and the transformation of inherent oxygen in biochar during the course of steam gasification; (4) investigate the evolution of biochar structure during biochar gasification, focusing on differences in the mechanisms between steam and carbon dioxide gasification. These objectives have been successfully achieved in this PhD study.

Firstly, due to the significant differences in the chemistry of various mallee biomass components (leaf, bark and wood), there are significant difference in the thermal decomposition of various biomass components. While leaf and bark contains substaintial inorganic nutrients (hence good for soil application) due to their high ash contents, wood component is more suitable for AC production. A larger particle size favours the production of biochar production. The optimum holding time for pyrolysis appears to be 1h for producing biochars from wood particles of 1-2mm at 500℃. Temperature and heating rate played significant roles in the chemical and physical structure of biochars. The surface area of slow-heating and fast-heating biochars produced from pyrolysis at 350-600℃ generally have low BET surface area (<50 m^2/g). Such data may have important implications to applying biochar for soil application.It is known that biochar applied in soil can change the porosity of soil so that change the percolation model, holding time, the pathway of soil moisture and keep the soil water. The carbon content of biochar can increase soil organic matter while inorganic matter of biochar can be treated as fertilizer. The pore structure of biochar may provide more space for the development of roots and microbes. Due to the low BET surface area, regardless its applications in soil or for AC production, the results in this study show that biochar directly produced from pyrolysis need to be treated for increasing surface area and producing desirable pore structure.

Secondly, this PhD study carried out a systematic study on biochar steam gasification,

focusing on the reaction mechanism at low carbon conversions, with obvious objectives of maximizing product yet, at the same time also improving the properties of biochar products for applications such soil amendment and AC. For biochars produced from wood pyrolysis at 750℃ and 1h holding time, partial steam gasification can significantly increase the surface area of biochar from <50 to 950 m^2/g after 40 min activation in steam. At the same temperature, even with only 5 min steam gasification (corresponding to a carbon conversion of 5.5 %), the surface area of the partially-gasified biochars (with 15min holding time) can be increased to be 526 m^2/g. This provides a promising method to tune the biochar structure.

Efforts were also taken to understand the composition of evolved gas product during partial biochar steam gasification. The gas product contains mainly H_2, CO, CO_2. In agreement with related studies, the primary product of CO_x from gasification is CO while the formation of CO_2 is more likely from the water-gas-shift reaction. It was also found that while the majority of oxygen involved in biochar gasification was provided by steam, ~20% was supplied by the inherent oxygen present in the biochar. Therefore, it is clear that for solid samples like biochar which also contains abundant heteroatoms, the inherent oxygen can play an important role in the biochar gasification reactions, particular during the early conversion stage.

Thirdly, during the course of CO_2 gasification of wood char, the Raman results showed large aromatic-ring clusters in the biochar tend to be enriched in the reacting biochar as conversion increases. Also, it is interesting to note that at a carbon conversion below 15%, gasification of biochar in H_2O and CO_2 at 750℃ showed similar specific reactivity. At conversions >15%, the specific reactivity of biochar under steam gasification was higher obviously than that in CO_2 gasificaiton. CO_2 gasification also leads to a slower increase in the BET surface area of partially-gasified biochar. Therefore, different optimal parameters are required for adjusting the biochar properties via gasification using steam and CO_2.

ACKNOWLEDGEMENTS

I gratefully acknowledge the Curtin International Postgraduate Research scholarships (CIPRS) from Curtin University for my PhD study.

I would like to express my deepest gratitude to my supervisors, Professor H.Ming Ang and Professor Hongwei Wu, for providing me the precious opportunity for this research and for their invaluable advice, enduring guidance, patience, inspiration, persistent supports as well as their devotion in supervision throughout the course of my PhD study. Without them, my PhD research would not be possible. I would also like to acknowledge my thesis committee chairperson Professor Moses Tadé for assistance and help as thesis committee members.

I am indebted to my beloved family for their support, encouragement, and understanding during my PhD study overseas.

I also would like to express my appreciation to Ms. Karen Haynes, Mr. Jason Wright, Ms. Ann Carroll, and Mr. Xiao Hua and other general staff for their laboratory assistances. Special thanks to Doctor John Bromly for the help of GC analysis and Doctor Gia Hung Pham for his advice and assistance in elemental analysis. Special thanks to Vlad Curteanu and Yasuhiro SAKURAI for their assistance in part of experiments. Centre for Materials Research (CMR) at Curtin is acknowledged for accessing SEM facilities.

I am also grateful to Dr. Kongvui Yip, Dr. Xiangpeng Gao, Ms. Zhaoying Kong, Mr. Muhammad Usman Rahim, Ms. Yi Li, Dr. Yun Yu, Mr. Alan Burton, Mr.SuiBoon Liaw, Mr. Dawei Liu, Ms. Mingming zhang and Mr. Syamsuddin Yani in our research group for their help in various ways. Thanks also go to all other people who have provided their assistances during my PhD study.

TABLE OF CONTENTS

LIST OF FIGURES

LIST OF TABLES

CHAPTER 1 INTRODUCTION

1.1 Background

Fossil fuels have been the cheap and available energy source for powering the global economy since industry revolution. However, there are two major issues related to fossil fuel use. One is the continuously depletion of fossil fuel sources; the other is the adverse environmental impacts eg carbon emissions that is believed to be at least partly responsible for global warming and climate change.[1] Therefore, renewable energy, particularly biomass, has been attracting increasing attention worldwide to address these issues. The International Energy Agency (IEA) predicted that biomass energy will increase to ~11.7% of the total global energy supply by 2030.[2]

In Western Australia, mallee planting is a key strategy for managing dry land salinity and preventing the loss of fertile agricultural land.[3] It does not compete with food production, rather it complements food production.[4] It is known that mallee biomass production is of large scale and has small energy and carbon footprints. [3, 5] Therefore, mallee biomass can be considered as a second-generation feedstock for the production of energy, chemicals and other value-added products.

Mallee biomass as a renewable energy feedstock has been extensively researched recently. [6-11] Particularly, via pyrolysis, bio-oil and biochar can be produced from mallee biomass. The characteristics of bio-oil from the pyrolysis of mallee biomass were also reported. [12-14] and biochar as a solid product is also found to have many properties including excellent grindability and high energy density.[8]

Besides used a solid fuel, biochar can find attractive applications in carbon sequestration and soil amendment. It is also a good feedstock for activated carbon (AC) production. For all of these applications, good properties of biochars are desired so that necessary treatment of biochars may realize such goals. However,

only scattered studies[15-18] can be found in the literature, focused on these aspects. Phussade Patunukao[15] worked on AC preparation from mallee bark using phosphoric acid gasification. Tancredi used Eucalyptus grandis to prepare AC via steam gasification but applied extensive carbonization at the pyrolysis temperature (2 hours) and a high burn-off (>25%) during steam gasification.[19] Arriagada compared the performance of AC production via CO_2 and steam gasification however the effect of char preparation during pyrolysis was not studied. [20] Therefore, there is substantial scope for research into these important aspects.

1.2 Scope and Objectives

Therefore, this PhD project carried a systematic experimental program to investigate the properties of biochars from mallee biomass (wood, leaf, and bark) after pyrolysis and partial gasification. A series of biochar under different conditions were produced. Steam and carbon dioxide were applied to activate biochar. Low carbon conversions were considered. To gain a fundamental understanding on the mechanism of biochar gasification, gas products were also analyzed during the course of biochar gasification reactions. The study considers various reaction conditions and key parameters (e.g. raw materials properties, operation conditions), deploying an array of facilities for characterizing the properties of biochar and AC.

The specific objectives of this research are as follows:

(1) To investigate the pyrolysis behavior of various mallee components (wood, leaf and bark) under various conditions;

(2) To understand the characteristics of biochar produced from pyrolysis and partial gasification and then further discuss the implication for biochar application including soil amendment and AC production;

(3) To investigate the role of inherent oxygen present in biochar and its implication to biochar gasification mechanism at low carbon conversion levels (<10%);

(4) To investigate the development of char structure under gasification in steam or CO_2 and further figure out the optimal conditions for AC production.

1.3 Thesis Outline

There are a total of 8 chapters in this thesis (including this chapter). Each chapter is listed as follows, and the thesis structure is schematically shown in the thesis map (see Figure 1-1).

- Chapter 1 introduces the background and objectives of the present research.
- Chapter 2 reviews the up-to-date literature on biochar production and gasification, identify research gaps then list the objectives of this research work.
- Chapter 3 summarizes the research methodology, including samples, experimental facilities and analytical techniques employed in this study.
- Chapter 4 investigates the properties of biochar produced from mallee biomass under various pyrolysis conditions, considering the effect of temperature, heating rate, holding time, and sample size.
- Chapter 5 reports the data on biochar steam gasification, including char gasification reactivity and the role of pyrolysis in the steam gasification.
- Chapter 6 focuses on the roles of inherent oxygen (present in biohars) on biochar gasification and their effect on gas composition.
- Chapter 7 further investigates the gasification of biochar in CO_2 conditions and the evolution of char structure during gasification.
- Chapter 8 concludes the present study and recommends future work.

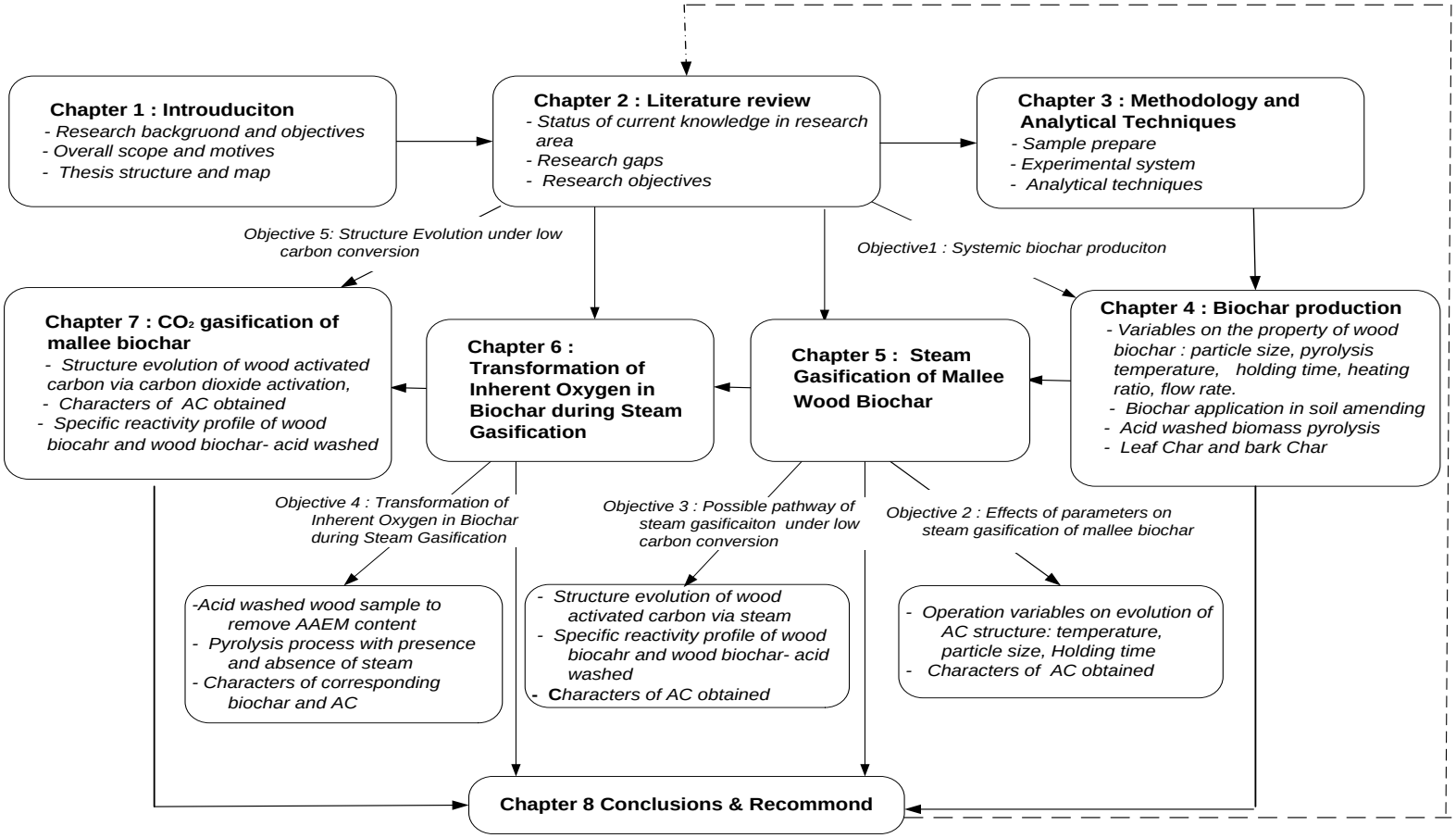

Figure 1-1: Thesis map

CHAPTER 2 LITERATURE REVIEW

2.1 Introduction

Biomass, any organic matter that can be used as an energy source, has been used by human beings for a longer time than any other energy source. There are four main ways to utilize it including burning, bacterial decay, fermentation, and conversion to gas/liquid fuel. At present, the conversion of biomass to gas/solid fuel contributes a new energy source which has been attracting world-wide attention to face future energy challenges sustainably. Pyrolysis and gasification of biomass can be a promising way to convert biomass to gas /liquid fuel/char. Most commercial plants control the process to realize the target of one of the fractions as primary products. [21] Biochar can be used directly as soil amendments to improve soil and sequestrate atmospherical carbon dioxide. Solid residue during gasification in industry is disposed of by burning. However, these solid residues can possibly be further treated as value-added activated carbon since porous structures have been developed during gasification.

Over the past two decades, there have been abundant studies on activated carbon production from coal and biomass; however, little literature has been found based on mallee biomass. This chapter starts with reviewing mallee biomass production in Western Australia followed by key issues regarding biomass supply. A brief review on activated carbon production and their characteristics is given. The research work of biochar steam gasification and carbon dioxide gasification was then summarized. Finally, the conclusions of the key research gaps and the thesis scope were identified.

2.2 Mallee Biomass in Western Australia (WA)

Mallee belongs to the eucalypt family and grows with multi-trunks arising from a lignotuber. It is fast growing (3~4years growth time) and can be planted in low rainfall (mean annual rainfall at 300-600 mm) zone. [3, 22, 23] More than 14 000 ha (30 million trees) have been planted across the "wheat-belt" region[24] of Western Australia.

Due to its large scale, small carbon and energy footprints production, [3, 23, 25-29] Mallee has been attracting increasing Research & Development recently. Mallee biomass can be ~10 million dry tonnes per annum. [33] In WA, mallee biomass was planted initially to manage the salinity problem since early 1990. Recent life cycle analysis[23] indicates that Mallee production in Western Australia can achieve an annual energy productivity of over 200 GJ ha^{-1} y^{-1} within a 75 kilometer transport radius. Such energy performance is considerably higher than that achieved by other annual or other short-lived agricultural crops like canola. All these characteristics of mallee make it a competitive source of biomass feedstock for activated carbon production in WA.

2.3 Mallee as Biomass Supply and Motivations of Using Mallee Biomass as Feedstock for Biochar and Activated Carbon Production

Mallee biomass can contribute greatly to energy security and local economy with the production of energy, chemicals and other value-added products. Since mallee biochar was obtained via the pyrolysis of mallee biomass and activated carbon (AC) was the final solid product of further gasification of biochar, the mechanism of pyrolysis and gasification of mallee biochar is the major focus of this study. Knowledge of AC production should be mentioned as well.

Although there is an abundance of mallee in WA, some challenges of using this biomass as a feedstock for AC production have to be overcome.

- ***Mallee biomass supply***

Usually AC production, like other industrial products, is based on its profit. The economics and availability of feed stock is of vital importance. Many issues have to be considered for the supply chain of mallee biomass including storage, sizing, transportation, pre-processing, etc. Biomass is characteristic of bulky, high-moisture-content, low-energy-density, and fibrous nature.[8] The moisture content and energy density of mallee biomass [30] is ~45% and ~10 GJ ton^{-1} respectively. Such characteristics lead to uneconomical transport of mallee biomass for long distances and are a major constraint of planting biomass as a dedicated bioenergy feedstock. [5] Moreover, due to the bulky and fibrous natures of biomass, the grindability of biomass is poor resulting in possible undesired consequences such as significant increase of the cost for size reduction (milling costs), expensive storage and drying, and maintenance cost. [8]

- ***Motivations of using mallee biomass as biochar and activated carbon feed stock***

To overcome the above shortcomings of direct use of biomass, various pre-treatment technologies have been developed such as drying, [31] pulverizing, [32] palletizing, [10] and pyrolysis. [8, 9] Among the processes, pyrolysis is a flexible technology. [33-37] By controlling the operating conditions, it is possible to convert bulky raw biomass into high-energy-density fuels such as gas, bio-oil[34, 35, 38, 39] and biochar. [8, 37, 40] Adding biochar to soil could realize soil amending and carbon sequestration. [41] By activating biochar, activated carbon can be produced. Various biomass such as coconut shells, [42] oil palm empty fruit bunches, [43] rice husk, [44] wheat straw[45] have been chosen as carbon source for activated carbon production. However, only few researches have used mallee biomass for the production of bio-oil and/or biochar from the pyrolysis of mallee biomass. [6, 13, 14] Scattered work has been done so far on treating mallee biomass biochar as AC production feedstock. [20, 17] Considering the production of

mallee and the promising market of AC, it is desirable to investigate its feasibility as the carbon source for AC preparation.

2.4 Activated Carbon Characteristics and Production Methods

2.4.1 AC Structure

The application of activated carbon has been known for at least 5000 years. [46] At present, predesigned activated structure was produced. The uniqueness and versatility of activated carbon broaden extent of its application even in many complicated separation processes. [46]

- ***Pore structure and functions***

The adsorption ability and strength of AC mostly depend on AC structure including the porosity and surface structure. The normal types of pores are defined by International Union of Applied Chemistry are shown[47] in Table 2-1. Micropore can be divided into ultramicropores (size <0.7 nm) and supermicropores (size between 0.7nm and 2 nm).

Table 2-1: The pore width and the type

Type	Width(nm) IUPAC	Width(nm) Convention	Volume(cm^3/g)	Specific surface area(m^2/g)
micropore	< 2	<1.5-1.6	0.2-0.6	400-100
mesopore	2-50	1.5-1.6~100-200	0.1-0.5	20-70
macropore	>50	>100-200	0.2-0.8	<0.5

The isotherms present a plot of volume of adsorbate (mmol/g, or ml/g) against the relative pressure (P/P_0). Considerable structural information of material can be obtained from visual inspection of their isotherms. In 1985, IUPAC developed a standard classification of general isotherm types. The detailed explanation is presented in Figure 2-1. [48]

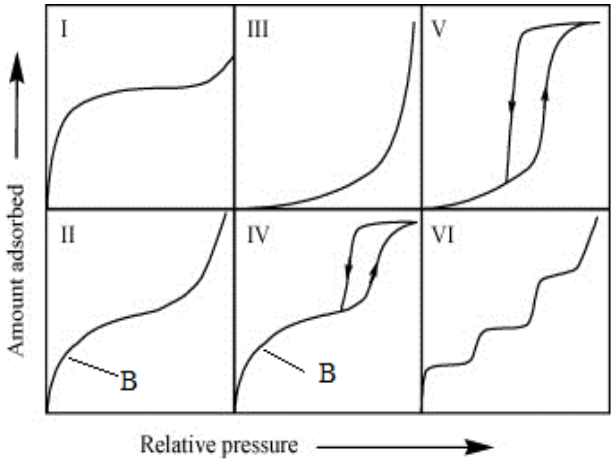

Figure 2-1: The IUPAC classification of adsorption isotherm shapes [48]

The reversible type I isotherm represents micro porous adsorbent with monomolecular adsorption. There is a steep increase at low relative pressure due to the filling of micro-pores. After that, the curve levels off indicating the entire coverage of adsorbate on the adsorbent.

The reversible type II isotherm represents a non-porous or macro porous adsorbent. There is an unrestricted monolayer-multilayer adsorption. Point B is often taken to the point of complete monolayer coverage followed subsequently by multilayer adsorption.

The reversible Type III isotherm is not common and there is no distinct point B. However, in a number of systems (eg. nitrogen polyethylene), isotherms with gradual curvature and an indistinct Point B may occur where the adsorbate-adsorbate interactions play an important role.

The type IV isotherm is characterized by its hysteresis loop where capillary condensations take place in mesopores. The initial part of the isotherm is due to the monolayer adsorption. These isotherms are common for many mesoporous industrial adsorbents.

The type V isotherm is uncommon, but is obtained with certain porous adsorbents.

The type VI isotherm represents stepwise multilayer adsorption on a uniform non-porous surface and step-height represents the monolayer capacity for each adsorbed layer.

The adsorption and desorption isotherms provide solutions to the industry use such as safe and efficient storage. The curves themselves can provide more information rather than values obtained from them. For example, the characteristic of AC with the same value of surface area may have different pore size structure resulting in varying performances in applications. In practice, the adsorption effect of AC is determined by both AC structure and molecular structure of adsorbate. In other words, the pore width of adsorbent must match the adsorbate molecules or ions，and only the porosity into which these molecules or ions can enter is effective porosity. The possible conditions are shown in Figure 2-2. The diameter ratio between adsorbent and adsorbate, at which the adsorption efficiency is the highest, is about 1.7~3.3. [49]

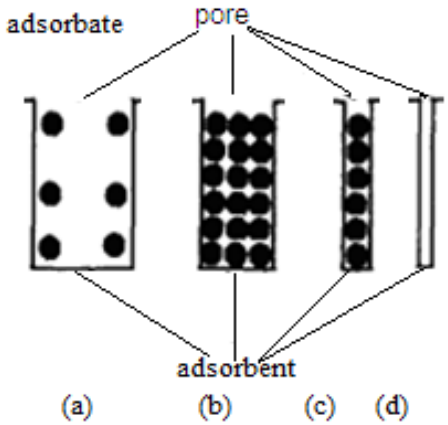

Figure 2-2: Adsorption model

According to the relationship between the pore width and adsorbate molecule diameter, the adsorption can be divided generally as follows:

(a) The molecule diameter of adsorbate is far smaller than pore width of adsorbent. Although it is easy to adsorb, it is also easy to desorb and the rate of desorption is very high, thus the overall adsorption ability is very low.

(b) The molecule diameter of adsorbate is relatively smaller than the pore width of adsorbent. Because capillary condensation will occur in the pores, adsorption capacity of AC will be high.

(c) The molecule diameter of adsorbate is nearly the same as the pore width of adsorbent. In this case, although the adsorption ability of AC is very strong, it can only be used in extremely low concentrations.

(d) The molecule diameter of adsorbate is bigger than the pore width of adsorbent. Due to the effect of molecule size, molecules cannot enter into the pores. Thus the adsorption ability of AC cannot be realized.

Although the adsorption ability of AC is controlled by the quantity and structure of micropores, it is the primary condition that there are macropores and mesopores which can act as the pathway of adsorption; thus, a good quality of AC requires not only micropore, but also appropriate ratio and array of the structure of mesopores and macropores.

Generally speaking, microporous carbon (70~90%) is used mostly in the gas phase [50]treatment like gasoline emission control, low-pressure gas storage, industrial emission gas treatment, solvent recovery, cigarette filters, and electrode. Mesoporous carbon is applied in liquid phase treatment such as drinking water purification, waste-water treatment, sweetener discoloration, food, and chemical processing.

- ***Chemical structure of AC surface***

Chemical properties of AC are determined by hetero atoms such as H, O, N, and S assembled on the surface. Surface oxides are the most common groups on AC surface. There are many types of functional groups (shown as Figure 2-3) of surface oxides such as acidic groups like (a), (b), (c), neutral functional groups (d) , and alkaline group like (e). Methods such as exchanging reaction with diazomethane, esterification reaction with methanol, and other chemical reaction can be used to

identify these groups. [51]

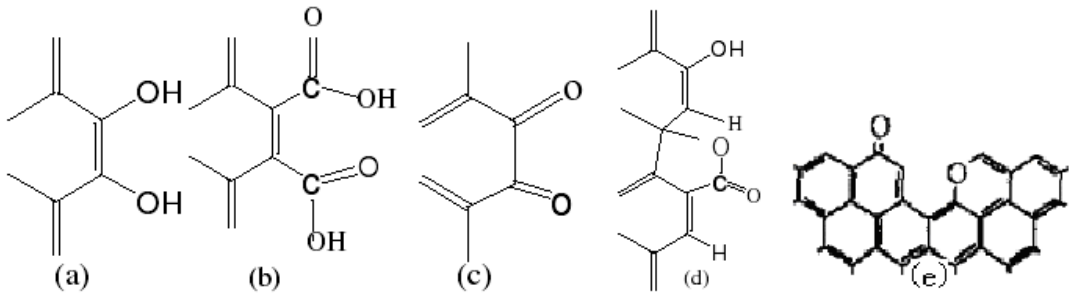

Figure 2-3: Possible functional groups: (a) phenolic hydroxyl group, (b) carboxyl group, (c) carbonyl group, (d) base-lactone and, (e) pyranoid ketone.

When acid or alkali surface compounds are formed, hydroxyl with acid or alkali is produced after hydrolysis. Through ion exchange, the compounds with alkali (or acid) are adsorbed in aqueous solution. So the different adsorption abilities to alkali (or acid) solution appear. Generally, the surface of AC generated by $ZnCl_2$ and steam gasification is acid and alkali respectively. [52]

- ***Characteristics of AC***

To test and characterize the quality of AC, various techniques are developed (shown in Table 2-2). Comprehensive evaluation methods are usually applied to evaluate the adsorption performance of AC. For example, iodine value [representing micropores (0~2nm)] and methylene blue adsorption value [representing 1.5nm micropores, mesopore (2~5nm)] are used to evaluate the micropore specific surface; some big molecules with a given structure are applied to demonstrate the development of mesopore; a phenol as a delegate of complex organisms is applied to determine the adsorption ability of activated carbon. Certain index such as alkyl benzene sulfonate (ABS) value is commonly used to indicate the adsorption ability of AC to remove foreign odour of water.

Table 2-2: Summary of the methods for characterization of raw materials and AC

Objective		Method
Chemical Compositions		Inductively coupled plasma-mass spectroscopy (ICP-MS); Organic element analyzer; Perkin Elmer GCs; Transmission Electron Microscope (TEM); X-ray fluorescence spectroscopy (XRF); SEM-EDX;
Compound Structure		FT-Raman spectroscopy; Raman;
Morphology		Micrometrics Tri-Star II Model ;surface area, surface area distribution; Mercury intrusion porosimetry; Small angle scattering; Scan Electron Microscope (SEM) ; X-ray diffractometry (XRD); Infrared spectroscopy;
Thermal Analysis		Differential thermal analysis (DTA) and thermo gravimetric analysis (TGA);
Mineralogy		X-ray diffractometry (XRD); Infrared spectroscopy;
Particle Size Distribution		Sieving analysis; Laser particle size analyzer; SEM;
Physical index	Hardness /abrasion number impact strength Density	ASTM standard measurement methods.
Adsorption	Methylene blue Iodine number Molasses Tannin	

2.4.2 Key Issues of AC Production from Biomass

- ***Biomass cell structure***

Investigating the cell structure of mallee biomass is important to understand the

structure and application of AC produced from such feedstock, benchmarking with those from other substrates. Biomass consists mostly of the polymers cellulose, hemi-cellulose, lignin and extractives. The molecular structure of these three components and typical interactive plant cell wall showing their constitution are shown in Figure 2-4. Cellulose forms the structure of micell and is surrounded by hemicellulos, pectin and associated with lignin. Usually for wood biomass, the contents of hemicellulose, cellulose, and lignin are 10-30%, 40-50%, 20-30% respectively.

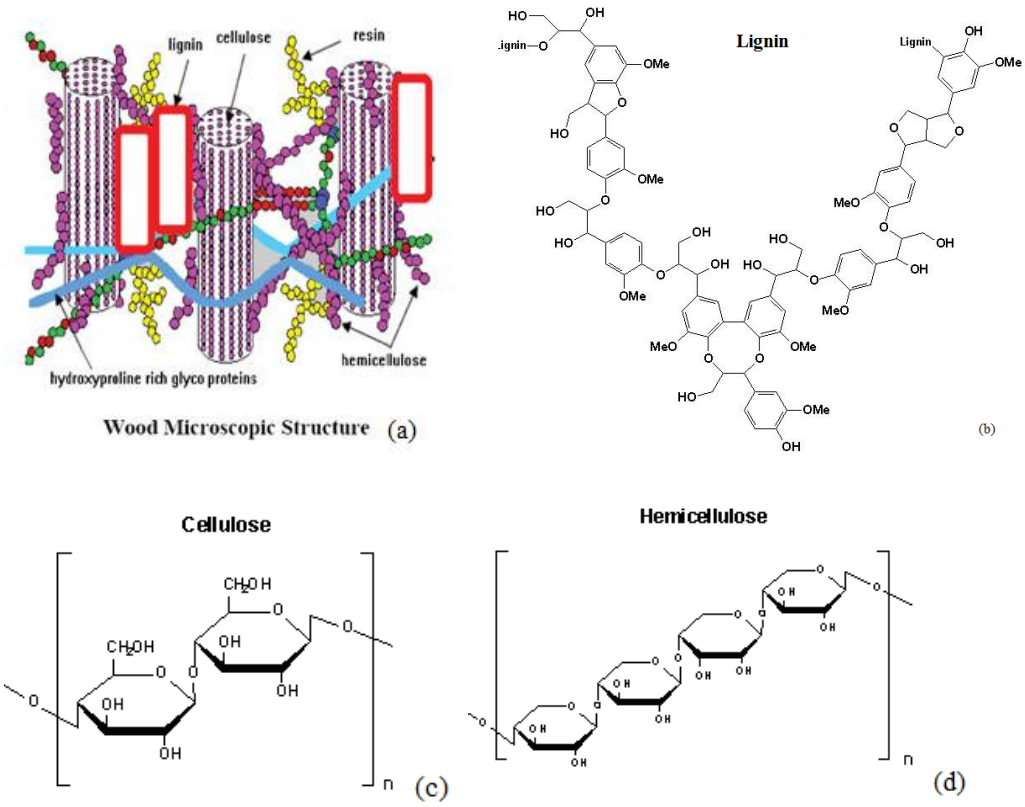

Figure 2-4: (a) Interactive plant cell wall[53]; (b) molecular structure of lignin; (c) molecular structure of cellulose; (d) molecular structure of hemicellulose.

Development of porosity of AC during gasification depends on the lignocellulosic composition of substrates [54] and the retention and dilation of cellular structure. [55] It is also known that feedstock with low structure order can be easier to be activated for porosity development. [56] Therefore, the coarse-cellular of the raw materials rather

than material-specific features (element composition) plays an important role in production of AC. If the porosity of raw materials is >35%, it will not be advantageous to produce AC with high quality. [57]

- ***Inherent inorganic species***

It is also well known that the additive gasification agents like transition metal Fe, Co, Ni, alkaline metal Ca can be used to produce mesopores of AC. [58-59] However, the effect of inherent inorganic species on biochar to produce AC via pyrolysis/gasification is still not clear. Some studies showed that de-ashing led to the increase of liquid yield and decrease of char yield during pyrolysis. [60] While biomass with high lignin, potassium and zinc (e.g. groundnut shell and coir pith), char yield increases on de-ashing. [60] It was also found that Kraft lignin experienced a rapid decrease of weight at a temperature above 750℃ because of the presence of Na_2CO_3.Na_2SO_4. [61] Apricot stones with low sulphur contents(external 0.04%) are useful for producing high BET surface. [62] The results are different for Pakistani coals, de-ashing results in decreased yield of tar and gas. [63] High ash content usually is not beneficial to the gasification so that pretreatment may be considered for ash removal. After gasification, coconut samples with lower total ash contents leads to the production of AC of higher iodine numbers. [64] So, inherent inorganic species may act as catalysts. [56]

2.4.3 Process of AC Production from Biochar

Considering the original structure, the economics and the availability [62] of feed material, the most common feedstock [65-70] for AC preparation are plants (e.g. wood, nut-core),[39,56, 57, 71-73, 202] coal (e.g. anthracite),[70] petroleum (petroleum asphalt), [74] waste materials [69] (e.g. sewage sludge, used tyre) and plastic materials.

Physical gasification and chemical gasification are generally employed to produce AC. Physical gasification process involves two steps known as pyrolysis and

gasification. Pyrolysis determines the characteristics of resulting solid including structure and chemical composition thus playing a dominant role in structure evolution of biochar. [75] Biochar produced from pyrolysis is subjected to gasification process using gasification agents such as steam, carbon dioxide, air, oxygen or a mixture of them. The scheme of physical gasification is shown in Figure 2-5. In a chemical gasification process, such chemicals as potassium carbonate, zinc chloride, and phosphoric acid are commonly used. Firstly, the feedstock is mixed with chemicals directly or impregnated in chemical solution, after that the mixture is carbonized, and then products are washed to obtain the final AC product. These chemicals can physically or chemically modify the thermal decomposition of the precursors by inhibiting the shrinkage of feedstock and reducing the evolution of volatile matter and the formation of tars.[75] Sometimes these two gasification methods are combined. For example, impregnating the biochar obtained through pyrolysis with chemicals then running gasification under CO_2 was applied together. [76]

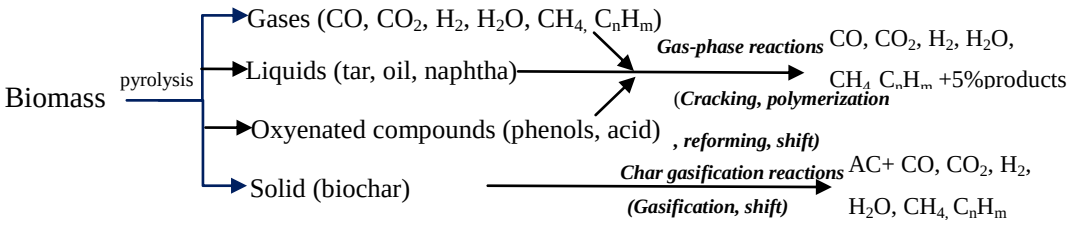

Figure 2-5: AC production via pyrolysis and gasification[77]

- ***Pyrolysis***

As discussed above, pyrolysis plays a significantly important role in the development of the structure of activated carbon. Thus it is necessary to obtain basic understanding of the pyrolysis process.

Carbonization is a kind of extreme pyrolysis where mostly carbon is the main residue. It is a thermochemical decomposition of organic material which is typically carried out in a relatively low temperature in the range of 450℃ and 900℃ .[78] This process

can be run either without the presence of oxidizing agents or with a limited supply where gasification does not occur to an appreciable extent. As shown in Figure 2-6, large complex hydrocarbon molecules of biomass break down to relatively smaller molecules thus producing gas, liquid, and char during pyrolysis. Pyrolysis occurs in the way of dehydration, decarboxylation, slow depolymerization and recombination of the decomposition at low temperature or with the presence of inorganic matter. [79] The three biomass components have different decomposition temperatures: hemicellulose at 200℃~260℃ resulting in high yield of CO_2, cellulose at 260℃ ~300℃; lignin at 370℃~400℃ resulting in high yield of H_2 and CH_4. At higher temperature above than 550℃, the primary gas produced is CO.

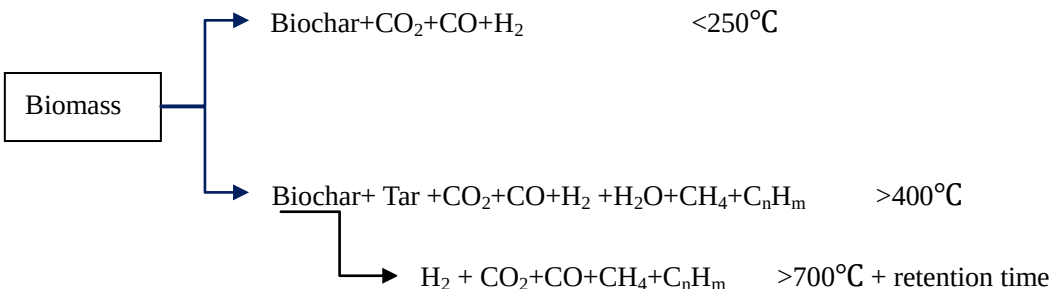

Figure 2-6: Model of Pyrolysis[77]

Various distribution of different pyrolysis products (gas, liquid, and solid) can be obtained by controlling the pyrolysis process (see Table 2-3). However, many competing reactions like cracking, devolatilization attribut to complexity of the pyrolysis. To understand the pyrolysis process, three main stages are mentiond and it should be noted that the temperature boundaries are not sharp and there are always some overlap between stages.

(1) The first stage includes mainly dehydration and degassing (low than 300℃ to 400℃). Main gas products such as CO_2, CO, and H_2S and small amounts of acetic

acid, formic acid, acetic acid, and second aldehyde are produced. Usually, the temperature of this stage for wood and coal is 180℃~200℃and 300℃ ~ 400℃ respectively. This stage is accompanied with heat release, so it is an exothermic reaction phase.

(2) The second stage includes the thermal pyrolysis mainly（300℃~600℃）. The cracking and reformation of functional groups such as O-H, C-C, C=C, C≡C, C=O, -COOH,-OCH_3 ,and C-O-(C) lead to the production of CO_2, CO, CH_4, C_2H_6, H_2 , methanol, formaldehyde, formic acid, acetone, and phenols. The rest of the solid residue is mainly carbon frame combined with hydrogen and oxygen. Wood starts pyrolysis at about 270℃ and this process will finish at 450℃. As for coal, the thermal pyrolysis will finish at around 600℃~700℃. The mechanical strength of char increased in this stage.

(3) The third stage includes the polycondensation reaction mainly (above 600℃). The reformation and breakdown of function groups like C-O, C-H continues and the hydrogen, oxygen carbon in the char skeleton is further removed. Only small amount of gas is released. Aromatic structures are formed continuously and net microcrystalline structure increases. Carbon graphite is formed at higher temperature 1000℃. The pyrolysis temperature determines the structure of biochar.

- ***Gasification***

Gasification is different from pyrolysis which is usually carried out in none/poor oxygen atmosphere. During gasification, pyrolysis/gasification exists in the same time and gasification agents introduced to react with the biochar. Through gasification, [75] porous structure of AC is formed. With temperature increasing, more volatile matters will be released and plenty of secondary reactions take place in the physical production method. The main final products are AC, CO, and CO_2.

Table 2-3: Characteristics of some pyrolysis process[77]

Aim:*To maximize CARBON production : Heating rate(HR) (<0.01~2.0℃/s), Final temperature℃(FT)（below 500℃）, long Residence time(RT)*				
Pyrolysis type	RT	HR	FT	Main products
Carbonization	Several hours or days	Very low	400	charcoal
Conventional	5~30min	Low	600	Gas, bio-oil, char
Aim: *To maximize LIQUID production : high HR, medium FT(450℃~650℃), short RT To maximize GAS production : low HR, high FT(700℃~1100℃), long RT*				
Pyrolysis type	RT	HR	FT	Main products
Fast	0.5~5s	Very high	650	Bio-oil
Flash	<1s	High	<650	Bio-oil
Flash	<1s	High	>650	gas
Ultra-rapid	<0.5s	Very high	~1000	Chemicals ,gas
vacuum	2~30s	Medium	400	Bio-oil
Reactive pyrolysis Medium（500℃~650℃） High HR（10^4~10^5℃/S） short RT(below 2s) bio-oil				
Hydro-pyrolysis	<10s	High	<500	Bio-oil
Methano-pyrolysis	0.5~10s	High	1050	Chemicals

Residence time(RT); Heating rate(HR); Final temperature℃(FT).

- ***Pore structure***

Porosity of activated carbon can be obtained by several ways including the creation of further porosity, widening of existing porosity, modifications to the surfaces of pores. [80] Much effort has been spent to stimulate the pore structure of activated carbon. The model of non-graphitzable carbon by Fralin,[81, 82] shown in Figure 2-7, is remarkably accurate.

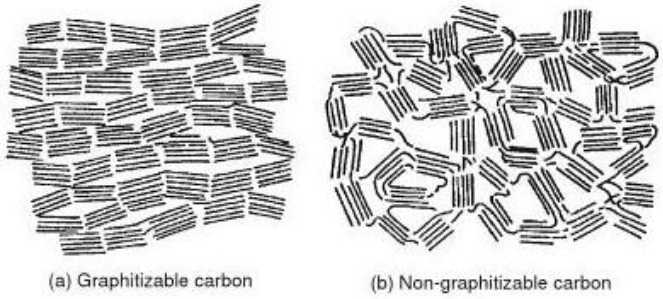

Figure 2-7: Drawings to illustrate the essential differences between (a) garphitizable (b) non-graphitizable carbons[83- 84]

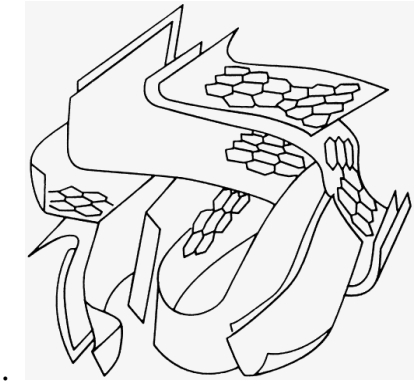

Figure 2-8: Schematic representation of the structure of activated carbon[83- 84]

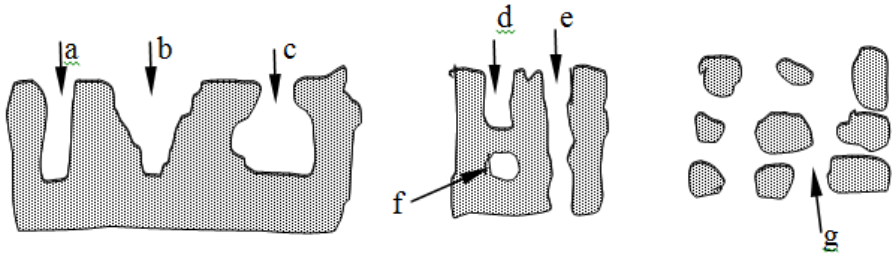

Figure 2-9: Types of pores: a- uniform size; b- funnel shaped ; c- ink bottle shaped; d- blind pore; e- through pore; f- closed pore; g porous net work. [85]

Figure 2-8 shows that the spaces between imperfect sections of graphitic lamellas constitute porosity of carbon. These sections, with many structural defects, can be bonded together to create a three-dimensional network. The pore types are shown in

Figure 2-9. [85]

2.5 Parameters Affecting Pyrolysis and Gasification

The major parameters that determine the process of pyrolysis and gasification includes temperature, heating rate, burning off, gasification time, gasification agent, and partial pressure of gasification agent.

- ***Temperature***

As for gasification process, temperature must be high enough to guarantee the reaction between biochar and gasification agent. Generally speaking, the total pore volume of AC will increase with temperature in some temperature range. After the porosity volume reaches the peak, it will then decrease probably because of the sintering and collapse of pores. [86] Usually the higher the gasification temperature, the less amount of AC is obtained. [87] In the case of pyrolysis, Table 2-3 illustrates the fraction of products. A liquid fraction is the main fraction of product at low temperature and the gas produced including CO_2， CO, CH_4. Above around 500℃, amorphous carbon is formed and evolved gases are mainly CO, CO_2. At 750 ℃, biochar is decomposed fiercely, C and gases are generated.

- ***Heating rate***

Heating rate determines the process of pyrolysis thus leading to different product fractions. For fast pyrolysis, reactions mostly happen in stage three (shown in 2.4.3) leading to higher release of evolved gas. Solid residues are macroporous chars which are useful to form micropore after the gasification. [57] On the contrary, slow pyrolysis experiences three stages completely. Jiang found that slow carbonization is good to the increase of specific surface area. [88] In industry AC production, heating rate

0.17K/s is commonly used, while the heating rate above 1000K/s is for gas reforming.

- ***Burn off***

Under traditional process with H_2O gasification, the porosity of different raw materials will increase with the increase of burn off. Micropore can be obtained at low burn off, with different volumes of meospores and macropores.[54] Gonzalez found that the porosity and micropore volume development as a function of burn-off is similar for six precursors, especially at low burn off level. [54] The decrease of adsorption of low concentration n-butane by activated carbon justified the removal of an effective porosity with increase of burn-off. [89]

- ***Gasification agent***

The attributions of different gasification agents to the pore development of AC are different. CO_2 (aerodynamic diameter 0.33nm) plays an important role to widen micropores in the late stages of gasification, and water vapor (aerodynamic diameter 0.27~0.32nm) broadens micropores in the early stages. The pore volume activated by steam was less than that of CO_2. However the microporous volumes of the two methods approached the same due to the dissolving effect of water volatilization and gasification in the high temperature. The effect of gasification was more prominent by water vapor in macropore and mesopore than the effect of CO_2 gasification. [90]

- ***Partial pressure of gasification agents***

Wigmans [91] believed the increase of pore volume of AC, which was activated by steam at high temperature and low steam partial pressure, was mainly developed by the effect of steam deepening the pore rather than widening the pore; while, at low temperature and high steam partial pressure, the function of H_2O was widening the pore. That means micro porous AC was easily obtained at high temperature and low

steam partial pressure, and mesoporous and macro porous AC was easily obtained at low temperature and high steam partial pressure. Chiung and Fenchang obtained a similar conclusion at high temperature and low steam partial pressure with CO_2 gasification，while only mesoporous AC is easily obtained at low temperature and high steam partial pressure. [92] Take CO_2 for example, micropores and mesopores are found to remain unchanged with burn off with adding small amount of CO to CO_2, decreasing reaction temperature, and reducing the particle size. Due to the high diffusion resistance of air, reaction cannot proceed uniformly inside the char, leading to the generation of mainly meso- and macro-pores. [50]

- ***Gasification time***

Appropriate gasification time can influence the pore structure greatly. Wheeler et al found that both gasification temperature and gasification time determined the component of carbon.[93] At a given gasification temperature, the extension of holding time will make the gasification more complete and pores be continuously developed. When temperature is above 800℃, long enough holding time is needed for the occurrence of secondary reactions.While the holding time exceeds the optimum, micropores will decrease while meso- and macro-pores increase.

2.6 The Study of Biochar in Gasification

2.6.1 Effect of Biochar Structure in Gasification

Specific reactivity was determined by three main characteristics: chemical structure of surface, inorganic constituents, and porosity. [94]

- ***Physical structure of biochar***

Compared with other chars that have been intensively researched for AC preparation，mallee biochar has different properties. As far as mallee biomass is

concerned, the pore structures of wood, leaf, and bark are different. Wood chars have higher porosities at the value of 40~50% and pore size at 20~30 nm than that of coal char with 2~18% porosity and around 5A pore size. [95] Meanwhile, wood biochar shows higher reactivity than coal char during steam gasification. [96] Generally, the rate of solid devolatilization is higher than that of char oxidation which is higher than the rate of biochar gasification. [97] Accessible porosity (usually micro porosity) impacts the gasification from within the interior. [80]

The porosity of biochar was developed during pyrolysis. Such porosity provides the basic structure to further gasification. Some authors believed that the largest increase of porosity was produced during the early stage of gasification by removing the constriction in the char porosity and forming new pores. [98]

- ***The effect of indigenous inorganic species of biochar***

Indigenous inorganic species in mallee biomass impact the pyrolysis [60] and steam and carbon dioxide gasification. It can change not only the chemical kinetics of reactions but also the topographical kinetics (reaction anisotropy). [80]

Mallee biomass components contain abundant amount of inherent inorganic species including alkali and alkaline earth metallic (AAEM) species, i.e. mainly Ca, Mg, Na, K, and S, P, Si, Cl, Al, Ti. (Table 2-4). As shown in Table 2-4, different mallee components (leaf, wood, and bark) have very different quantities of inorganic species. Therefore, it is expected that each component may lead to the production of char and AC of different quality and quantity. Thus, both individual biomass components and their mixtures should be considered.

Basically, the order of ash content of biomass components is bark > leaf > wood. It clearly shows the dominant role of AAEM species with highest content of Ca. Therefore, only AAEM species were taken into account in the following discussion.

Table 2-4: Contents of inorganic species in biomass, wt%db[14]

Mallee tree		Wood	Leaf	Bark
AAEM(analyzed by IC)	Na	0.03	0.544	0.223
	K	0.06	0.335	0.104
	Mg	0.036	0.154	0.098
	Ca	0.107	0.668	1.517
Other inorganic species (analyzed by ICT-AES)	Si	0.0041	0.0498	0.0508
	Al	0.0025	0.0192	0.0028
	Ba	0.0002	0.001	0.00[12]
	Fe	0.0001	0.0142	0.0019
	P	0.0159	0.0939	0.0204
	S	0.0061	0.068	0.0137
	Sr	0.0021	0.0078	0.0223
	Ti	Not detected	0.0008	0.0002

Inorganic species in biomass can be present in different ways, i.e. soluble ions, (present in moisture and pores), organically associated, as included minerals or as free inorganic particles excluding minerals.[99] A schematic diagram of the different forms of inorganic species in biomass is shown in Figure 2-10.

It is known that the form of alkalis determines their performances such as transformation and release during pyrolysis. [100] Basically, the sodium in woody biomass may exist as salts and/or organically bound structures [101] such as carboxylates. Potassium may exist in the form of salts like KCl, K_2SO_4, KOH, and K_2CO_3 or in the form of organically bound like carboxylic groups. [102] Magnisium and calcium is largely found as ion-exchangeable and acid soluble material. Especially, calcium may exist as crystallized calcium oxalate ($Ca(COO^-)_2$) in plants. [103]

AAEM in the biochar acts as important catalyst in the further process of gasification. It impacts on the reactivity of biochar and may change the steam gasification pathway. It is reported that the occurrence of AAEM depress the pyrolysis process thus increase the biochar yield. [60, 104,105] Thus a thorough understanding of AAEM dispersion on the biochar and the possible release of AAEM during the steam gasification are demanded.

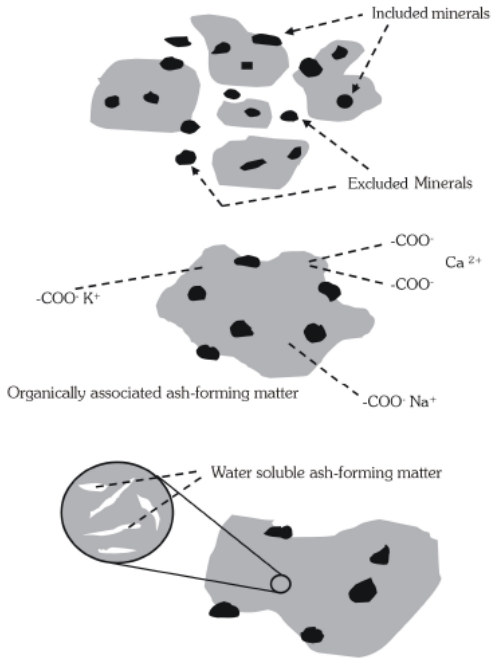

Figure 2-10: Schematic diagram of the different forms of inorganic species in biomass[99]

Some studies[106-108] reported that considerable amounts of alkali metals can be released even at low pyrolysis temperature at 500 ℃. The larger molecular carboxylates may be retained in char matrix and a form char-bond alkali which is relatively stable with little additional release with any increase of pyrolysis temperature at slow heating rate (fixed bed condition). [106] The same mechanism may be used for the release of Mg and Ca. However, the amounts of released Mg and Ca are generally lower than those of K and Na as observed in the pyrolysis of both sugar cane biomass[106] and Victorian brown coal, [109, 110] probably due to the difference in the nature of valence, i.e., monovalent of K (and Na) and divalent of Mg (and Ca).

- ***The effect of chemical structure of biochar***

As discussed before, three biomass components decompose thermally at different temperatures. Hemicellulose and cellulose is mainly decomposed at low temperature

while lignin decomposition covers a wider pyrolysis temperature range. At higher pyrolysis temperature such as above 700℃, the volatile matter is mainly released and amorphous char is formed. Thus the effect of chemical structure of biochar on steam gasification is highly related to the thermal decomposition of lignin during the gasification. In the thermal decomposition of lignin, the ring opening of benzene and bond-breakage of C-O, C-C, and C-H in the side/main chains take place. Caojun[111] used TGA-FTIR to analyze evolution of biochar and gas during the pyrolysis of lignin. The results show that at 500℃~900℃ ring-opening of benzene and aromatization occurred. Macromolecules aromatic began to rearrange and C=C was formed. [112]

2.6.2 Mechanism Study of Mallee Wood during Steam Gasification under Low Carbon Conversion

Main reactions during steam gasification are shown in Table 2-5. [113] Table 2-5 gives the function of reaction equilibrium constant with temperature. The Gibbs free energies ΔG and the reaction equilibrium constant logK as a function of temperature of these equations were calculated for the temperature range of 550℃~900℃ using HSC Chemistry ver.5.0 as shown in Figure 2-11. Reactions between steam and carbon produce CO and H_2. Under certain conditions the steam and carbon reaction can also produce CH_4 and CO_2. [114] As it can be seen, below 700℃, steam gasification speed is slow and it speeds up with the increase of temperature to 800℃.

Some researchers have researched the mechanism of gasification of biochar under the atmosphere of CO_2 and steam. They found that the reactivity of biochar under CO_2 is much lower than that under steam.[115] The higher pyrolysis degree of coal char leads to low steam reactivity. The inorganic matters in coal biochar catalyze the CO_2 gasification. At higher temperature of 1100℃, gasification reaction was changed

from chemical reaction control to diffusion reaction control.[116] The gasification dynamics of different classes of coal were also investigated. [117]

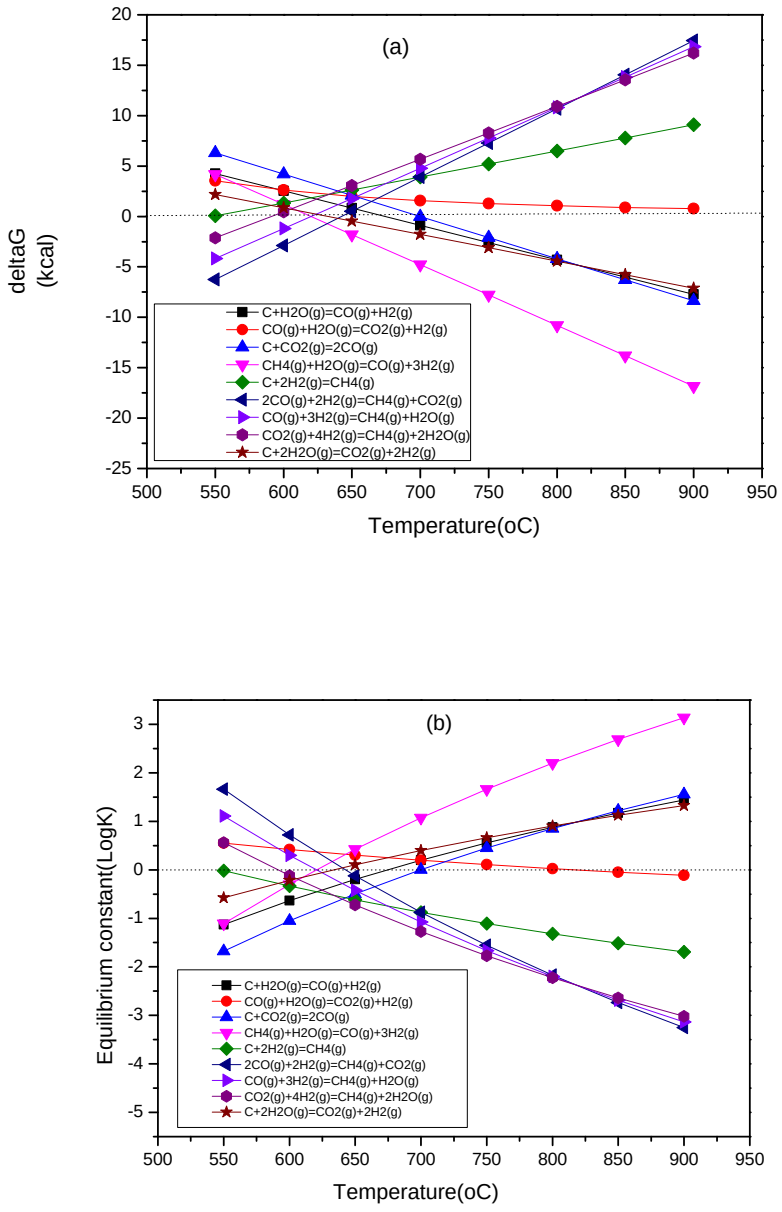

Figure 2-11: Main reactions in the process of steam gasification of biochar: (a) Gibbs free energy, ΔG (kcal.mol^{-1}), against temperature; (b) equilibrium constant against temperature [114]

Table 2-5: Main reactions during steam gasification [113]

Reaction type	Reaction		
steam reforming	$C + H_2O \rightarrow H_2 + CO$	Δ H=+118.628kj /mol	$\lg K_r = \frac{6740.5}{T} + 1.5561\lg T - 0.081092T - 0.06371T^2 + 2.554$
	$C + 2H_2O \rightarrow 2H_2 + CO_2$	Δ H=+75.114kj /mol	$\lg K_r = \frac{4533.3}{T} + 0.6446\lg T + 0.083646T - 0.0818587T^2 + 2.336$
Water gas Shift reaction(WGS)	$CO + H_2O \rightarrow H_2 + CO_2$	Δ H= -43.514kj /mol	$\lg K_r = \frac{207.2}{T} + 0..9115\lg T - 0.09738T + 0.0818487T^2 + 0.098$
Boudouard reaction	$C + CO_2 \rightarrow 2CO$	Δ H=+162.14kj/mol	$\lg K_r = \frac{8947.7}{T} + 2.4675\lg T - 0.0010824T + 0.0611T^2 + 2.772$
Steam reforming reaction of methane	$CH_4 + H_2O \rightarrow CO + 3H_2(g)$	Δ H= +206kj /mol	
hydrogasification	$C + 2H_2 \rightarrow CH_{4\,(5)}$	Δ H= -75.2400kj /mol	$\lg K_r = \frac{3348}{T} - 5.975 + 0.001867T - 0.061095T^2 + 11.79$
	$2CO + 2H_2 \rightarrow CH_4 + CO_2(g)$	Δ H= -247kj /mol	
	$CO + 3H_2 \rightarrow CH_4 + H_2O(g)$	Δ H= -203.556kj /mol	
	$CO_2 + 4H_2 \rightarrow CH_4 + 2H_2O(g)$	Δ H= -82.7514kj /mol	

2.6.3 Transformation of Inherent Oxygen in Biochar during Steam Gasification

Ko, Tse-Hao[118] mentioned the effect of pyrolysis outweighs the effect of the degradation of carbon dioxide. It is likely to be true that the attribution of pyrolysis may also occur during steam gasification. Both pyrolysis and steam gasification are essentially the process of release of heteroatoms (oxygen, hydrogen, nitrogen and sulphur). Thus the insight to the role of pyrolysis may provide information of steam gasification pathway.

Hydrogen is bonded to edge atoms but the oxygen can be bonded both at edges of graphene layers and also in-ring within the graphene layers. Among them, the oxygen in particular edge-bonded-oxygen (surface oxygen complexes) has more effect on the process. [119] It was estimated that there may be several types of oxygen functional groups, as shown in Figure 2-12. [84]

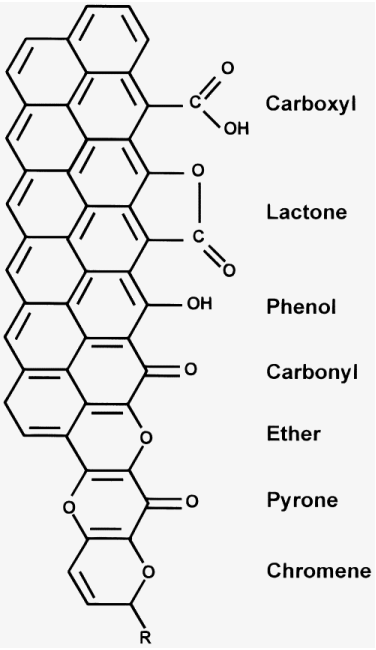

Figure 2-12: Examples of oxygen functional groups on carbon surfaces [84]

A summary of the functional groups on carbon for gas formation during the process of thermal desorption of carbon shown in Table 2-6. [120]

Table 2-6: The function group on carbon for the gas formation[120]

Carbonyl	CO
Quinone	CO
Ether	CO
carboxyiic anhydride	CO,CO_2
Lactone	CO_2
Iactolt	CO_2,H_2O
carboxylic acid	CO_2,H_2O
phenol (hydroxyl)	CO,H_2O
hydroquinone	CO,H_2O
Aldehyde	CO,H_2O

The oxides remaining on the surface of the carbon have been characterized by temperature-programmed desorption (TPD). Isotopic oxygen $^{18}O_2$ combined with $^{16}O_2$ was used to understand gasification. The final overall reaction proceeds as C (^{18}O) + $^{16}O_2$→ C (^{16}O) + $C^{18}O$. $C^{16}O^{18}O$ suggests the mobility of oxygen complex over the carbon surface. [121] Char oxidation experiments[122] suggests lower CO/CO_2 ratio of char produced at slow heating rates is attributed to the more ordered char structure with lower content of oxygen namely limited reactive complexes. Therefore, oxygen transformation of biochar indicates that pyrolysis makes a contribution to gasification.

2.6.4 Mechanism of Gasification via Carbon Dioxide

The mechanism of carbon dioxide gasification[123] has been postulated as the following.

$$C_f + CO_2 \rightarrow C(O) + CO \quad (2\text{-}1)$$

$$C(O) + CO \rightarrow C_f + CO \quad (2\text{-}2)$$

$$C(O) \leftrightarrow CO \quad (2\text{-}3)$$

Where C_f : active carbon site, $C(O)$: Carbon–oxygen complex. One possible form of

carbon-oxygen complex postulated is shown in Figure 2-13. [124]

The reaction of carbon and carbon dioxide is basically irreversible, [125] the use of CO_2 proved[13] that that carbon from the gas phase reactant is inserted in the carbon structure. If the CO is adsorbed on to the active point, the reaction will be hindered. The phenomena that carbon content decreased with the increase of carbon conversion were observed. [50 ,118,124]

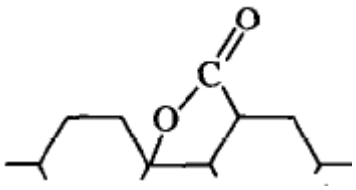

Figure 2-13: Examples of oxygen functional groups on carbon surfaces [124]

Carbon dioxide has different gasification mechanism with steam.[126] During gasification, H_2 is a much stronger inhibitor in steam gasification than C (O) in carbon dioxide gasification.[133, 134] The rate of the steam gasification is about two to five times faster than that of carbon dioxide gasification. [127]

Carbon dioxide is also a common gasification agent in activated carbon industry production, although only few biomass like oil palm, [90] wood, [128] olive residue[129-131] have been researched using carbon dioxide as gasification agent. Unlike the intensive researches on the comparison of gasification of coal[132-133] between CO_2 and H_2O, fewer biomass such as corn cob, [92] olive stones,[142] grape fruit skin[134] have been investigated under both steam gasification and carbon dioxide gasification.

In the case of eucalyptus, only limited literature have been done under both gasification of steam and carbon dioxide[16, 20, 135] or only carbon dioxide. [18] Therefore, the activated carbon was obtained under gasification of carbon dioxide. The pore structure evolution was also investigated to compare with steam gasification of mallee wood.

2.7 Biochar Used as Soil Amendment

Apart from being the feed stock of AC, biochar is proposed to be used in amending soil. This is a novel technology having the potential in reducing emissions, leading to a net sequestration of atmospheric greenhouse gas CO_2 with respect to global warming, and a rapid improvement of the soil fertility.[41] Figure 2-14 shows the pathway of biomass being transformed into C and other products via pyrolysis. Higher carbon of 50% was retained after pyrolysis as compared to burning of 3% and biological decomposition of < 10-20% after 10 years. [136] It was estimated that a total of 9.5 billion tons of carbon could potentially be stored in soils by the year 2100. [136] Due to its polycyclic aromatic structure, biochar is chemically and microbially stable. Some biochars may decompose relatively rapidly in soils, [41] while others may persist in the environment for centuries ranging from 1,000 to 10,000 years. [137-139] Therefore, large amounts of CO_2 could be sequestrated in the biochar for long periods rather than being released into the atmosphere.

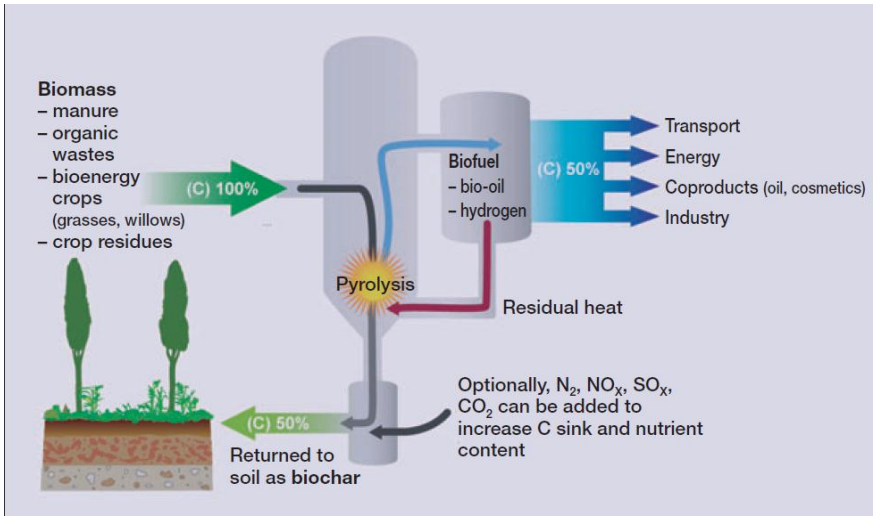

Figure 2-14: Concept of low-temperature pyrolysis bio-energy with biochar sequestration[41]

Amazon's dark earths, "*terra preta do índio*", were anthropogenic soils by the river basin's original human residents, and some soils are thought to be 7,000 years old. [140] These soils contained not only higher concentrations of nutrients like N, P, and K,

but also greater amounts of stable soil organic matter (SOM). [141] They were more productive compared with neighbouring soils. The soil fertility was found to be due to it containing charred trash of all sorts such as charcoal.

Biochar is a pyrolysis product of biomass.With higher porosity, range of surface acidity/basicity, [142] higher carbon content and accumulated inorganic matter, biochar can be an important long-term nutrient source and a soil structuring agent. [143] It is mainly composed of carbon and small fractions of other chemical compositions such as hydrogen, oxygen, nitrogen, and ash including inorganic matters such as Na, K, Mg, and Ca. With the increase of pyrolysis temperature, the carbon content and ash content increase while oxygen and hydrogen content decrease[8, 144] and P solubility decreased. [145, 146] pH values [41, 147, 148] of biochar varied from near neutral to highly alkaline.

The addition of biochar to soil will lead to the increase in the quality of soil by increasing the field capacity, pH value, organic carbon, and exchangeable cations as well as reducing soil tensile strength. [142]

Biochar addition increased the content of soil organic matter (SOM).[149-150] With biochar addition and the presence of N, exchangeable Na, K, Ca, and extractable P increased in soli. [151] Due to the pore structure of biochar, it could also improve water retention of soil. [152] Surface temperature of biochar charcoal-site soils increased up to 4℃ on average as the consequence of darker colour.[153] It has been found that biochar can strongly affect soil microbial populations, including mycorrhizal fungi, and biogeochemistry. [136,154-155]

Biochar has greater potential for cation exchange capacity (CEC measured at pH 7) per unit organic C as the consequence of the higher surface, great surface charger, and greater charge density. [156] The pore structure of charcoal may provide microsites for the microbes and prevent them from soil faunal predators. [157] Biochar obtained at

low temperature contains higher fraction of easily biodegradable contents[158] thus favouring the activity of microbial biomass. [158]

It was found that adding biochar to a typical midwestern agricultural soil reduced nutrient leaching suggesting that addition of biochar could be an effective option to reduce the nutrient leaching. [159] There was an optimum value of the additon of biochar.[160]

2.8 Conclusions and Research Gaps

2.8.1 Conclusions

The contents of this chapter have revealed the basic knowledge of biochar and activated carbon such as its production process, characteristics and the research gaps. The main conclusions that can be drawn are:

(1) Mallee biomass is widely planted in the world especially in Australia. In Western Australia, it can be a potential bio-energy source due to its large scale and being carbon neutral. Utilization of mallee biomass is not only good for solving the crisis of energy and environment but also attributes to the local economy by the production of value-added product AC.

(2) The activated carbon properties and production methods have been well illustrated. Suitable pore size distribution of AC determines the adsorption capacity as an adsorbate. Factors influencing the pore distribution and surface structure of the biochar and AC are discussed such as temperature, holding time, and heating rate.

(3) The catalytic effect of AAEM on gasification has been well accepted, but the mechanism is still not clear. The occurrence and release behavior of AAEM (K, Na, Mg, and Ca) were extensively elaborated in this chapter.

(4) Temperature is a key parameter for both pyrolysis and gasification. The process

of pyrolysis can be divided roughly into three stages. The heating rate leads to the different retention time in these three stages resulting in the pronounced effect on the structure evolution of biochar. Gasification agents (steam and carbon dioxide) have different gasification mechanisms. The partial pressure influences the pore formation by broadening or/and deepening the pores. Burning off of biochar during gasification determines pore size distribution of AC. A suitable gasification time is needed for any desirable pore size distribution.

(5) The research progress of steam gasification and CO_2 gasification of biochar was discussed. Most researches were based on coal. As for mallee biomass, researches were mainly focused on the preparation of bio oil and its optimization at the experimental scale.

2.8.2 Research Gaps

(1) In the last two decades, lots of investigation focused on pyrolysis of biomass. The study of relationship between pyrolysis and gasification is lacking.

(2) Little research of gasification under low carbon conversion has been done.

(3) Research on relationship between gas evolution and AC structure evolution in pyrolysis/gasification is lacking.

(4) Inherent oxygen transformation of biochar based on the chemical structure evolution during steam gasification is hardly mentioned in the literature.

2.8.3 Research Objectives of the Present Study

Based on the above discussion, it clearly shows the necessity of systematic experimental study of production of biochar and activated carbon from mallee biomass. Furthermore, further research & development is needed to gain the fundamental understanding on the pathway of steam gasification and carbon dioxide

gasification.

Thus, this study aims to investigate the key factors that influence the pyrolysis of mallee wood and the development of the physical and chemical structure of pyrolysis product and AC obtained via steam gasification and carbon dioxide gasification. More focus will be put on the mechanisms of steam gasification under low carbon conversion and carbon dioxide gasification to understand the development of pore structure.

Therefore, the main research objectives of this study are:

(1) Firstly, study on the preparation method of mallee biochar sample from mallee wood biomass to exploit the physical and chemical properties of the biochar.

(2) To investigate the mechanism of pyrolysis/gasification of mallee biochar under low carbon conversion, the property of pyrolysis has to be investigated in advance. In this part the possibility of biochar obtained from fast pyrolysis will be assessed to be the feed stock of activated carbon production.

(3) To investigate the transformation of inherent oxygen of biochar during steam gasification by analytical and mathematical means and to determine the relationship between pyrolysis/steam gasification.

(4) To investigate the mechanism of pyrolysis/gasification of mallee biochar under CO_2 gasification.

(5) To compare and evaluate the pore evolution by gasification of steam and carbon dioxide.

CHAPTER 3 RESEARCH METHODOLOGY AND ANALYTICAL TECHNIQUES

3.1 Introduction

This chapter illustrates the general research methodologies used to achieve the targets of the thesis. Experimental and analytical techniques are described in detail.

3.2 Methodology

Three components of mallee biomass including wood, bark and leaf were used in this study. Two gasification agents including steam and carbon dioxide were applied in the experiment. A series of systematical experiments were conducted as listed as the following:

- Pyrolysis of raw and acid washed biomass in a fixed-bed quartz reactor system to produce biochar such as raw-biochar and acid washed biomass-biochar for further combustion, gasification, and characterization.
- Combustion of the prepared biochar under well-controlled conditions in the same reactor system to obtain the carbon content of biochar.
- Gasification of either preload biochar or in-situ biochar was run in the same reactor system as the pyrolysis.
- Analyses of the biochar and activated carbon via a series of techniques such as nitrogen adsorption, Raman analysis, gravimetrical analysis, chemical composition and morphology analysis were conducted.

Figure 3-1 gives the overall research methodology and its detail.

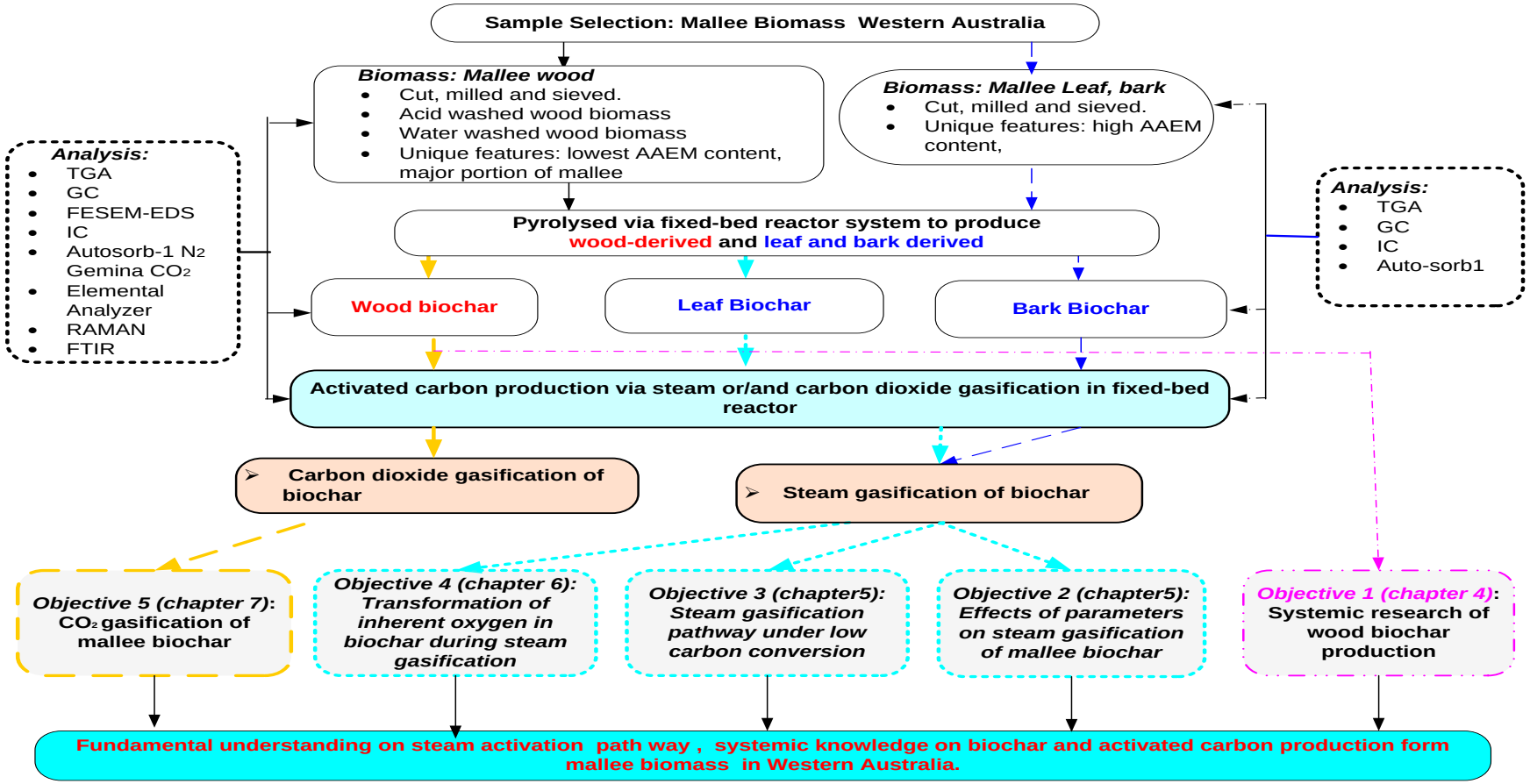

Figure 3-1: Research methodology

3.2.1 Effect of Sampling Temperature on the Properties of Biochar

Pyrolysis temperature takes a vital role in the evolution of biochar especially with reference to biochar yield and biochar structure. Important reactions such as the release of the volatiles, the formation of the intermediate melt were mainly influenced by temperature. Carbonization temperature of around 500℃~800℃ and gasification temperature between 800℃~900℃ are normally accepted for industrial AC production. To gain insight into the possible pathway of gasification, a mild temperature should be applied to ensure the experiment to be under the regime of chemical reaction control. Therefore, a series of experiments under a wide range of temperatures (from 350℃~850℃) were carried out to produce biochar samples from wood biomass in a fixed bed reactor. After that, pyrolysis of leaf and bark were conducted under optimized temperature which was obtained from wood pyrolysis.

3.2.2 Effect of Heating Rate on the Properties of Biochar

To gain a basic idea about the possible application of solid residue, systematical experiments were then designed and carried out. Firstly, biochar samples were produced from both slow and fast pyrolysis of mallee wood via a fixed-bed quartz reactor system at 750℃. This selected temperature is mild but high enough to guarantee the reaction of the consequent gasification either in the atmosphere of steam or carbon dioxide. The detailed results and discussion for this work are presented in Chapter 4.

3.2.3 Effect of Holding Time, Gas Flow Rate on the Properties of Biochar

The results in Chapter 4 also provided the effect of holding time and gas flow rate on the properties of biochar. Such results give the basic knowledge of the pyrolysis process. In Chapter 5.2, steam gasification under low carbon conversion and transformation of inherent oxygen in biochar during steam gasification were carried out to explore the possible gasification pathway.

3.2.4 Effect of Gasification Agent on the Properties of Activated Carbon

To investigate the roles of gasification in the evolution of pore structure, both steam gasification and carbon dioxide gasification were applied. A series of AC were obtained under various operating parameters such as different carbon conversion, temperature, with the absence or presence of AAEM. The focused ion beam scanning electron microscopy (FIBSEM) analysis was carried out to quantify the process of the development of pore. The results of this work are presented in Chapters 5, 6 and 7.

3.2.5 Significant Roles of Inherent Mineral Species on the Reactivity of Biochar in the Course of Gasification

To investigate the roles of indigenous mineral content in biomass in the development of the structure of AC, a wood biomass was washed with dilute acid to produce a sample that is free of AAEM mineral particles. To obtain partially demineralized sample, water washing biomass was applied. The procedure is the same as acid washing sample except the acid solution replaced by Milli-Q water and with shorter wash time. During the gasification, the produced gas were collected by gas bag and analyzed by Gas Chromatograph (GC). The characteristics of AC were obtained through an array of analytical techniques such as gas adsorption analysis, Raman, fourier transform infrared spectroscopy (FTIR), and FEBSEM-EDS. The significant roles of the evolution of pore and the role of AAEM were then clearly evidenced. The detailed results of this part of work are reported in Chapters 6 and 7.

3.3 Experimental

A series of preliminary blank experiments without samples or with graphite were performed to ensure the seal of experiment system before gasification run. Repeated experiments were conducted to obtain enough samples for analysis and determining the experimental reproducibility.

3.3.1 Sample Preparations

- ***Mallee biomass.***

Three mallee biomass components as leaf, wood and bark were obtained by cutting the green mallee tree (E.loxophleba lissophloia) harvested from farms in Narrogin, Western Australia. These samples were dried in a large lab oven at 40℃ then were ground by cutting mill (Fritsch Laboratory cutting mill "Pulverizette 15"). All three biomass samples were then sieved into different size fraction 106 μm ~150μm, 150 μm ~250 μm, 250μm~1000 μm, and 1mm ~2mm. Then these samples were sealed with double plastic bags. The effect of different size on biochar and AC production will be analyzed. Only size 150 μm ~250 μm woody portion of the mallee tree were used in gasification mechanism study without further mention. The properties of these three types of samples have been listed in Table 2-4.

- ***Acid washed mallee wood***

Acid washed mallee wood biomass was prepared for the experiments in Chapter 4 and Chapter 6. Table 3-1 shows the properties of acid washed mallee wood.

Table 3-1: Properties of acid washed mallee wood

Sample	Moisture (% ad)	Proximate(wt% db)			Ultimate analysis(wt% daf)			
		FC[b]	VM[c]	Ash	C	H	N	O[*]
A[a]	2.9	88.2	11.8	-	46.49	6.36	0.51	45.84

[a]A means acid washed biomass , [b]Fixed carbon（FC）, [c]Volatile matter(VM), *O by difference.

Acid washed raw wood was obtained by acid washing biomass. It consisted of soaking approximate 2g sample in 1L 0.2 M HCl solution and stirred gently for 72 hours before filtering and then washing with ultrapure water (Milli-Q water) repeatedly until there is no Cl^- detected by a ion chromatography (IC). After that, the sample obtained was put in oven drying at 40 ℃ for 72 hours.

3.3.2 Experimental Rigs

The pyrolysis experiments were carried out to prepare biochar and activated carbon in a quartz fixed-bed reactor. A schematic diagram of the reactor system is shown in Figure 3-2. It mainly consists of a quartz reactor with an inner diameter of 40 mm and a two-heating zone electrical temperature-controlled tube-furnace. Other parts include a clod trap, a quartz filter, and a steam/ carbon dioxide introduction system. A key feature of the reactor system is that both slow-heating pyrolysis and fast-heating pyrolysis can be realized easily.

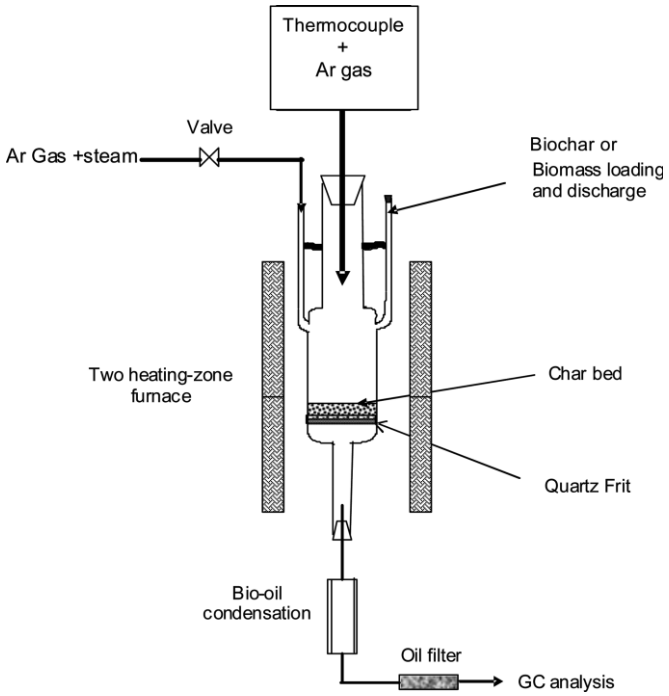

Figure 3-2: Steam gasification system used in present experiment[161]

Thermocouple and mass flow control were used to monitor temperature and gas flow rate. The thermocouple was inserted from the top of the reactor and its end was placed on the top of the sample bed as close as possible without touching it. It should be noted that the reactor was always lift out of furnace vertically to avoid the contact between the char bed and the tip of the thermal couple. The readings of thermocouple give the instantaneous temperature inside the reactor.

3.3.3 Preparations of Biochar

In Chapter 4, two types of char were prepared from the pyrolysis of the raw wood biomass sample. Both types of biochar were prepared in a fixed-bed quartz reactor. For pyrolysis experiments at a slow-heating rate (slow pyrolysis), a quartz reactor with preweight sample was put into furnace, then was heated up to a final stable temperature (between 350℃ and 850℃ which covers the common temperature used in activated carbon production in practice) at a heating rate 10K/min (unless mentioned) with chosen argon flow rate (UPH 99.999%) as an inert gas (at room temperature). Due to its similarity to industrial carbonizations process and wide application in other literatures, heating rate 10℃/min was applied. [162] At the final temperature, reactor was kept in furnace for 1h. When pyrolysis was finished, the reactor was lifted out of the furnace immediately keeping argon continuously blowing and cooling down to room temperature naturally. For pyrolysis experiments at a fast-heating rate (fast pyrolysis), firstly an empty quartz reactor was connected with a feeder then it was put into furnace and heated up to a terminal temperature (between 350℃ and 850 ℃). After a final stable temperature was obtained, argon was purged through the empty reactor for around 20 minutes to ensure the absence of oxygen. After that, wood particles were fed to a reactor at a rate of about 110 mg/min under 1.5L/min argon atmosphere. When all the particles were in the reactor, the particles were held for a further 10 minutes before discharging. Cooling down method applied is the same method used for SB above. Once sample particles were injected into the hot reactor zone, rapid pyrolysis took place similar to than in a normal drop-tube reactor.

Hereafter, nomenclatures “SB” and “FB” were used to represent biochar obtained under slow heating rate or fast heating rate. In Chapter 4, biochar from leaf and bark were also prepared for the purpose of comparison with wood biochar.

- ***Activated carbon production***

Biochar sample production and gasification of the biochar were carried out in the same fixed-bed reactor. The procedure of gasification of steam or carbon dioxide is the same. Basically, once the above biochar was obtained, the gasification agent was introduced immediately into heated reactor zone by switching on the three-way valve. Once the desired gasification time was reached, the gasification agents were switched off and the reactor was lifted out of furnace immediately cooling down naturally with keeping argon blowing through. About 0.1 g biochar sample was employed in each experiment. The steam was produced by the evaporation of Milli-Q water which was pumped through a HPLC pump (Alltech Model 626) into the reactor. The selected concentrations of steam (8.2 vol %, 10 vol %, and 15.2 vol %) were applied in this study. And the reactor was operated at atmospheric pressure. The concentration of carbon dioxide was fixed at 7.7 vol % from pre-mixed gas. The various parameters of activated carbon production result in the complexity of nomenclatures of activated carbon. Therefore, different nomenclatures used to represent the products were explained in detail in the separate sections. For instance, in Chapter 6, "Sample-AC-temperature" was normally used to identify the activated carbon obtained. Here, AAC550-760 means activated carbon was obtained from acid washed biomass biochar which was pyrolyzed at 550 ℃ then heated to 750 ℃.

- ***Mechanism study of gasification***

It is very important to keep the gasification agent partial pressure constant so that the reactor can be treated as a differential reactor. However, steam was consumed as a gasification agent. In this study, reaction conditions were controlled to minimize the consumption of steam. The actual steam concentration was determined from the amount of feed. Gasification was well controlled under chemical-reaction-controlled

regime, where mass transport effects are minimized. To keep steam partial pressure constant, minimal steam consumption should be achieved. In all steam gasification experiments, approximately 1g raw sample was used.

The amounts and the composition of gas produced in the pyrolysis and gasification were collected and measured systematically. The gaseous product (like H_2, CH_4, CO, CO_2) that went through the cooling system were collected by gas bags at predetermined time intervals after being cooled down through condensation system and filtered by quartz wool. They were then analyzed by two PERKIN-Elmer Gas Chromatographs (GCs).

The specific reactivity of biochar (R) was calculated by the following equation:

$$R = \frac{-dc}{cdt} \tag{3-1}$$

Where, c is the amount of carbon in mol at any time t. The total carbon of biochar sample was determined by combustion. The specific reactivity is calculated being based on the instaneous remaining amount of carbon, therefore, it indicated an instaneous rate thus displaying the real reactivity.[163]

For carbon dioxide gasification, the same experimental conditions as steam gasification including temperature, flow rate were employed. The further experiments prove the reaction is under chemical reaction control in Chapter 5.3.1 and Chapter 7.2.

The combustion of biochar was carried out in the fixed-bed quartz reactor. The gaseous product were collected and analyzed to determine the carbon content of biochar.

Biochar and activated carbon were collected for further analysis.

3.4 Instruments and Analytical Techniques

3.4.1 Proximate Analysis and Ultimate Analysis

METTLER thermo gravimetric analyzer (TGA) was applied to determine the proximate analysis of biomass, biochar and activated carbon. A method based on American Society for Testing and Materials (ASTM) international standard ASTME870-82[164] was applied as shown in Figure 3-3. About 10 mg of sample was loaded into a TGA 150 µl alumina crucible. Firstly the sample was purged with Argon gas for 15 min and then was heated to 110℃ followed by 40 minutes holding time until no further weight loss was observed. The total weight loss of the sample was calculated as moisture content. Then the sample was further heated to 900℃ at a heating rate of 100 K min^{-1} in Argon holding 20 min at this temperature. Thirdly, the temperature was decreased to 700℃. The weight loss was calculated as volatile matter and the remaining material is biochar. The argon gas was then replaced by air, and the biochar residue was burned at the air atmosphere for 25 min until no further weight loss was observed. The weight of the residual ash in the sample crucible is used to calculate the ash content (ash content percentage), of biochar while the difference between the weights of the char and residue ash is calculated as the fixed carbon content.

Ultimate analysis of these samples was determined via the PerkinElmer 2400 Series II CHNS/O Elemental Analyzer. To prevent the possible picking up of oxygen of heavily pyrolyzed chars, [165] all samples were dried under an atmosphere of argon before elemental analysis. The oxygen content was determined by the difference from the C, H, and N contents of the samples on a dry-ash-free (daf) basis.

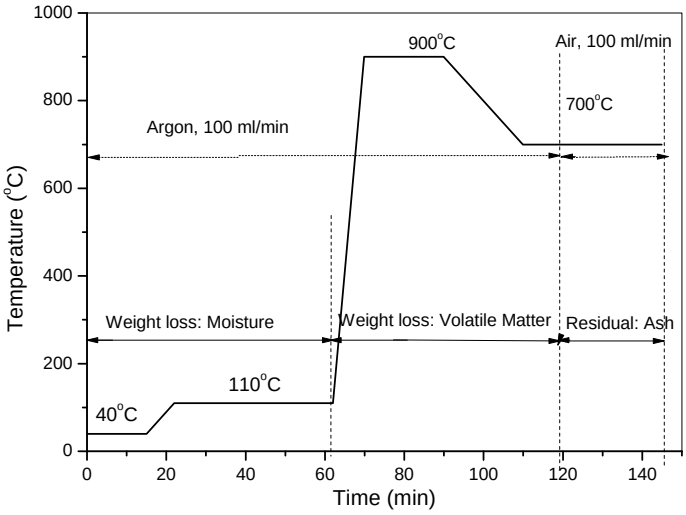

Figure 3-3: Temperature program of TGA for proximate analysis of biomass, biochar, and activated carbon

3.4.2 Quantification of AAEM Species and Other Inorganic Species

The alkali and alkaline earth metallic (AAEM) species, especially sodium (Na), potassium (K), magnesium (Mg), and calcium (Ca) are not only dominant metallic species (~90%) in raw samples but also play an important catalytic role in gasification. [166] Therefore, the amount of alkali and alkaline earth metallic species (AAEM) like Na, K, Mg, and Ca were analyzed by ion chromatography Dionex ICS-3000 ion chromatography (IC). Briefly, around 20mg samples were put onto platinum (Pt) crucibles then followed by ashing in air using a specially designed heating program which is shown in Figure 3-4 to guarantee no loss of AAEM during ashing. After that, Pt crucibles with ash sample were put in Teflon vials for acid digestion using a mixture of HNO_3: HF (1:1) solution at 120 ℃ for 12h. Excessive acids were then evaporated on a hot plate. The digested ash with Pt crucibles was dissolved in 20mM methane sulfonic acid (MSA) solution. A Dionex ICS-3000 ion chromatography with a CS12A column and 20mM MSA solution as effluent was used to detect the AAEM species in the solution. The relative standard

errors of were Na ±4%, K±5%, Mg ±5%, and Ca ±7%.

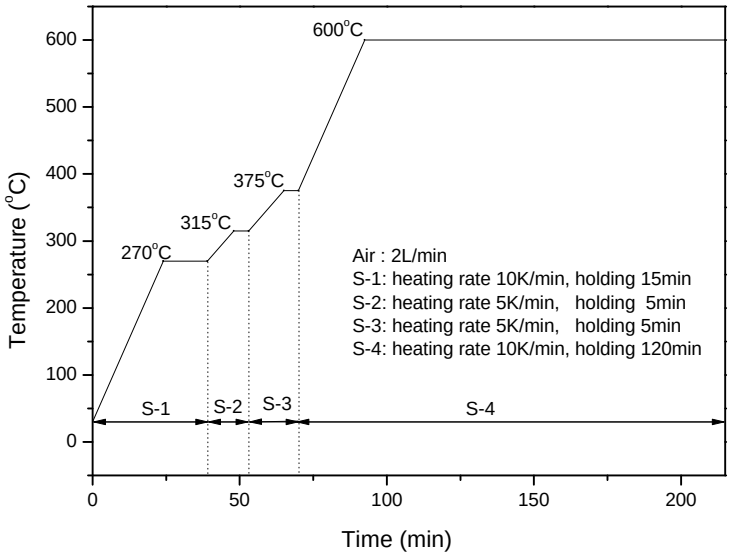

Figure 3-4: Temperature program of ashing fuel samples such as biomass, biochar

3.4.3 Gas Chromatograph

Two PERKIN-Elmer Gas Chromatographs (GCs) were applied to analyze produced gas. One contains a molecular sieve 5 column and with argon as a carrier gas, the other contains a Porapak-N column and a molecular sieve 5 column and with helium as a carrier gas. Both GCs were equipped with thermal conductivity detectors (TCD).

3.4.4 Pore Size Distribution of Biochars and Activated Carbon

The main methods of measuring porosity distribution are electron microscopy, the molecular sieve, adsorption (gas adsorption method) and small angle X-ray scattering method. Due to its convenience and in-expensive cost, gas adsorption and desorption method is commonly used. Molecular probe method [167] was used to evaluate the pore where a series of organic vapors of different molecular size (molecular diameters: dichloromethane 0.33nm, benzene 0.41nm, cyclohexane 0.54nm, and tetra

chloromethane 0.63nm) were applied to obtain isotherms at 25℃. Such different molecular sizes show different ability to access pore. For instance, adsorption benzene and carbon dioxide isotherms to evaluate mesopore (2~50nm), and micropore (0.4 ~2.0nm) is accessible to benzene while submicropores (<0.4nm) is only accessible to CO_2. [167] As for nitrogen at 77K and carbon dioxide at 273K, the nitrogen adsorption has diffusional restriction into narrow micropores as compared with CO_2. [119] Marsh, Harry [119] summarized three possible comparable results of N_2 and CO_2 adsorption: (1) N_2< CO_2. The possible reason is the restricted activated diffusion of the nitrogen at 77K into narrow microspores or pore entrances. This phenomena happens to the following material (a) of heat treatment temperature (HTT) <600℃ and >800℃; (b) the molecular sieve carbons with their limited PSD (pore size distribution) and; (c) activated carbons with <5wt% burn-off; (2) N_2～CO_2. This happens to materials with relatively narrow (about 1 nm dimension) micro porosity and a narrow PSD such as activated carbons with <35wt% burn-off and some molecular sieve carbons ; (3) N_2>CO_2 . This happens to material with a wider micro porosity and a broader PSD. Most activated carbons behave this way with >35wt%.

Quanta chrome Autosorb AS-1 instrument was used to run N_2 adsorption-desorption isotherm of biochar and activated carbon at 77K. Gemini was applied to run CO_2 adsorption isotherm at 273K and 195K. The molecular area for nitrogen (77K) is 0.162nm^2, and CO_2's is 0.170 nm^2 at 195K and 0.187 at 273K. [168] The density of liquid N_2 is 0.808g cm^{-3} and β factor is 0.33, and the density of CO_2 at 273K is 0.818gcm^{-3} and β factor is 0.35. All samples were degassed under vacuum overnight at 100 ℃ [169] prior to analysis.

The software used for calculation is provided by Quanta Chrome Corporation (ASWIN) and Micrometrics. Apparent surface area (SBET m^2/g) was calculated by Stephen Brunauer, Paul Hugh Emmett, and Edward Teller equation (BET). BET surface is a main index to illustrate the pore evolution, so it will be explained

thoroughly. Pore volume of micropore (cc/g) and average half pore width (A) was calculated by Dubbin-Radushkevich (DR) plot.[163, 170] Total volume was obtained at around p/p_0=0.9998 (cc/g). All these data analysis were completed by ASWIN software. The detailed theory and discussion of models are summarized and given in Autosorb AS-1 AS1Win gas sorption system operation manual.[171] The relative standard deviations of SBET, total volume and AHPW are 0.8~2.2%, 0.8~2.1% and 1.4~3.2% respectively. To get better understanding of the pore structure, quenched-solid density functional theory (QSDFT) [172, 173] was used to get the pore size distribution profile which takes into account the surface geometrical heterogeneity in terms of a single roughness parameter, δ and was proved to be accurate. [174]

BET Surface area

Multi point BET method was used in this study. Usually the range of P/P_0 of adsorption isotherm using nitrogen as the adsorbate is limited to 0.05 to 0.35. However, this linear region may shift to lower relative pressures for microporous materials.

Apparent surface area (SBET m^2/g) was calculated by Stephen Brunauer, Paul Hugh Emmett, and Edward Teller equation (BET).

$$\frac{1}{W((p_0/p)-1)} = \frac{1}{W_m C} + \frac{C-1}{W_m C}\left(\frac{P}{P_0}\right) \qquad (3\text{-}2)$$

Where W is the weight of adsorbate adsorbed at a relative pressure P/P_0; W_m is the weight of adsorbate constituting a monolayer of surface coverage; C is the BET Constant. This constant illustrates the energy of adsorption in the first adsorbed layer and it is also an indication of the magnitude of the consequent adsorbent/adsorbate interactions.

W_m can then be calculated from the slope s and intercept *i* of the BET plot. From equation (1):

$$s = \frac{C-1}{W_m C} \tag{3-3}$$

$$i = \frac{1}{W_m C} \tag{3-4}$$

Thus

$$W_m = \frac{1}{s+i} \tag{3-5}$$

The total surface area S_t can be expressed as:

$$S_t = \frac{W_m N A_{cs}}{M} \tag{3-6}$$

where, N is Avogadro's number (6.023×10^{23} molecules/mol) and M is the molecular weight of the adsorbate. A_{cs} the cross-sectional area of adsorbate. For the hexagonal close-packed nitrogen monolayer at 77 K, the cross-sectional area A_{cs} for nitrogen is 16.2 Å. The specific surface area S of the solid can be determined from the total surface area S_t t and the sample weight w as the following equation:

$$S = \frac{S_t}{w} \tag{3-7}$$

Dubinin-Radushkevich

Micropore information was calculated using the Dubinin–Radushkevich (DR) equation.

$$\log V = \log Vo - D \log^2 (P/P_0) \tag{3-8}$$

Where, $D = 2.303\ k R^2T^2/\beta^{2;}$ V = Volume of adsorbate adsorbed at relative pressure

P/P_0; V_0 = Micropore volume within the adsorbent; *k* and ***β*** are shifting factors (β = 0.33 for N_2). *R* = Gas constant *R* = 8.3145 J mol^{-1} K^{-1}; *T* = temperature.

3.4.5 Ion Beam Scanning Electron Microscopy (FIBSEM)

Zeiss Neon 40ESB[175] focused ion beam scanning electron microscopy (FIBSEM) equipped with an energy dispersive X-ray spectrometer (EDS) was used for morphology and chemistry analysis of samples. In-lens SE detector was applied to get higher solution of images of selected biochar and activated carbon. A back scattering mode detector (BSE) combined with an integrated EDS/EBSD facility is used to obtain the chemical composition and dispersion on the surface of samples. Samples were firstly dispersive on the carbon tape sticking to the aluminum stub then were coated by carbon (2nm) or platinum (2nm). Platinum coating is better for high-resolution images while carbon coating is used for chemical composition analysis using EDS and BSE.

3.4.6 Raman Analysis

ISA (Dilor) Dispersive Raman spectrometer (HeNe, 632 nm lasers) is used in this study. Biochar particles are black bodies and can be easy to heat up resulting in the possibility of biochar structure alteration. So firstly D=0.3 was chosen and analysis of the same particle were repeated four times. Results show the Raman spectral intensity does not change showing no evidence of alteration of biochar, so D=0.3 was chosen. The minimum of 15 measurements were taken per sample and their average was taken as the final results. [170]

Usually the Raman spectral contain two bands of major interest, namely D (~1350cm^{-1}) band which reflects the disordered structure in graphite or other highly ordered carbonaceous materials and G band which (~1580cm^{-1}graphite E22g band) implies graphitic carbon. However it should be noticed that a G band in carbonaceous material does mean it was graphitic and conversely that D-band may

appear in a relatively well-ordered carbon. [176] Qian believed that the increase of the intensity of D-band is attributed to the increased number of defects within multi-walled carbon nanotubes. [177]

However, the "overlap" of G band and D band of highly disordered carbonaceous may cause the miss of the information. Thus the Raman spectral data over the range of 800 cm^{-1} ~1800cm^{-1} were curve-fitted using 10 bands[178] (see in Table 3-2) which represent the major structure of biochar and activated carbon. Therefore, the detailed information of skeletal carbon structure such as the information of size of aromatic rings, the nature of substitutional groups, and cross-links in char can be acquired. Origin 8.1 was used to run curve fitting.

Table 3-2: Summary of Raman band assignment[178]

Band name	standing	Band position (cm^{-1})	Description Bond	type
Gl	G left	1700	Carbonyl group C=O	sp^2
G		1590	Graphite $E^2$2g; aromatic ring quadrant breathing; alkene C=C	sp^2
Gr	G right	1540	Aromatics with 3–5 rings; amorphous carbon structures	sp^2
Vl	valley left	1465	Methylene or methyl; semicircle breathing of aromatic rings; amorphous carbon structures	sp^2, sp^3
Vr	valley right	1380	Methyl group; semicircle breathing of aromatic rings; amorphous carbon structures	sp^2, sp^3
D		1300	D band on highly ordered carbonaceous materials; C-C between aromatic rings and aromatics with not less than 6 rings	sp^2
Sl	S band left	1230	Aryl–alkyl ether; para-aromatics	sp^2, sp^3
S	on the side of the D band	1185	Caromatic-Calkyl; aromatic (aliphatic) ethers; C-C on hydroaromatic rings; hexagonal diamond carbon sp3; C-H on aromatic rings	sp^2, sp^3
Sr	S band right	1060	C-H on aromatic rings; benzene (ortho-di-substituted) ring	sp^2
R	right band	960–800	C-C on alkanes and cyclic alkanes; C-H on aromatic rings	sp^2, sp^3

3.4.7 Fourier Transform Infrared Spectroscopy (FTIR)

Perkin-Elmer Spectrum 100 ATR-FTIR spectrometer was used to analyze the raw biomass and activated carbon. Before analysis, samples were pulverised into powder using an agate mortar and then air-dried overnight in an oven at 40 ℃. A scanning resolution 2 cm^{-1} was applied. A constant force of 80 N was applied on the sample during the analysis. Software attached was used to process data including ATR corrections, baseline corrections, and automatic data smoothing. Table 3-3 gives the main atomic groups and structures of maize stalk.

Table 3-3: The main atomic groups and structures of maize stalk[179]

Wavenumber (cm^{-1})	Infrared adsorption	Atomic groups and structures
3200 -3700	O-H stretching	Hydroxyl
2800-3000	C-H stretching	Aliphatic structures
1650-1770	C=O stretching	Carbonyl
1610-1680	C=C stretching	Olefinic structures
1450-1600	C=C stretching	Aromatic structures
1420-1480	C-H bending	Aliphatic structures
1360-1430	O-H and C-H bending	Hydroxyl, acid, phenol, olefines and methyl
1200-1300	C-O stretching	Unsaturated ethers
1000-1200	C-H out of plane bending	Aromatic structures
1000-1160	C-O stretching	Saturated ethers
1050-1160	C-O stretching	Tertiary hydroxyl
1070-1120	C-O stretching	Secondary hydroxyl
1000-1060	C-O stretching	Primary hydroxyl
625-1000	C-H out of plane bending	Olefinic and aromatic structures

3.5 Summary

Mallee biomass sample was selected as feed stock to prepare biochar and AC. Mallee wood with different size fractions was initially pyrolyzed under variable operating conditions using a quartz fixed-bed reactor system. Optimized conditions were then obtained from the initial experiments. Through the subsequent gasification of biochar,

activated carbon based from mallee wood was produced. To gain insight into the possible steam gasification pathway, size fraction 150~250 of leaf, bark, and wood were used to guarantee the reaction was under chemical reaction control regime. The raw samples, derived biochars, and activated carbon, gas produced in pyrolysis and gasification were characterized via various analytical techniques.

CHAPTER 4 PYROLYSIS CHARACTERISTICS OF MALLEE BIOMASS

4.1 Introduction

Pyrolysis is an important step for activated carbon production and its consequent mechanism during gasification.[180,181,182] Biochar obtained at 450℃ is the most reactive while a char obtained at 900 ℃ [80] is unable to form ether and carbonyl groups. Different size fractions such as 1mm~1.6 mm (grapefruit peels), [134] 1mm~2 mm (poplar wood), [104] and 2mm~4 mm (lignocellulosic chars) [127] were applied. Biochar itself can be used as fuel source for combustion, soil adjuster, and reducing iron ore to iron in the blast furnace in steel industries. During the research on pyrolysis and gasification of biomass, biochar preparation is the first step. A certain structure developed during this process has a vital effect on the subsequent soil amending and subsequent AC structure. The knowledge of the properties of biochar offers us basic informaiton not only in choosing operating parameters of gasification of biochar but also in the other biochar application yiled such as carbon sequestration,[136] soil amending, [41] and combustion of solid biochar.[163] However, there are still no systematic studies of biochar produced from mallee biomass.

Therefore, this chapter aims to discuss key factors that influence the pyrolysis of mallee wood, as the majority of mallee biomass, and the systematic development of the physical and chemical structure of the pyrolysis product. Pyrolysis of mallee wood was carried out under different operating variables including particle size, pyrolysis, temperature, holding time, heating rate and acid washing biomass. The consequent biochar have been further analyzed to obtain their characteristics such as AAEM contents and ultimate analysis. The mechanism of biochar addition effecting on soil performance was discussed as well.

4.2 Mallee Wood, Mallee Leaf, and Mallee Bark

Thermal decomposition of leaf, bark, wood, and the mixture of three biomass component were carried out. Since results show mallee wood had the lowest ash content which is beneficial to obtain carbonaceous solids, mallee wood particle was applied to produce activated carbon. Furthermore, the properties of pre-treated mallee wood particle like acid washed mallee wood and water washed mallee wood were also investigated. Without further mention, mallee wood particle was used in the following experiments.

4.2.1 Mallee Wood

Figure 4-1 illustrates SEM images of mallee wood biomass sample. It shows the shape of both 106 µm ~150 µm sample and 150 µm ~250 µm are irregular. Samples with size 106 µm ~150 µm showed more cracking structures and less complete cells which were probably due to longer milling time. Table 4-1 presents the property of wood particle used in this section.

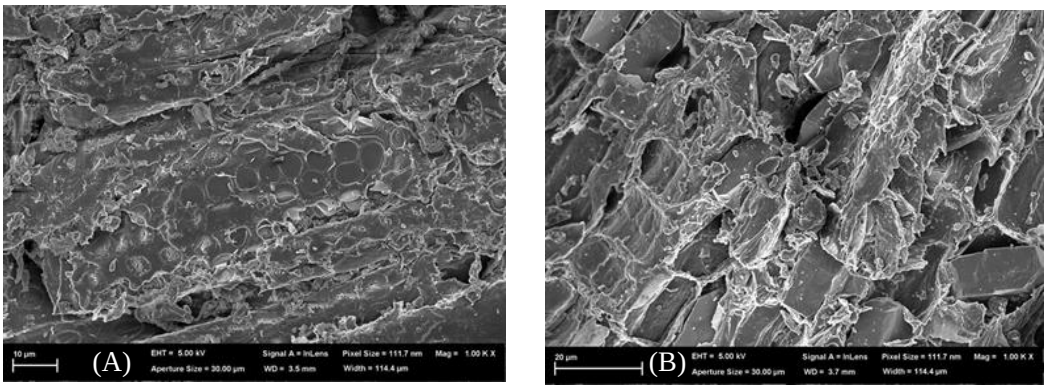

Figure 4-1: SEM of mallee wood biomass used in this experiment: (A) 150~250 µm (B) 106~150 µm.

Table 4-1: The property of mallee wood particle

Sample	Moisture (wt% [a]ad)	Proximate analysis (wt% db)			Ultimate analysis(wt% daf)					AAEM content(% db)			
		FC[b]	VM[c]	Ash	C	H	S	N	O*	Na[d]	K[d]	Mg[d]	Ca[d]
Raw	3.1	16.8	82.7	0.5	46.11	6.41	0.74	0.15	46.58	0.021	0.064	0.032	0.124

[a]ad means air dried; db means dry basis; daf means dry-ash- free basis; [b]Fixed carbon（FC）, [c]Volatile matter(VM), [d] Analysed by IC; * by difference

Thermo gravimetry (TG) and differential thermo gravimetry (DTG) curves of raw wood were obtained under argon atmosphere. The curves at heating rates between 1K/min and 10K/min based on ASTM E1641 were performed and are shown in Figure 4-2.

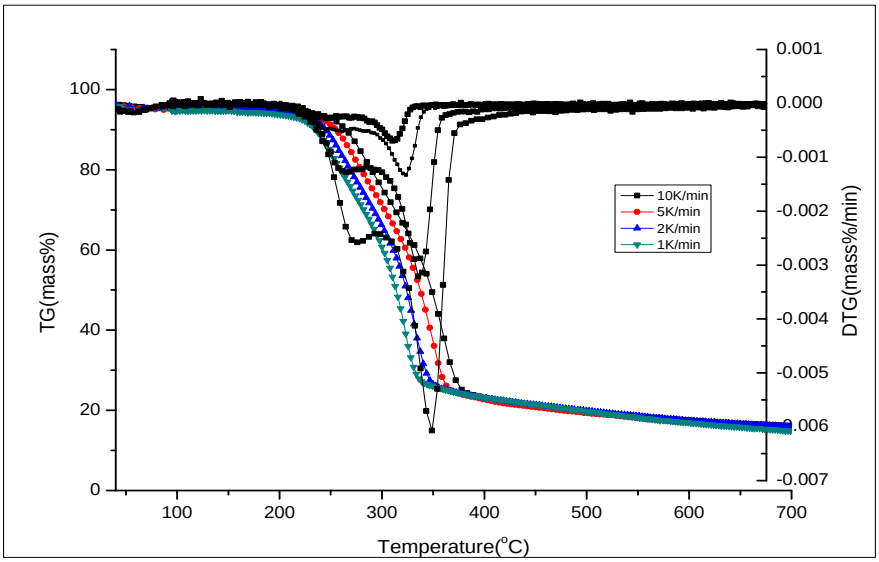

Figure 4-2: TG and DTG curve of raw wood particle under heating rate 1K/min, 2K/min , 5K and 10K/min

The separated regions of TG and DTG curve are very clear indicating the thermal degradation process of mallee wood. According to TG curve, the first weight loss at around 100℃ is mainly due to the loss of moisture. Then continuous weight loss took place and these can be explained by the degradation of lignocellulosic compostion.As for the degradation temperature of these three components

（hemicellulose, cellulose, and lignin）, different temperature ranges have been given by different authors. Decomposition temperatures of hemicellulose, cellulose and lignin are180 ℃ ~240 ℃ , 230 ℃ ~310 ℃ , and 300 ℃ ~400 ℃ respectively[183]. Hemicellulose and cellulose started thermal degradation at 200~260℃ and 240℃ ~350℃ respectively. [170, 171,184, 185] Lignin is believed to be thermostable and shows a wide range degradation temperature 280℃~500℃ [186] or 175℃~800℃.[187] The reason for the difference of the degradation temperature is mainly due to the sample characteristics. Generally, hemicellulose starts to decompose followed by cellulose and lignin may decompose at low temperature.

As shown in Figure 4-2, in terms of DTG curve, there are two overlaping peaks and a flat tail section despite different heating rates. Based on the above discussion, the second peak (around 270℃) is attributed to hemicellulose and the third peaks occurred between 320 ℃ and 360℃ due to cellulose. The degradation of lignin covers a wide range and mainly accounts for the flat tail.

Figure 4-2 also presented that an increase in heating rates led to a tendency of shifting the peak to the right of of DTG curve. Under various heating rates 1K/min , 2K/min, 5K/min, and 10K/min, the second peak point of DTG curve happened at temperature 253 ℃, 264 ℃, 274 ℃, 279 ℃ respectively, and the third peak point occurred at 320 ℃, 334 ℃, 342 ℃, 360℃. The reason was that the heat resistance occuring at higer heating rate which delayed the decomposition. However, the percentage of solid residue weight after pyrolysis under different heating rate are similar at around 14%. It is obvious that TG curve levels off after 600℃ which indicated that most volatile matter was released above that temperature.

To obtain the temperature of biomass combustion, combustion of sample under air

atmosphere was also carried out shown in Figure 4-3. It clearly shows 600℃ is high enough to ensure the complete combustion of mallee wood.

To understand the effect of AAEM contents on thermal decomposition of wood sample, the DTG curve of acid washed wood and water washed wood were also given in Figure 4-4. The temperature where the peak of decomposition rate occurred according to DTG cure were shown in Table 4-2.

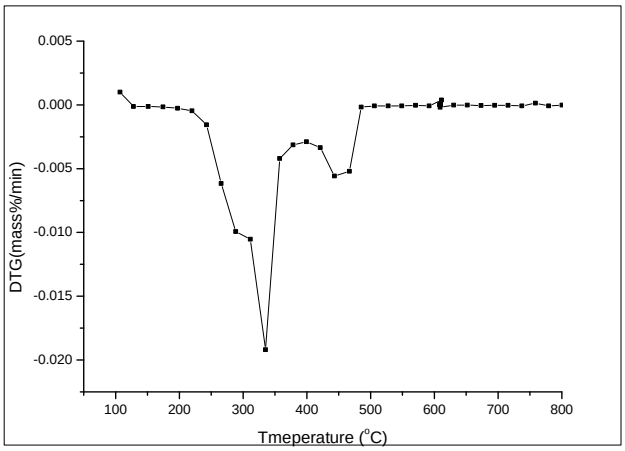

Figure 4-3: Combustion of raw wood particle under air atmosphere (heating rate 10K/min)

Table 4-2: The peak temperature of decomposition of DTG curves of three types of wood sample

sample	Heating rate											
	1K			2K			5K			10K		
	2nd	3rd	D	2nd	3rd	D	2nd	3rd	D	2nd	3rd	D
raw sample	253	320	67	265	332	67	274	347	73	285	360	75
acid washed sample	250	322	72	258	332	74	274	348	74	286	354	68
water washed 15min sample	254	329	75	258	340	82	274	355	81	287	364	77

D means difference; 2nd and 3rd means the second peak and the third peak of decompositon of DTG curve.

Combining Figure 4-2 and Figure 4-4, the altitude of peak of raw wood sample is higher than acid washed and water washed sample. However, temperature points with peaks and the range between peaks of these three types of samples are similar as

shown in Table 4-2. With the increase of heating rate, the peak points moved to right namely to higher temperature obviously. The second peak temperature of decomposition of acid washed wood shows the lowst tempeatuer.

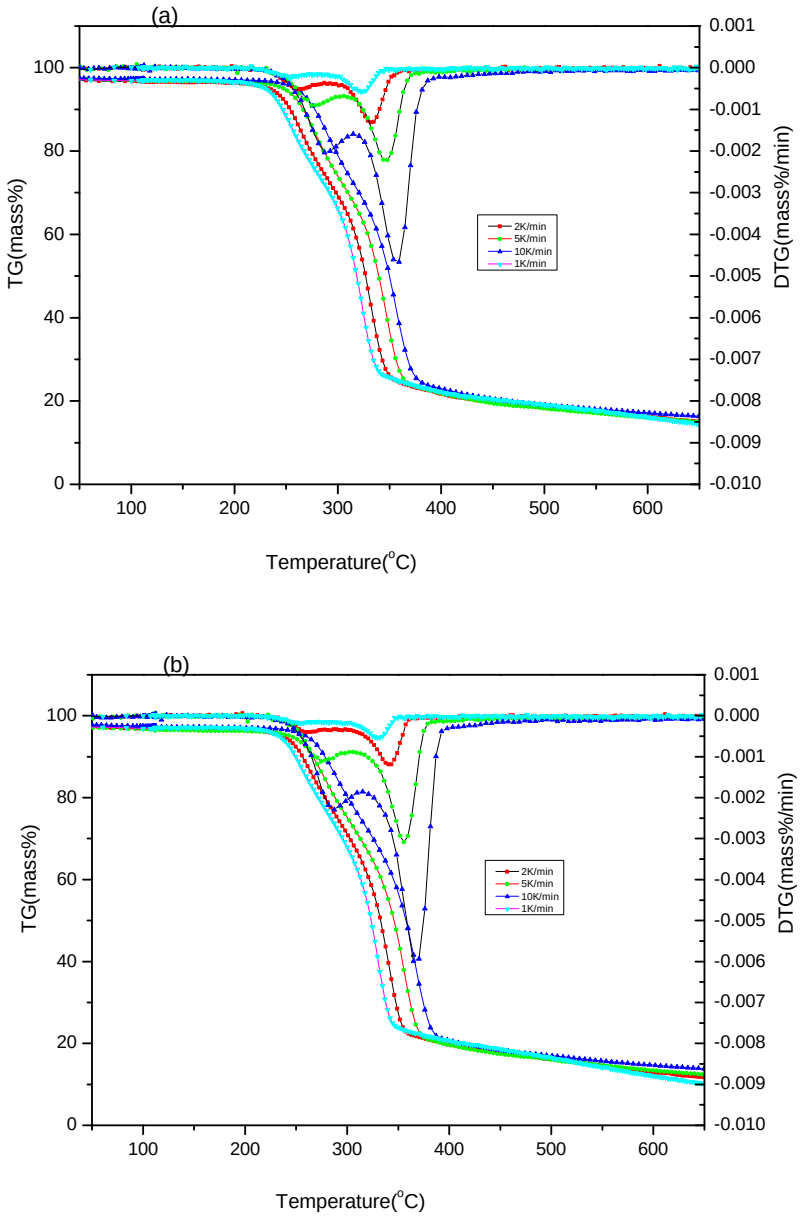

Figure 4-4: DTG curves under heating rate 1K/min, 2K/min, 3K and 5K/min: (a) acid washed wood sample and (b) water washed wood sample.

The slight lower peak temperature of decomposition of acid washed sample and water-washed sample under lower heating rate is likely attributed to the release of organic compounds during washing treatment of samples. It seems like, under

heating rate at 10K/min , the release of volatile matter is slow thus the peak altitude is lower.

On the contrast, in the analysis of proximate analysis where the heating rate increases to 100K/min, higher volatile matter content of acid washed biomass may be due to the easier release of volatile matter because of the the "voidage " left by the release of organic compounds caused by acid washing. In the following section, acid washed biochar showed much higher surface area which further support this assumption. It was found inherent mineral matter effect the biomass pyrolysis slightly, but influenced the sensitivity of the reaction. [188]

4.2.2 Mallee Leaf and Mallee Bark

During havesting mallee biomass, the three biomass components (leaf, wood, and bark) are usually just mixed or are roughly separated. Therefore, knowledge of leaf and bark is of primary importance. Table 4-3 and Figure 4-5 show the properties of raw leaf and raw bark.

Table 4-3: Properties of raw leaf and raw bark

		Proximate analysis			AAEM content			
Sample	M[a], % ad	Ash, % db	VM[b], % db	FC[c], % db	Na [d]	K [d]	Mg [d]	Ca [d]
leaf raw	6.6	3.9	74.5	21.7	0.5917	0.3232	0.1706	0.7031
bark raw	5.1	4.4	70.9	24.8	0.2503	0.1102	0.0888	2.1646

ad means air dried; db means dry basis; daf means dry-ash- free basis; M[a] means moisture; bFixed carbon（FC）; [c]Volatile matter (VM); [d] Analyzed by IC.

It is obvious that leaf and bark showed much higher ash content. The bark also showed the highest calcuim content. The DTG curve of leaf and bark demonstrate different thermal decomposition behaviour. Bark had two more peaks at around 500 ℃ and 700℃. Leaf showed wider thermal decomposition range and gives two peaks at around 420℃and 645℃. This information suggests two important issues: (1) bark and leaf will have higher biochar yield than wood; (2) due to their different

thermal behavior, mixing of these three components may lead to positive impacts on biochar yield by negative impacts on the following AC structure. Apart from that, leaf and bark biomass exhibit higher ash and low fixed carbon.That indicates that leaf and bark may have higher reactivity due to the catalyst of inorganic but higher biochar yield is the consequence of higher ash content. Such high ash content are not good for AC production, however, maybe good as soil fertilizer. Therefore, wood was mainly investigated in this work.

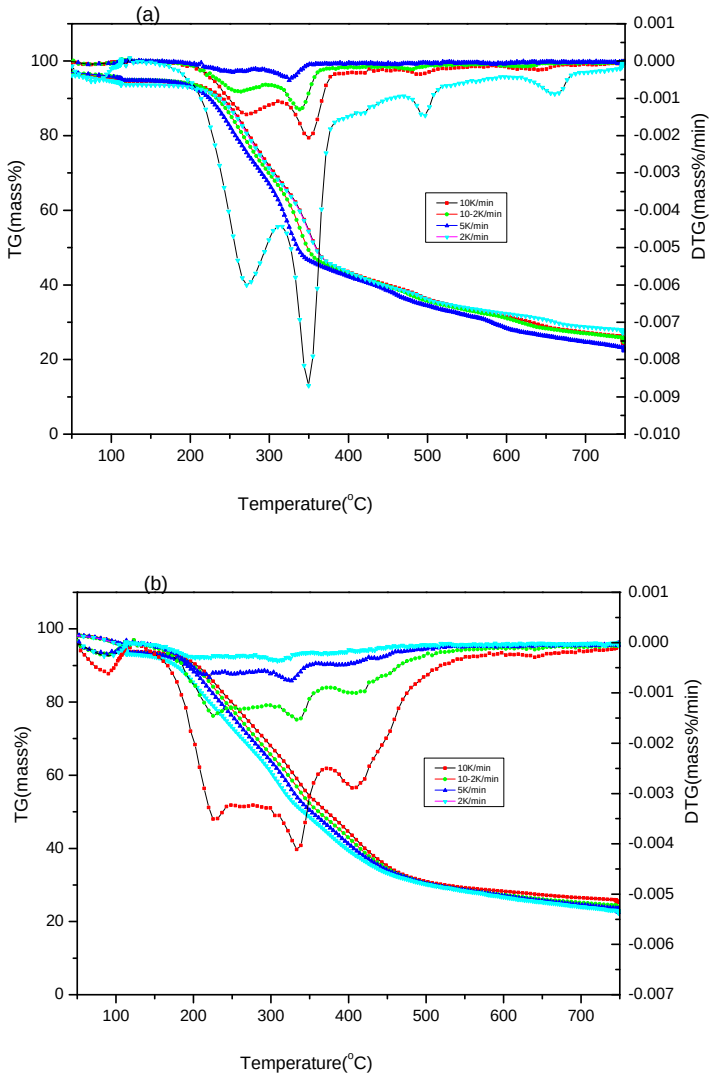

Figure 4-5: DTG curve of leave and bark sample under heating rate 1K/min, 2K/min, 3K/min and 5K/min: (a) bark sample; (b) leaf sample.

4.3 Pyrolysis Characteristics of Mallee Wood

4.3.1 Effect of Holding Time on Biochar Yield

Figure 4-6 presents the effect of holding time at 350 ℃ and 500℃ on biochar yield of 1mm~2mm mallee wood particle. When the temperature was held at 350℃, increasing holding time from 1 to 2 hours, the biochar yield decreased from around 36.6% to 27.5 %. That meant that volatile matter was continuously released during the extension of holding time. The biochar yield remained nearly steady when the pyrolysis time increased beyond 2 hours. As for 500℃, the char yield remained constant between 1 and 2 h holding time. It shows that 1h holding time was enough for the release of volatile when pyrolysis temperature is at 500℃. From Figure 4-2, it can be seen that when temperature is higher than 500 ℃, the weight loss leveled off. Thus in the following experiments, 1 h of holding time was used for all runs.

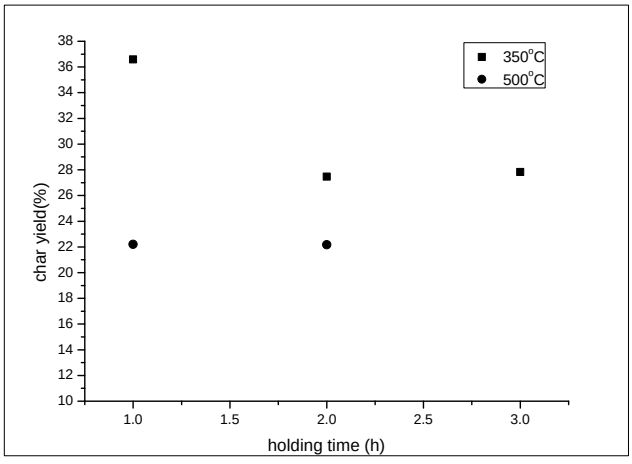

Figure 4-6: The effect of holding time on biochar yield at 350℃and 500℃

4.3.2 Effect of Sample Size, Temperature, and Heating Rate on Biochar Yield

For commercial powder activated carbon production, the particle of raw material is less than 1mm in size with an average diameter between 0.15 mm and 0.25mm was

used. [78] Thus in this section, size 1mm~2mm and 150 μm ~250μm are chosen for slow pyrolysis. During the process of fast pyrolysis, sample was fed into reactor through a feeder. The smaller sample size 106 μm ~150μm was used to avoid the risk of jam in the line.

For slow pyrolysis, holding time and carrier gas flow rate were maintained at 1h and 2L/min respectively. For fast pyrolysis, the requirement of gas flow rate was stricter. As a carrier gas (argon) was used to feed the sample into reactor, the flow rate of argon must be high enough to blow up sample particle. However, the flow rate cannot be too higher, otherwise the back pressure in reactor would increase leading to the risk of leakage of reactor and change sample feeding rate. Therefore, a flow rate of 1.5L/min was chosen. Considering the quicker release of volatile matter during fast heating rate, holding time was chosen as 10 min.

The most significant factor on biochar product is temperature. Pyrolysis process has a vital effect on characteristics of biochar thus impacting on the subsequent AC structure. Normally, in industrial production of AC, pyrolysis temperature is usually 600℃~900℃.[75] Gasification temperature range is 600℃~900℃ [72] or 800℃ ~1000℃. [75] And we know from Figure 4-2, the second and third peaks of weight loss took place at 279℃ and 360℃ respectively. So in this chapter the main pyrolysis temperature range was chosen as 500℃~750℃. Pyrolysis under lower temperature 350℃ was also carried out to investigate the property and yield of biochar with only partial thermal decomposition.

For comparison purpose, the effects of these variables are shown in Figure 4-7.

Fast pyrolysis biochar was obtained for only a 10 min holding time and 1.5L/min carrier gas rate at various temperatures between 350 ℃ and 850 ℃. Figure 4-7 illustrates the biochar yields obtained under slow pyrolysis with three particle sizes

of samples and a single fast pyrolysis for 106~150μm mallee wood. The char yields plotted in Figure 4-7 are obtained on the basis of dry sample.

Figure 4-7 illustrates the effect of particle size on the biochar yield. It is obvious that biochar yield decreased with lower particle sizes. Particles with 1mm~2mm show higher char yield through the whole temperature range compared with sample with size 150μm~250μm and 106μm~150μm. It is because the heat transfer through larger particle size needs a longer pyrolysis time to reach the interior of the particle. As a result, a thermal decomposition delay took place. Thus at the same holding time 1h, they show higher biochar yield.

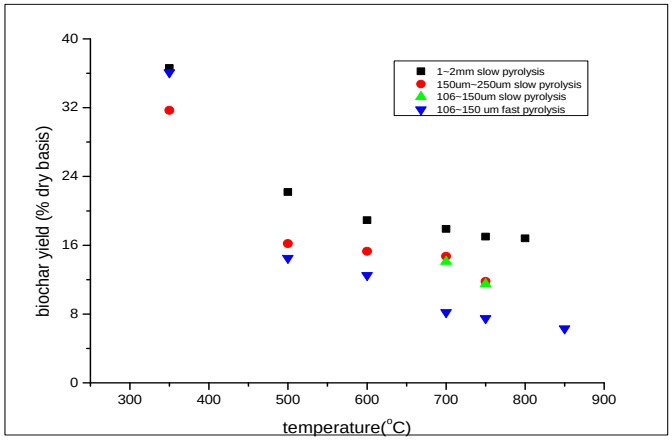

Figure 4-7: The relationship between char yield , particle size and temperaure.

It is shown in Figure 4-7, for sample size with 1~2mm the yield of biochar decreased significantly when the pyrolysis temperature was between 350 ℃ and 600℃ but it changed slightly between 700 ℃ and 800℃. This indicated at higer temperture, 1 h soaking time was enough for the thermal decomposition of hemi-cellulose and cellulose of larger particle size sample. As for sample size 150 μm ~250μm and size 106 μm ~150 μm, there was nearly no biochar yield difference between them when pyrolysis temperature was 700 ℃ and above. The reason was that the volatile matter had been mostly released after 1h holding time. As for sample size 150 μm ~250μm, the yield of biochar was nearly the same between 600 ℃ and 700 ℃ but

decreased when pyrolysis temperature was 750℃. The temperature for stable biochar yield of samll size sample of 600℃ is lower than that of large particle of 700℃. This is because there was less heat resistance for smaller size samples. The drop of biochar yield at 750 ℃may due to the further decomposition of large fraction of lignin. This phenomena consistent with TGA curve (see Figure 4-2) which shows volitle matter has released mostly at 500 ℃.

Biochar char yields are obviously affected by heating rate. Generally, biochar yield at fast heating rate was lower than that obtained at slow heating rate. At 750℃, the difference between the biochar yield of FB (11.8%) and SB (7.5%) was 4.3 % (see Figure 4-7). However, it is very interesting to notice that at low temperature of 350℃, the char yield of biochar obtained under fast heating rate (FB) are similar as that of biochr produced via slow pyrolysis (SB). The reason is that only partial decompositon of sample occurred at this low temperature. At pyrolysis temperature of 500 ℃, there was a more significant drop of FB yield. However at temperature of 700 ℃, the effect of temperature on biochar yield became less significant. It is because more cellulose and hemicellulose decomposed at 500℃ as shown in TGA curve (see Figure 4-2); the third weight loss peak took place at 390 ℃. Decomposition was completed at above 700 ℃ so that the biochar yield remained nearly constant above 700℃.

As shown in Figure 4-7, at current experimental conditions, FB yield and SB yield at 750℃ was around 7.5% and 11.8% respectively. These results indicated both type of biochar could be a feedstock for AC production.

To further understand the cause of the above observations, the properties of

corresponding biochar were analyzed in chapters 4.3.3 and 4.3.4.

4.3.3 Effect of Sample Size, Temperature, and Heating Rate on Biochar Chemical Composition

Both inherent catalytic species (AAEM) and chemical composition of biochar take important roles in increasing the biochar specific reactivity during the subsequent gasification thus affecting the structure of AC. So knowledge of AAEM content, the proximate and ultimate analysis of biochar and biomass are necessary to understand the effect of biochar on the subsequent process of gasification. Table 4-4 gives the properties of selected biochar.

Table 4-4 shows that fixed carbon content and ash content increased dramatically with the increase of temperature below 600℃ but increased slightly at higher temperature above 600℃. When pyrolysis temperature was above 500℃, ash content of SB did not change a lot. Unlike SB, ash content of FB increased obviously with increase of pyrolysis temperature. The tendency of volatile matter decreased with the increase of pyrolysis temperature. In the case of biochar obtained under slow pyrolysis of 150~250μm, the volatile matter contents of biochar decreased from 48.4% to 14.2%, fixed carbon correspondingly increased from 48.7% to 81.6% with the increase of pyrolysis temperature from 350℃ to 750℃. This is can be explained by the release of volatile matter. While for FB, the volatile matter contents of biochar decreased from 63% to 17.4%, fixed carbon correspondingly increased from 35.4% to 73.1% with the increase of pyrolysis temperature from 350℃ to 750℃. The value of ash content increased from 1.6% to 9.5% dramatically. At low pyrolysis temperature 350℃, ash content of FB is lower than that of SB. The reason is likely to be the partial pyrolysis due to the lower temperature（350℃）and shorter retention time (10min). As discussed above, cellulose and lignin was only partially pyrolyzed at low temperature. However SB experienced longer pyrolysis time and would have

more volotile relased than FB. Thus SB has higher ash content. It can also be seen from the VM content of FB and SB. It is obvious from Table 4-4 that FB at 350℃has much higher volatile content 63% compared to 48.4% for SB . At 750℃, due to higher ash of FB, the fixed carbon content of FB was lower than that of SB. The reason for the phenomena is likely to be the different pathway of release of volatile matter. During fast pyrolysis, volatile matter was released rapidly compared with the slow release during slow pyrolysis.

It can also explain the different moisture content between FB and SB. The moisture content of FB is lower than that of SB but distribute randomly without any distinct trend which was similar as Lua's observation. [75] This suggests the different capacity of adsorption of moisture between FB and SB indicating the different surfaces of FB and SB. That means structure of fast biochar could be more inert (shown in Figure 4-8). As for SB, the moisture is nearly same.

Biochar reactivity was determined by parameters such as the concentration of heteroatoms, active sites in the char, the accessibility of active site to the gas, and catalytic effect of inorganic impurities.[189] Hydrogen–rich region are easier to be oxidized after fast pyrolysis.[190] Higher content of H and O indicates more active sites thus improve the reactivity.[123] It is believed that alkali metals like sodium and potassium and alkaline earth in biomass act as catalysts in steam and carbon dioxide gasification. In addition, alkali metals also catalyze polymerization thus increasing the biochar char yield. [191] So data of ultimate analysis and AAEM content of biochar were also determined and shown in Table 4-4 in attempt of understanding the possible effect of biochar structure on gasification reactivity.

Similar to the tendency of fixed carbon, C content also increased with the increase of temperature quickly at low pyrolysis temperature and only slowly at higher pyrolysis temperature. Oxygen content and Hydrogen content decreased with temperature correspondingly may be due to the release of volatile matter. [192] The disappearance of

ether bond indicates the development of more ordered carbon structure. The H content of FB was relatively higher than that of SB as expected. Slow pyrolysis biochar showed higher C content compared with FB. The difference, however, becomes minor at higher temperatures.

Similarly, AAEM contents of SB also did not change a lot especially at higher pyrolysis temperature. In contrast to SB, AAEM content of FB showed significant changes. FB has higher content of K, Mg, and Ca and little lower content of Na than SB .

For particle size (<250μm), there was little effect on contents of biochar at pyrolysis temperature above 700 ℃.

Table 4-4: Properties of wood biochar

Pyrolysis type	PT[a] (℃)	Moisture (% ad)	Proximate(wt% db)			Ultimate analysis (wt% daf)					AAEM content (% db)			
			FC[b]	VM[c]	Ash	C	H	S	N	O*	Na[d]	K[d]	Mg[d]	Ca[d]
150~250 μm slow	750	6.1	81.6	14.2	4.2	82.38	1.76	0.14	0.3	15.42	0.1634	0.5149	0.2483	0.8863
	700	5.6	78.8	17.0	4.2	80.04	2.02	0.19	0.35	17.4	0.1633	0.3848	0.1997	1.0915
	600	5.2	74.7	21.3	4.0	81.04	2.64	0.25	0.34	15.73	0.1364	0.3809	0.2087	1.0422
	500	5.8	66.5	29.1	4.4	76.18	3.38	0.32	0.39	19.73	0.1243	0.3424	0.1920	1.2629
	350	5.5	48.7	48.4	2.9	65.9	4.51	0.48	0.35	28.76	0.0928	0.2527	0.1374	0.7195
106~150 μm fast	750	0.4	73.1	17.4	9.5	79.33	1.98	0.26	1.41	17.02	0.1176	0.9009	0.5522	2.4364
	600	0.5	73.4	19.0	7.6	75.79	2.8	0.40	1.18	19.83	0.1741	0.5959	0.4765	2.0955
	450	2.9	62.8	32.4	4.8	69.39	3.58	0.36	0.45	26.22	0.1773	0.4225	0.2818	1.1285
	350	1.1	35.4	63.0	1.6	57.05	5.15	0.53	0.28	36.99	0.0495	0.1563	0.1038	0.3860

[a]Pyrolysis temperature, [b]Fixed carbon（FC）, [c]Volatile matter (VM), [d] Analyzed by IC, O* by difference slow: 2L/min Holding time 1h fast : 1.5L/min holding time 10min.

4.3.4 Effect of Temperature and Heating Rate on Biochar Physical Structure

Figure 4-8 and Figure 4-9 present FIBSEM images of FB and SB prepared from pyrolysis of 106 μm ~ 150 μm samples at various temperatures respectively. As shown below, no major change of morphology of SB was obtained at variours pyrolysis temperature. The surface of SB kept botanical structure. The structure of FB, however, are of a loose structure and melting phenomena at higher pyrolysis temperature can be observed showing larger internal cavities .[186] Intermediate melt in the char structure is very obvious on the surface of FB. It seemed that molten melt blocked the pore give resulting in lower surface area of biochar. The reason may lie in the internal over-pressure caused by the quick release of volotile matters during fast pyrolysis. Only for pyrolysis temperature of below 400 ℃ seeing Figure 4-8 (A), FB kept the raw wood sample skeleton. With pyrolysis temperature increasing, pore of FB widened as shown from Figuress 4-8 (B) and 4-8 (C). The surface of FB (see Figures 4-8 (E1) and 4-8 (E2)) look molten and sintered. There were more asperities on the surface of FB. The tendency was more obvious as shown at higher pyrolyis temperature (see Figures 4-8 (F) and 4-8 (G)). The reason may due to the increase in temperature causing volatiles of biochar to evaporate more resulting in more ash left on the surface of biochar. Table 4-4 also shows FB has higher ash content. According to Figures 4-9 (A) to Figure 4-9 (E), SB obtained under various pyrolysis temperature seemed to maintain the original sample skeleton. This may be due to slow release of volatile during slow pyrolysis. The series of FIBSEM images in Figure 4-9 also show that the pore width of SB on the surface widened slowly with increase of pyrolysis temperature. However unlike FB, there were no obvious asperities on the surface of SB.

The pore structure of SB and FB at the range of pyrolysis temperatures between 350℃~600℃ did not developed well showing lower BET at lower than 50 m^2/g.

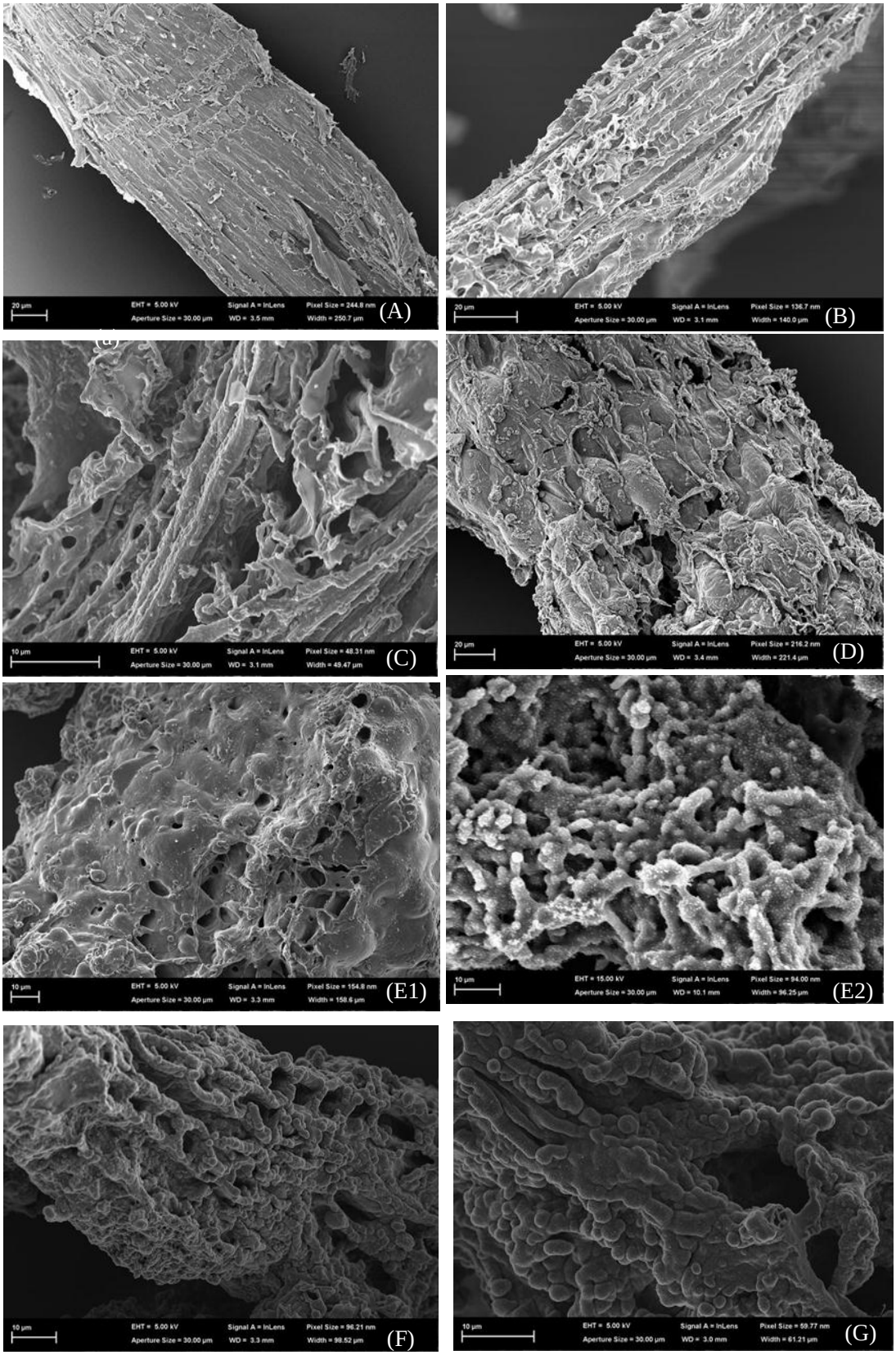

Figure 4-8: SEM images of FB at various pyrolysis temperatures: (A) 350℃ (B)450 ℃, (C) 500 ℃, (D) 600℃, (E1) (E2)750 ℃, (F) 800℃, (G) 850 ℃.

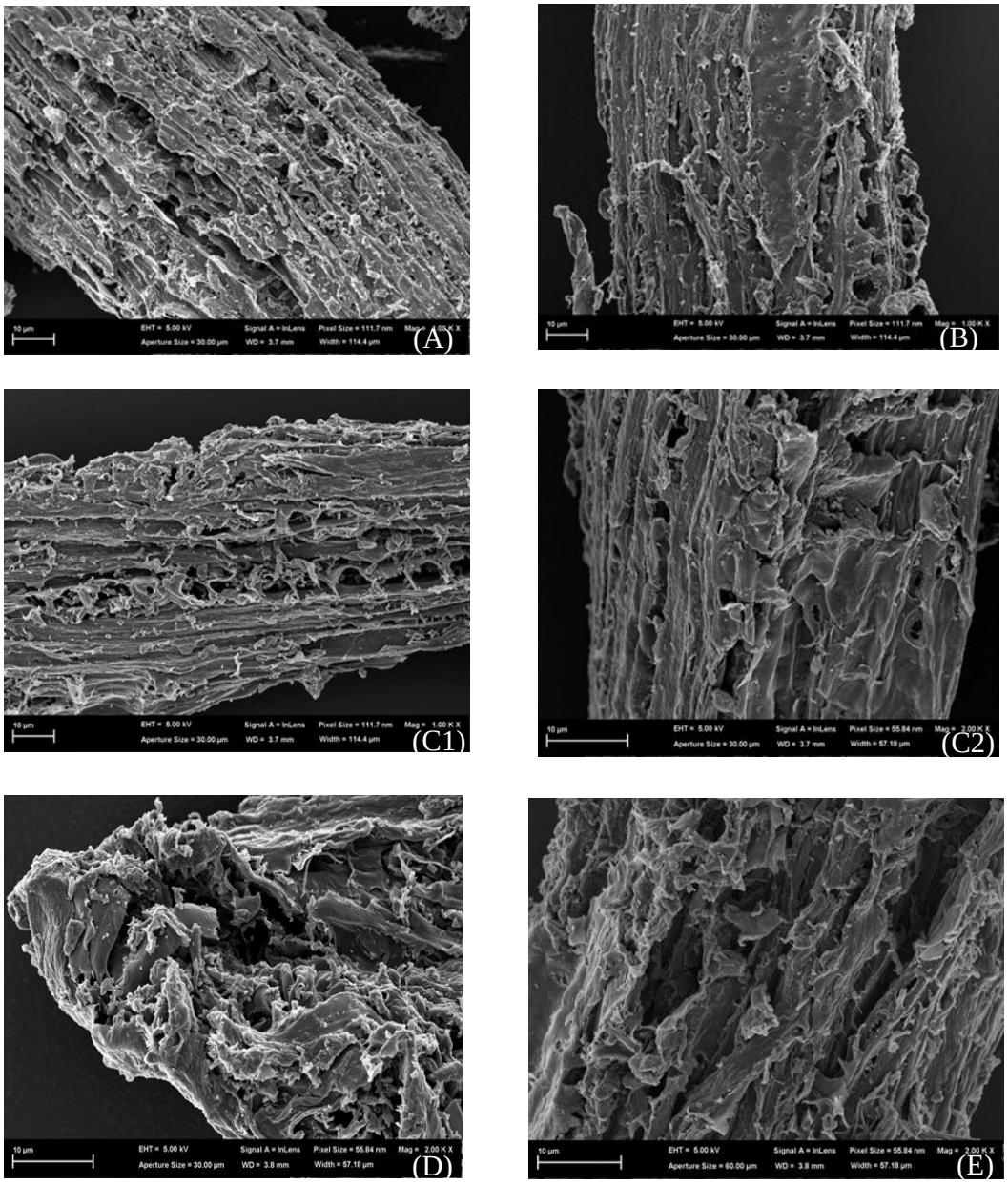

Figure 4- 9: SEM images of SB under various pyrolysis temperatures: (A) 600 ℃ (B)700 ℃, (C1)(C2) 750℃, (D) 800 ℃, (E) 850℃.

4.3.5 FTIR Spectra of FB and SB

Figure 4-10 shows the FT-IR spectra of FB and SB obtained at different temperatures.

In general, the shape of FT-IR spectra of FB and SB were similar. However, FB

showed stronger absorbance than SB at the same pyrolysis temperature. For both FB and SB, functional groups were obvious at low temperature and finally diminished at higher temperature. The higher level of absorbance of spectrum was the consequence of large amount of black carbon.[37]

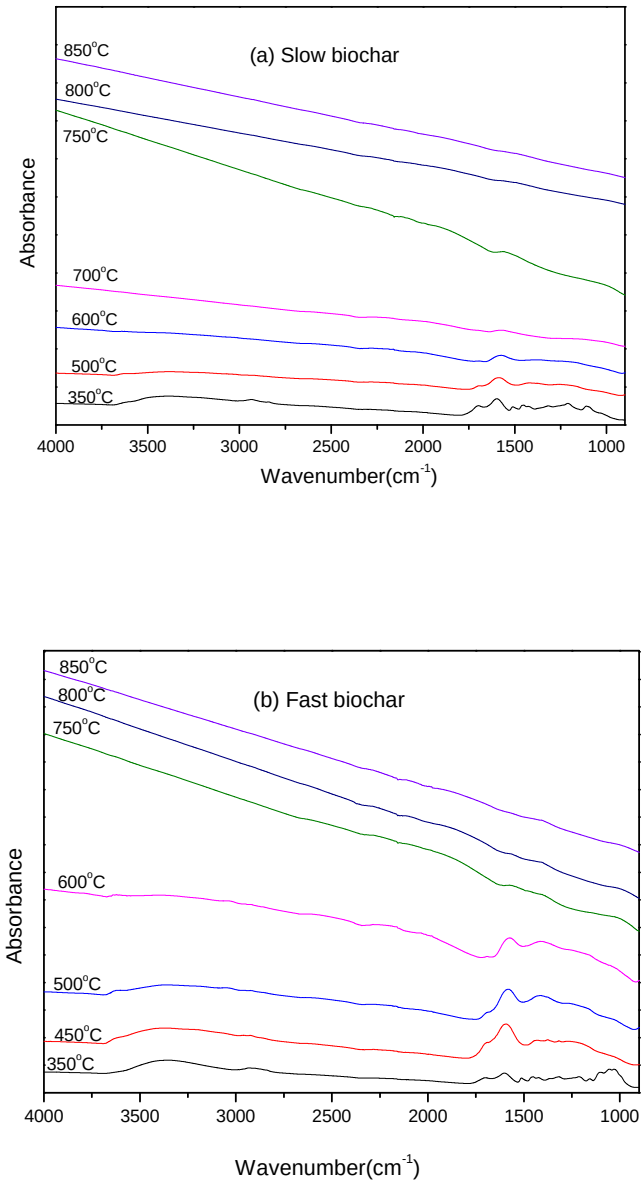

Figure 4-10: FT-IR spectra of biochar (a) SB and (b) FB

O-H stretching was apparent in the broad absorption range of 3600–3200 cm^{-1}. This suggested the possible presence of phenols and carboxylic acids. [193] The absorption range of 1800–1700 cm^{-1} may represent carbonyl structures such as carboxylic acids,

lactones, anhydrides, esters, and other acetyl derivative groups.[194-195] C=C stretching were found in the region of 1680–1620 cm^{-1}. The strong absorption at1600 cm^{-1} was likely to be the consequence of C═C bonds such as diene. With the increase of temperature, this peak was not observable as the consequence of developing aromatic rings structures.1360~1430 cm^{-1} corresponded to the infrared adsorption of O-H and C-H bending such as hydroxyl, acid, phenol, olefines and methyl.[179] For SB and FB at low temperature 350℃, the peak at around 1100cm^{-1} could be the stretching of C-O bonds such as saturated ethers and tertiary hydroxyl.[179]

4.4 Mechanism of Biochar Addition Effecting on Soil Performance

The properties of mallee wood biochar are highly dependent on the pyrolysis temperature and heating rate. Despite the limited development of pore structure of FB and SB, there were still observable changes of biochar surface. (see Figures 4-8 and 4-9). SB kept original skeletons on the surface during low pyrolysis of raw biomass while FB showed rougher surface with obvious macropores.

With increase of temperature, the degree of aromatization increased suggesting the stable structure of biochar. As shown in Table 4-4, both FB and SB obtained at lower temperature showed lower aromatization degree and had higher volatile matter content. These indicated lower temperature biochar was more active and could be easier to biodegrade thus being a more efficient fertilizer. Mallee biochar obtained at higher pyrolysis temperature contained higher AAEM content (see Table 4-4) whatever the sample size was. It was found that FB showed higher K, Mg, and Ca content but lower C and Na content than SB.

As shown in Figure 4-10, FB showed similar shape of FTIR spectra to SB but had higher intensity of spectra indicating more functional groups of FB. There were obvious oxygen-containing functional groups on the surface of both FB and SB especially obtained at lower temperature. These functional groups could exist as

anions at higher pH being another status of alkalis in biochar.

Due to its developed pore structure and chemical composition such as functional groups and AAEM, mallee wood biochar could be applied for soil amendment to hold nutrient, improve microenvironment, and increase the fertility of soil (see Chapter 2). The possible mechanisms of amending soil with biochar are as follows:

(1) Mechanism of improving the micro environment around plant root

It is accepted that CO_2 is captured through photosynthesis of plants. Through the pyrolysis process of biomass, these carbons were sequestered in the biochar. On the one hand, adding biochar to soil increases the carbon content of soil. On the other hand, it enlarged the space which was beneficial to the growth of roots, [196] especially the roots in xerosols. [151] Apart from that, a considerable vertical transport of biochar was observed to improve the deep soil.[197]

(2) Mechanism of keeping moistures and nutrients

Biochar applied in soil can change the porosity of soil so that it could change the percolation model, holding time, the pathway of soil moisture and keep the water in the soil.[198] Biochar can be both carbon source and carrier of polar or nonpolar compounds due to its porosity and functional groups. [199,200] Bio-char was applied to improve N input into agro ecosystems and the mechanism of restraining N leaching was due to its changing soil nitrogen fixation style and the activities of nitration microbes. [160] Biochar was able to strongly adsorb phosphate [41, 156, 201] although it is an anion.

(3) Mechanism of improving the living space of microbes

Biochar in soils with the addition of glucose promoted growth of microorganisms and the activity and degradation ability of microbes increased.[202] The porosity of biochar provided more living space for microbes. As a result, FB of mallee biochar may be better due to its macropores and rough surface area (see Figures 4-8 and 4-9).

(4) Mechanism of pollutant adsorbed

Due to the increased surface area, functional group, and AAEM content, biochar showed higher adsorption ability and cation exchange capacity (CEC). The CEC of soil increased with the addition of biochar to soil. So biochar has a strong adsorption ability of heavy metal ions. It was observed that the CEC of fast biochar from corn stover [203]showed about twice as much as that of slow biochar. The CEC value was correlated with the ratio of O/C. The higher O/C ratio indicated the presence of more hydroxyl, carboxylate, and carbonyl groups. [203] A study[204] showed that ion exchange was predominated with the increase of carbonization degree and amount of biochar. It was deduced as the consequence of light oxidation of surface of biochar and the electronegativity caused by the functional group of biochar. Higher pyrolysis temperature had good affinity for many organic pollutants due to its strong polarity of biochar obtained under higher temperature. [205] The emission of NO_2 and the eluviation of NH_4^+ of alfisol and vertisol in Australia were dropped dramatically with the addition of biochar. [206]

4.5 Conclusions

Leaf, bark, and wood have different chemical composition. Leaf, bark and mixture of three biomass components showed higher ash content than wood did. Thus their behaviors in thermal gravimetric studies were different. In contrast, acid-washed and water-washed treatment of wood did not change their thermal decomposition temperature. However acid washed wood showed highest content of volatile matter.

Wood is good for AC production as consequence of its higher carbon content and low ash content. Thus it was applied to investigate the mechanism of pyrolysis. The key factors such as particle size, pyrolysis temperature, and holding time which influence the physical and chemical structure of biochar were investigated. Temperature and heating rate played a significant role in the chemical and physical structure of biochar. Generally speaking, the biochar yield of 1~2mm particle size was higher than

150~250 μm and 106 μm ~150 μm particle. The char yield of SB at holding time 1h and 2h hours were similar at 500℃. With increase of pyrolysis temperature, FB and SB biochar yield decreased. However significant biochar yield difference took place when pyrolysis temperature was below 500℃. At higher pyrolysis temperature, the biochar yield of 150 μm ~250μm sample and 106~150 μm were nearly the same. Results showed pyrolysis temperature had more significant effects on FB in both physical and chemical structures of biochar products.

The processes of pore development of SB and FB through various pyrolysis temperatures were different. SB still kept the skeleton of raw material while FB appeared to experience ash sintering or melting. Consequently, FB showed more asperities than SB. FB showed higher oxygen and hydrogen content indicating higher reactivity in subsequent gasification. The cause of it was due to more AAEM dispersed on the surface of FB than that of SB. Generally FB had higher ash content compared with SB with one exception at lower temperature 350℃.The cause of the exception was shorter pyrolysis time (10min) and low pyrolysis temperature 350℃. FB had higher K, Mg, and Ca content and a little lower Na content than those of SB.

Under current experimental conditions, FB yield was 7.5% and SB yield was 11.8% at 750℃. So both types of biochar were applied to prepare AC in Chapter 5.

Due to the physical structures and chemical structures of mallee biochar, it could be added into soil thus realizing carbon sequestration, improving the fertility of soil through increase of SOM and CEC of soil, and even reducing the contamination of soil.

CHAPTER 5 STEAM GASIFICATION OF MALLEE WOOD BIOCHAR

5.1 Introduction

Activated carbon could be used as conditioners for soil [219] and applied to treat contaminated soils. [220] Compared with biochar, the development of pore structure leads to its higher surface area thus improving its performance in its applications.

However, steam gasification is a complex process. In the stage of steam gasification, concurrent pyrolysis takes place. During the process of pyrolysis, both cellulose and hemi-cellulose are almost decomposed mostly due to their low decomposition temperature. Lignin is different from the other two. It plays an important role in steam gasification as the consequence of its wider decomposition temperature range. At higher temperature (750℃ in this chapter), the breakage of ether bonds between large molecules and C-C, C-O, C-H bonds on the side chains or main chain results in unstable intermediate products leading to secondary reactions. Such complexity of pyrolysis and steam gasification leads to the difficulty of doing quantitative research on chemical structure. However, since the final product of pyrolysis/steam gasification is AC, properties of AC can reflect the evolution of steam gasification.

The development of micropore structure with a narrow size distribution can be obtained under low carbon conversion. With the process of steam gasification, submicropores/micropores decrease gradually, and mesopores increase slightly. It has been reported[98,167,207] that largest increase of porosity is produced in early stages due to the instantaneous reactions occurring once gasification agents was fed to the reactor. Understanding the process of steam gasification especially in the initial stage provides the knowledge about the evolution of pores, and also gives the possibility of increasing AC yield with shorter steam gasification time which usually means higher

char yield.

Therefore, to investigate the mechanism of steam gasification of mallee biochar, two main aspects of investigation were carried out in this Chapter.

(1) Variables including HTT (heat treatment temperature), particle size , flow rate of inert gas, holding time and biochar for the steam gasification of biochar; [21, 208]

(2) Possible pathway of steam gasification under low carbon conversion.

The mixture of three biomass components were obtained by mixing leaf, bark ,and wood at the ratio of 35:25:40 by weight. Table 5-1 gives the properties of biochar produced from leaf, bark, and mixture of leaf, bark , and wood .

Table 5-1: AAEM content and proximate analysis of biochar obtained from mallee leaf , bark, and mixture of three components

	Proximate analysis				AAEM content			
Sample	M[a], % ad	Ash, % db	VM[b], % db	FC[c], % db	Na [d]	K [d]	Mg [d]	Ca [d]
leaf	5.1	14.9	18.3	66.8	1.9459	1.8505	0.6906	2.9684
bark	3.1	12.9	19.7	67.5	0.7225	0.3191	0.2205	5.5853
wood	5.4	3.4	11.7	84.9	0.1515	0.4222	0.2235	0.8831
Mixturee	4.0	12.6	17.9	69.5	1.1885	0.8154	0.4064	3.4114

[a] moisture; [b] volatile matter; [c] fixed carbon;[d] wt% dry basis; [e]Mixture (leaf 35%,bark 25%, wood 40%)
all types of biochar was obtained at 750℃, holding time 15min, gas flow rate 3L/min.

It is obvious that leaf, bark, and mixture of these three components has much higher ash content and low fixed carbon compared with wood biochar. Higher ash content may led to the blockage of pore of AC, therefore wood was applied to AC production in the following experiments.

5.2 Effects of Parameters on Steam Gasification of Mallee Wood Biochar

5.2.1 Effect of Pyrolysis/Gasification Temperature on Mallee Wood Biochar Structure

- ***Determination of pyrolysis /gasification temperature and time***

Mallee wood with size 150 µm ~250 µm was used in this section to investigate the effect of temperature range between 550℃ and 750℃ on mallee biochar. Pyrolysis and gasification were carried out at the same temperature and in the same reactor to keep the reaction consistent. Mallee wood biochar was obtained at slow heating rate 10K/min with holding time 15 min at pre-set temperatures. The biochar was subsequently steam gasified at the same pre-set temperature for 5 min with 8.2 vol % steam to obtain AC.

Figure 5-1 shows N_2 adsorption-desorption isotherm at 77K of AC obtained at different pyrolysis/ gasification temperatures between 550℃ and 750 ℃ with 5 min steam gasification. It should be noted that the legend 550550 means AC was obtained via pyrolysis and gasification at the same 550 ℃. Table 5-2 shows textural characteristics of AC obtained their respective temperatures.

Both Figure 5-2 and Table 5-2 suggest the pronounced effect of temperature on AC structure. From Figure 5-2, it can be seen that the adsorption capability of AC increased with increase of temperature. At lower temperature of 650 ℃ and below, the value of Vd and total volume were lower, while the AHPW was higher indicating less micropores namely the porous structure of AC was undeveloped. Thus the surface area of AC was low at between 19 m^2/g and 46m^2/g showing low adsorption ability. It is primarily the consequence of small amount of released volatiles during pyrolysis and the gasification temperature was also low. According to thermal dynamics and chemical reaction of carbon and steam, gasification starts at above

400 ℃ and chemical reaction increases at 750 ℃ and above (see Figure 2-11). When temperature was increased to 750 ℃, the adsorption capacity of AC increased to above 100cc/g (see Figure 5-2) immediately at lower relative pressure which meant that there were microspores under these conditions. Besides, it is very clear that hysteresis loop appear at higher temperature indicating the existence of mesopore. As shown in Table 5-2, the value of SBET (surface area obtained by BET equation) of AC at 750 ℃ is already high as 526 m^2/g. Considering shorter gasification time and reasonable higher surface area 526 m^2/g obtained at temperature 750℃, parameters 5min gasification and 750℃ were applied for further experiments.

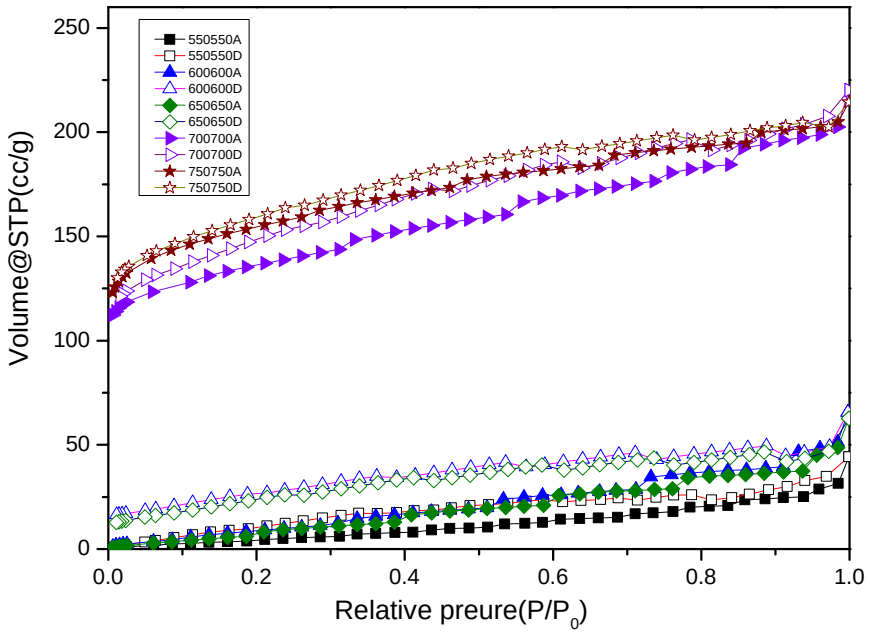

Figure 5-1: N_2 adsorption-desorption isotherm at 77K of AC obtained at different temperatures (the same shape of symbol means the same sample while open one means desorption curves and solid one means adsorption curves; A means adsorption, D means desorption)

Table 5-2: Textural Characteristics of AC obtained at different temperatures

Parameters(holding 15min AC5min)		SBET (m^2/g)	DR		Total volume (cc/g)
Pyrolysis (℃)	gasification ℃)		V_d(cc/g)	AHPW(A)	
550	550	19	0.01	22.81	0.07
600	600	35	0.01	23.64	0.10
650	650	46	0.01	19.66	0.10
700	700	481	0.231	14.68	0.33
750	750	526	0.24	7.533	0.42

SBET: surface area (m^2/g); Vd: micropore volume from DR plot (cc/g) ; AHPW: average half pore width from DR plot (A); Total volume obtained at p/p_0=0.9998(cc/g); DR: Dubinin-Radushkevich equation; BET: Stephen Brunauer, Paul Hugh Emmett, and Edward Teller equation.

- ***Effect of pyrolysis temperature on structure of activated carbon***

To understand the effect of pyrolysis temperature on subsequent activated carbon structure, biochars were obtained at different pyrolysis temperatures (550℃~900℃) with the same slow heating rate at 10K/min and holding time 15min. These biochar were then activated under the same steam gasification conditions namely steam containing 8.2 vol% at the same temperature of 750℃ for 5 min to produce AC.

The reactor with the biochar obtained was lifted out of the furnace cooling for 20 min with keeping argon going through, after that it was placed back into the tube furnace at 750℃. To prevent the further pyrolysis of biochar obtained at low temperature, the reactor was suited in the tube furnace holing for 2 min initially, then steam was introduced to the reactor system immediately. The holding time 2 min was determined by blank experiment (the same procedure but without samples) in advance that showed temperature will increase to 550℃ under this condition.

Figure 5-2 presents isothermal curves of AC via different temperatures pyrolysis and the same gasification process at the 750℃. All curves showed similar shape. They all

showed immediate increase at the lower relative pressure suggesting the existence of the micropore and all of them have hysteresis loops at high relative pressure region indicating the evolution of mesopore. Table 5-3 gives detailed information of AC structure which was calculated based adsorption-desorption isotherm in Figure 5-2. The calculations were described in Chapter 3.3.3. As shown in it Table 5-3, higher pyrolysis temperature led to higher surface area of subsequent AC. However, there was a distinct temperature 750℃ where BET surface area obtained under 750℃ was much lower than that obtained at higher temperature. The increase of pyrolysis temperature above 750℃ just led to a slight increase of surface area and total volume. The reason is that the short steam gasification time 5 min was not long enough to perform the pore development well and it was discussed in Chapter 5.2.4.

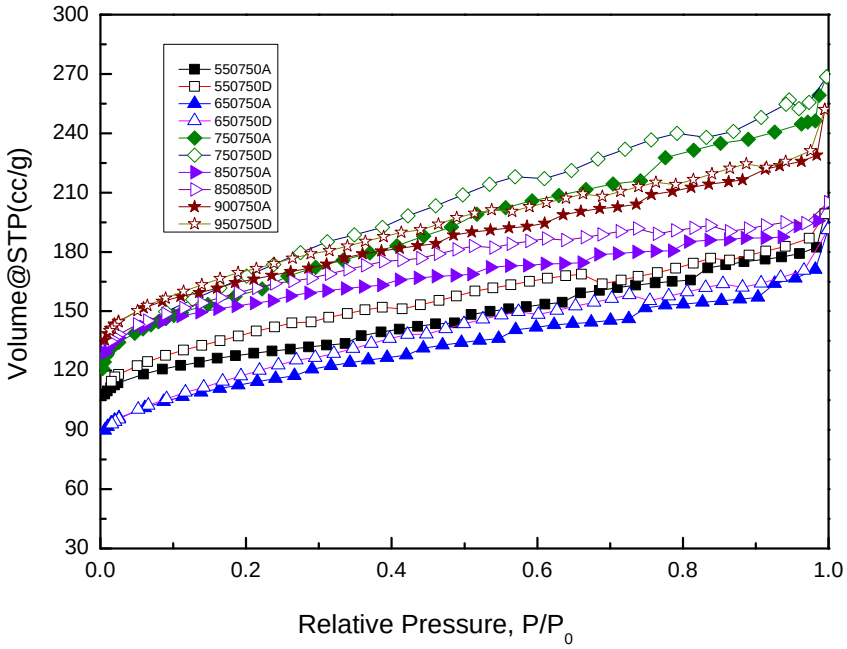

Figure 5-2: N_2 adsorption-desorption isotherm at 77K of AC from biochar obtained at different pyrolysis temperature (the same shape of symbol means the same sample while open one means desorption curves and solid one means adsorption curves; A means adsorption, D means desorption).

Examining Table 5-2 and Table 5-3 shows higher steam gasification temperature played a decisive role in the consequent AC structure. For AC obtained via steam gasification of biochar obtained at 550℃, the surface area increased from 19 m^2/g to 382m^2/g with the higher steam gasification temperature from 550 ℃ to 750℃. Similarly, the surface area of AC based on 650℃ biochar increased from 46 m^2/g to 366 m^2/g. However, increasing the pyrolysis temperature from 750℃ to 900 ℃ did not increase BET surface area of AC significantly.

Table 5-3: Characteristics of AC prepared from Different Biochar

Parameters (pyrolysis 15min +Gasification 5min)		SBET (m^2/g)	DR		Total volume (cc/g)
Pyrolysis (℃)	Gasification(℃)		AHPW(Å)	V_d(cc/g)	
550	750	382	6.48	0.19	0.31
650	750	366	7.53	0.17	0.30
750	750	526	7.54	0.24	0.42
850	750	540	6.51	0.23	0.32
900	750	561	6.90	0.25	0.39

SBET*:* surface area (m^2/g) based on Stephen Brunauer, Paul Hugh Emmett, and Edward Teller equation SBET; DR: Dubinin-Radushkevich equation*;* Total volume obtained at p/p_0=0.9998(cc/g); Vd: micropore volume from DR plot (cc/g) ; AHPW: average half pore width from DR plot (Å).

But what needs to be mentioned is that all biochar experienced the cooling and reheating process before steam gasification. Although the heating time was as short as 2 min and the temperature inside the reactor was only increased to 550℃ which was lower than the pyrolysis temperature used for production of biochar. Such pyrolysis history of biochar also contributed to the pore development of the subsequent activated carbon.

The original structure of biochar played an important role in the development of the pore size distribution. Accordingly, there is a significant difference between 650℃ and 750℃. To further understand the effect of pyrolysis/gasification temperature on

the structure of mallee biochar, Table 5-4 illustrates the AAEM content and proximate analysis of AC.

Table 5-4 clearly shows the effect of gasification process on the AC properties. For low temperature biochar at 550℃, despite the shorter gasification time of 5 min, the fixed carbon increased from 75.7% to 82.8% and volatile matter decreased from 20.3% to 12.8%. This could be due to appreciable amount of volatiles was released during the repyrolysis/gasification. Correspondingly, the surface area of biochar increased nearly 21 times from19 m^2/g to 383m^2/g (see Tables 5-2 and 5-3). Similarly, the same tendency happened to biochar obtained at 650℃. However, for biochar obtained at higher temperatures, the surface area only increased slightly. This is due to the nearly complete release of volatile matter at higher temperature. At higher temperature, a longer time was needed to reach high heat treatment (HHT), thus, biochar obtained at higher temperature experienced a longer heating history. [186] Based on the above results, the current procedure with cooling char firstly and then heating again can be applied to obtain AC with reasonable surface area.

Table 5-4: Proximate analysis AAEM content of AC (holding time 15min, gasification 5min)

T^d (℃)	Na	K	Mg	Ca	M[a], % ad	Ash, % db	VM[b], % db	FC[c], % db
550+750	0.1815	0.2935	0.2501	1.0158	1.8	4.4	12.8	82.8
650+750	0.1593	0.4615	0.2429	0.9346	1.8	4.4	11.7	83.9
850+750	0.1663	0.4936	0.2572	0.9895	2.2	5.3	7.6	87.2
900+750	0.1988	0.5213	0.2666	1.0599	1.9	5.2	8.3	86.5

[a] moisture; [b] volatile matter; [c] fixed carbon; T^d pyrolysis temperature + gasification temperature; holding time 15min+gasification 5min at 750℃.

5.2.2 Effect of Pyrolysis Heating Rate on Biochar Steam Gasification

To gain the idea of the possibility of fast biochar (see Chapter 4.3.4) being feed stock of AC, two kinds of AC were obtained from steam gasification of fast biochar (FB) at 750℃ with steam concentration 10 vol% and slow biochar (SB) at 750℃ with

steam concentration 8.2 vol % for 40 min. Figure 5-3 shows N_2 adsorption isotherm at 77K of AC produced from SB (slow AC) and FB (fast AC) via steam gasification. The volume of slow AC and fast AC increased immediately at lower relative pressure. It suggested that both slow AC and fast AC had micropores, while N_2 adsorption isotherm of slow AC increased dramatically up to around 200cc/g showing the existence of more micropores. The increases of the adsorption isotherm of both slow AC and fast AC at relative pressure around 1.0 illustrated the presence of macro pores. The BET surface area of fast AC and slow AC were 943 m^2/g and 991 m^2/g respectively.

To further understand the influence of pyrolysis/gasification on mallee biochar, SEM images of slow AC and fast AC were presented in Figure 5-4. It clearly showed pore development on the surface of AC. Honeycomb-like cavities were evident in slow AC and fast AC. This suggested that both SB and FB could be suitable the feedstock for AC production in terms of surface area (943 m^2/g and 991 m^2/g).

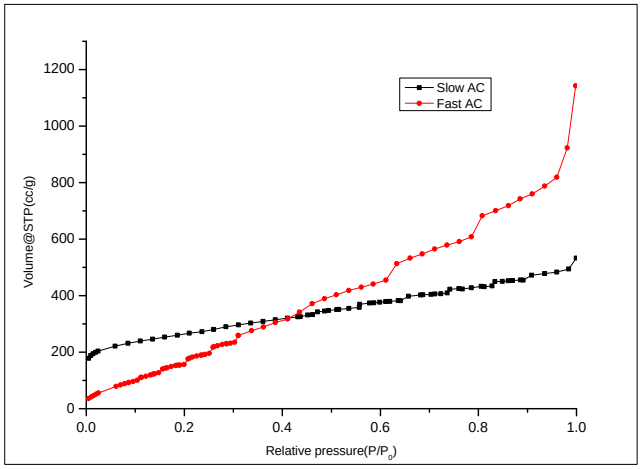

Figure 5-3: N_2 adsorption isotherm at 77K of AC produced from SB (Slow AC) and FB (Fast AC) via steam gasification

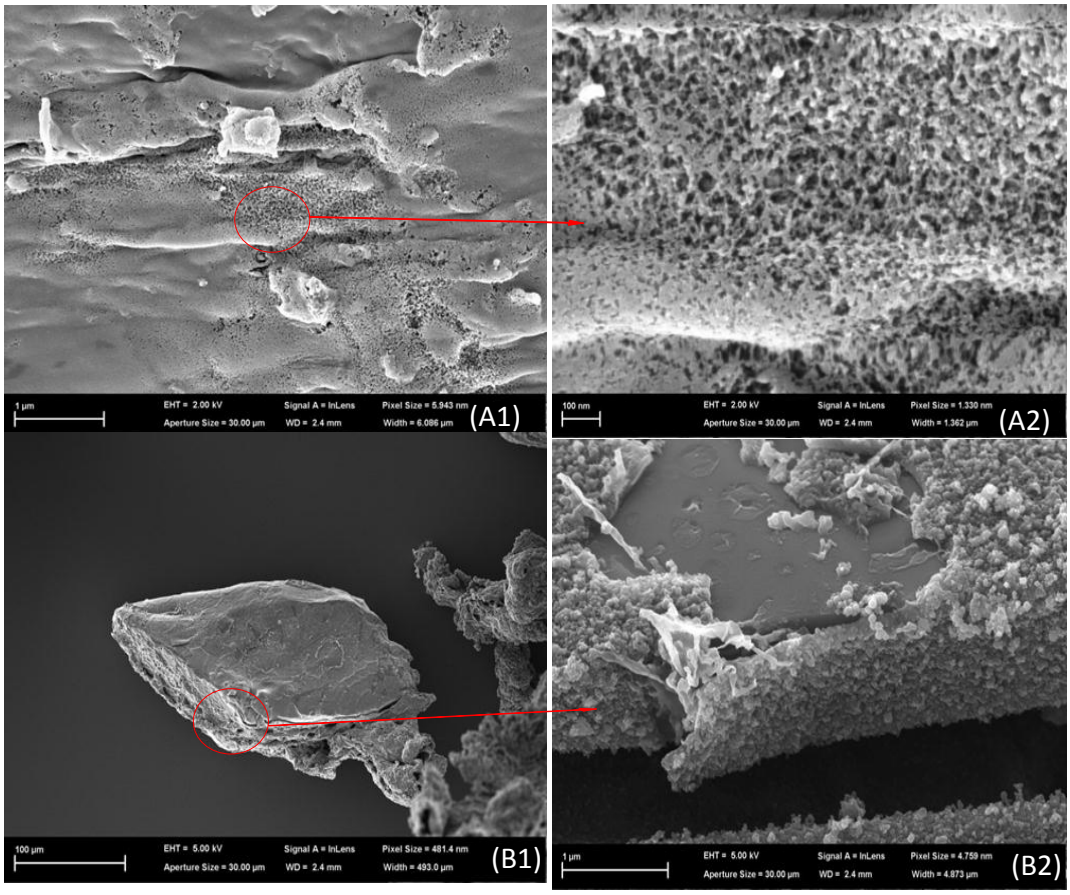

Figure 5-4: SEM images of AC produce d from SB and FB(A1)(A2) Slow AC with steam concentration 8.2 vol % at 750℃; (A2) is magnification of area of (A1); (B1)(B2) Fast AC with steam concentration10 vol % at 750℃; (B2) is magnification of area of (B1).

5.2.3 Effect of Sample Particle Size on Biochar Steam Gasification

Under the same conditions, larger particle size may cause temperature gradients inside the particle leading to higher AC yield. Thus samples with different particle size were applied to obtain AC in this chapter. The pyrolysis and gasification temperature were kept the same as 750℃. Pyrolysis holding time was 15min, and gasification time was 5 min. Table 5-5 presents the texture and chemical properties of AC obtained from different size raw sample.

Considering the possible under-development of pore size of AC due to the shorter gasification time and larger particle size of sample, both CO_2 adsorptions at 273K

using Gemina and N_2 adsorption at 77k using Autosorb-1 were carried out. As expected, N_2 adsorption at 77K was not suitable here. The isotherm of N_2 adsorption isotherm increased at lower relative pressure but decreased afterwards. Such phenomena indicated the pore structure of AC obtained did not develop well. So only surface area obtained under CO_2 adsorption was presented in Table 5-5. It shows larger particle size has lower surface area. Table 5-5 gives the properties including AAEM content, proximate analysis, and surface area of AC obtained using different particle sizes.

Table 5-5: Characteristics of AC obtained from different particle size

Size	Na	K	Mg	Ca	M[a], % ad	Ash, % db	VM[b], % db	FC[c], % db	yield	SBET
1	0.2274	0.5239	0.2862	1.689	1.2	6.7	17.1	76.2	9	255
2	0.1523	0.4156	0.2144	0.9646	2.1	4.0	11.5	84.5	16	178
3	0.1137	0.3866	0.1569	0.6341	1.9	2.9	11.7	85.4	19	75
4	0.1817	0.2968	0.2148	0.4385	1.4	2.5	11.3	86.2	20.7	57

[a] moisture; [b] volatile matter; [c] fixed carbon; SBET apparent surface area (m^2/g); Particle size 1 <106μm; 2 250μm~1mm; 3 1mm~2mm ; 4 500mm*500mm (pyrolysis holding time 15min , gasification time 5min ,pyrolysis(750℃) +gasification(750℃).

It can be seen from Table 5-5, particles with size <106μm showed the highest ash content and lowest fix carbon content. AC obtained from size range between 150μm and 1mm showed similar proximate analysis data. The proximate analysis of sample with size 1mm~2mm was similar to that of sample with 500mm*500mm. These results indicated that gasification time 5 min was possibly not long enough for pore development for larger particle size. Thus only small amount of rudimentary pores evolved. This can also be confirmed by higher AC yield at around 20%. These AC consisted of narrow pores which were blocked by deposition of tars and volatile matter. [209] For low burn-off, CO_2 adsorption can exhibit kinetic limitations on samples with narrow micropores. [210]

Therefore, under current experimental conditions, only the micropores were developed for these larger particle sizes. It indicated large particles might need longer gasification time to produce good AC.

5.2.4 Effect of Holding Time on Biochar Steam Gasification

- ***Pore structure***

To understand the effect of holding time on the structure development of biochar during steam gasification, biochar, which was obtained via pyrolysis of 150 μm ~250μm mallee wood at 750℃ for 15 min holding time, was steam gasified at 750 ℃ for various gasification time.

To gain a clear image of the relationship between the pore development of AC and the consumption of carbon atom of biochar during steam gasification, carbon conversion was also applied in this chapter. As discussed in Chapter 2, isothermal curves can demonstrate the structure of adsorbent so that Figure 5-5 gave the adsorption-desorption isotherms of AC under different carbon conversions in the range of 5 to 50%. Figure 5-6 shows the relationship between carbon conversion and surface area. The value of surface area and pore size distribution of AC are illustrated in Table 5-6.

The isotherms in Figure 5-5 show that at low carbon conversion the adsorption isotherms of AC are similar at low relative pressure with more open knee but diverge at higher carbon conversions.[211] The behaviors at low relative pressures suggest a wider micropore size distribution. The hysteresis loops between adsorption curve and desorption is due to the contribution of mesopore.

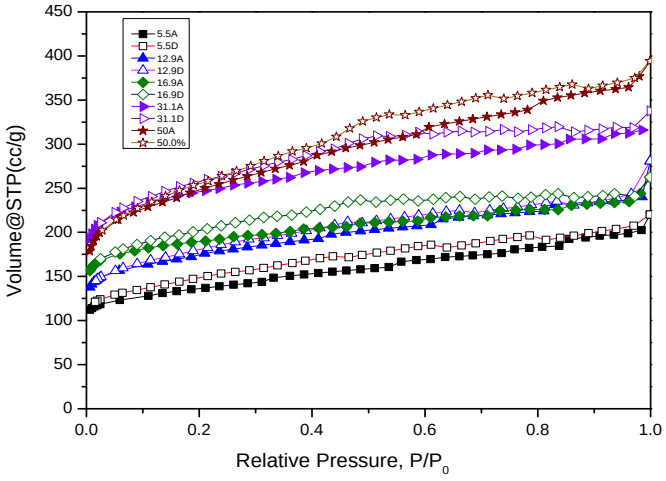

Figure 5-5: N_2 adsorption-desorption isotherm at 77K of AC obtained at different carbon conversion (x %) ; A means adsorption, D means desorption; the same shape of symbol means the same sample while open one means desorption curves and solid one means adsorption curves); (pyrolysis temperature 750℃ holding time 15min + gasification temperature 750℃,150 μm ~250μm).

As can be observed in Table 5-6 and Figure 5-6, the BET surface area increased with higher carbon conversion. With 50% carbon conversion, the BET surface area of AC increased to 819 m^2/g. BET surface area of only 600 m^2/g was obtained with the when carbon conversion was 16.9 %. Longer gasification time meant more carbon steam reaction, leaving more pores and greater surface area. However, average half pore width (AHPW) slightly decreased up to 16.9% carbon conversion then increased after that, indicating that some of the micropores were changed into mesopores and macropores.

From Figure 5-6, the conclusion that could be drawn was that higher carbon conversion (higher gasification time) played a positive role in increasing surface area of AC produced.

Table 5-6: Characteristics of AC obtained at the different level of carbon conversion

Carbon Conversion (%) (gasification time)	SBET (m^2/g)	DR		Total volume (cc/g)
		AHPW(Å)	Vd (cc/g)	
5.5 (5)	526	7.54	0.24	0.42
12.9 (10)	572	7.47	0.26	0.43
16.9 (15)	600	6.87	0.29	0.41
31.1 (30)	785	7.37	0.37	0.52
50.0 (50)	819	10.83	0.41	0.61

SBET: surface area (m^2/g) based on Stephen Brunauer, Paul Hugh Emmett, and Edward Teller equation SBET; DR: Dubinin-Radushkevich equation; Total volume obtained at p/p_0=0.9998(cc/g); Vd: micropore volume from DR plot (cc/g) ; AHPW: average half pore width from DR plot (Å).

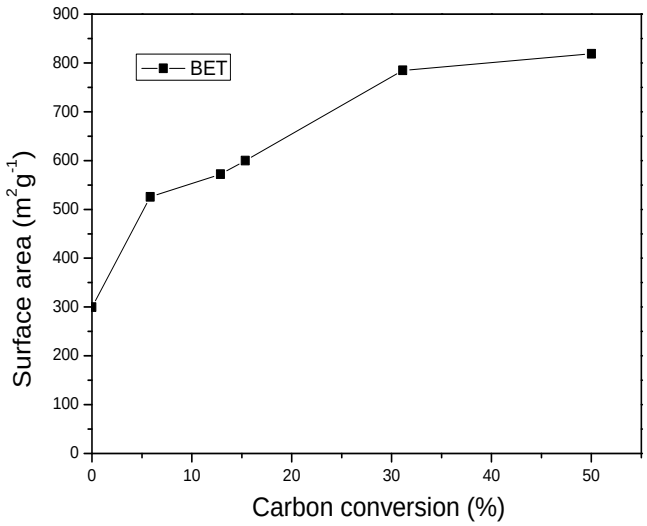

Figure 5-6: Surface area as the function of carbon conversion during the course of steam gasification (pyrolysis temperature 750℃ holding time 15min + gasification temperature 750℃ size150 μm ~250μm)

Figure 5-7 shows the pore size distribution of AC obtained by quenched solid density functional theory (QSDFT) for AC at different carbon conversions. It can be seen in Figure 5-7, half pore size >10 Å attributed to the pore volume suggesting the presence of mesopore. With gasification going on, the percentage of mesopore and macropore increased. At carbon conversion of 50%, mesopore and macropore are obvious. The pore size distribution expanded to mesopore with the increase of carbon

conversion. Noteworthy is the pore size distribution of AC obtained at carbon conversion 5.5% with BET surface area at 526m^2/g and pore volume of 0.42cc/g (see Table 5-6). According to IUPAC, pore width <2 nm is micropore and pore width between 2nm and 50nm is mesopore. As shown in Figure 5-7, even at such low carbon conversion 5.5%, there were two main peaks: one was at around 2 Å suggesting the contribution of micropore; the other was between around 6 Å and around 30 Å indicating the mesopore. Therefore, it seems the pore developed well. Therefore, a short gasification time as 5 min was enough to obtain AC with reasonable surface area 526m^2/g.

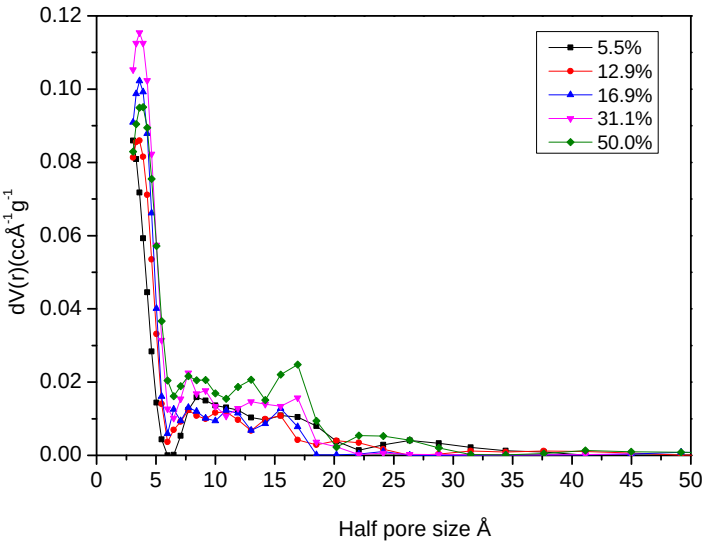

Figure 5-7: Pore size distribution by QSDFT for AC under different carbon conversion (x %) (pyrolysis temperature 750℃ holding time 15min + gasification temperature 750℃, 150~250μm)

To further understand the pore evolution of mallee biochar, Figure 5-8 presents selected images demonstrating the development of pore of activated carbon. It shows the edge of activated carbon obtained under different carbon conversions, while Figure 5-9 shows the morphology of AC under different carbon conversions and the energy dispersive spectrometry (EDS) results.

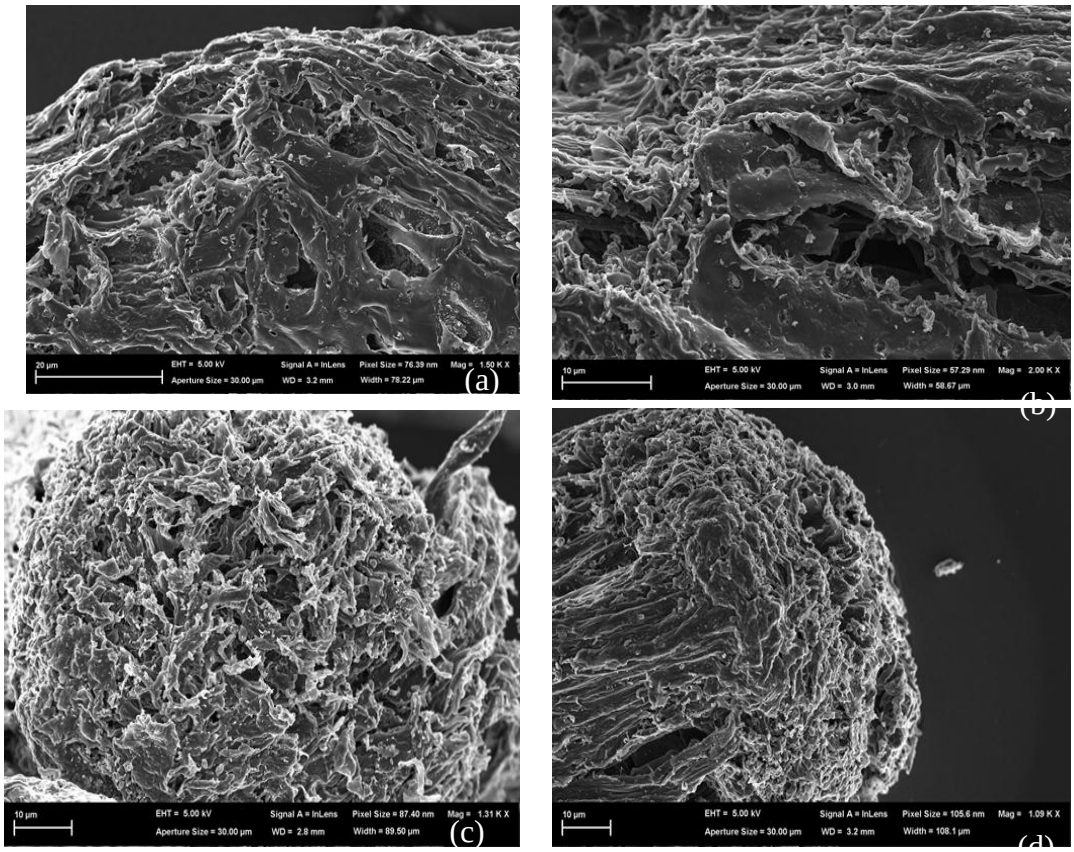

Figure 5-8: AC structure changing with carbon conversion (x %): (a) biochar (b)5.5% (c)16.9% (d)31.1%

From Figure 5-8, it can also be seen that surface of AC is more porous at higher carbon conversion 31.1%. It is very clear that the surface of biochar obtained via pyrolysis at 750℃ shows obvious pore and it can be verified by the BET surface area with the value of at the 270m^2/g. The surface structure of AC is porous, however, also orderliness. That indicated the ends of wood biochar were "attacked" by gasification agent steam. Even under low carbon conversion as low as 5.5%, the disorder of end of biochar increased leading to higher surface area at 526m^2/g. To further understand the evolution of pore on the surface, Figure 5-9 illustrates the morphology of AC with higher magnification of AC obtained under different carbon conversion. It proved surface of AC was more porous with higher carbon conversion. EDS results showed that bright points were AAEM dispersing on the surface of AC (5 min). The above discussions clearly show through the control of the carbon

conversion of mallee wood biochar during steam gasification, AC with different pore size distribution can be tuned correspondingly.

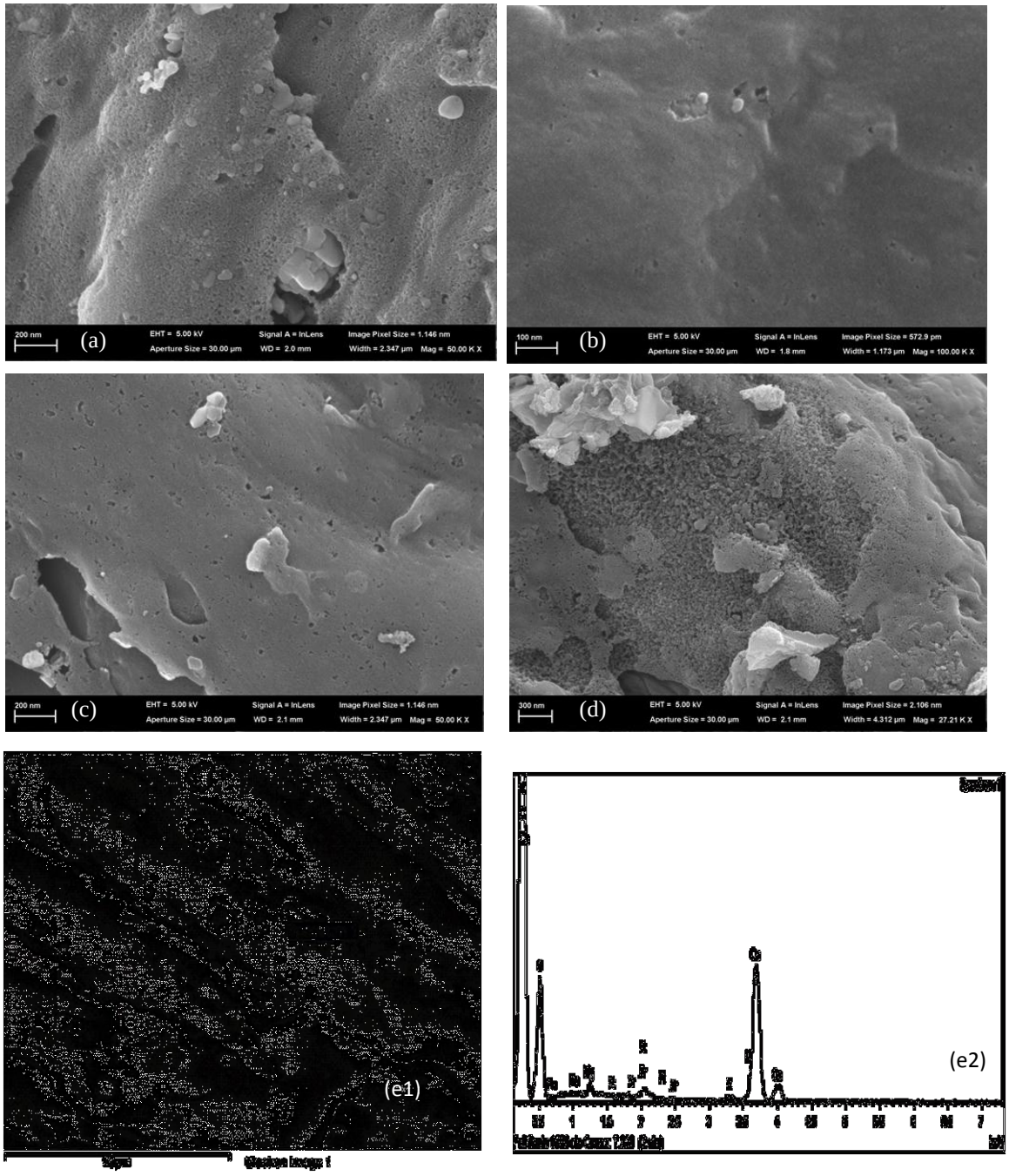

Figure 5-9: Morphology of AC under different carbon conversion (x %): (a) biochar (b)5.5%(c)16.9%(d)50% (e1)bright points on the surface of BESEM image of AC 5.5% (e2) EDS results of bright point.

- ***Chemical structure***

Considering short gasification time 5min (5.5% carbon conversion) and 15min (16.9% carbon conversion) resulting in reasonable surface area of 526m^2/g and 600m^2/g respectively, Table 5-7 presents these chemical characteristics of AC. As shown in Table 5-7, both the ash content and AAEM contents increased a little bit with the increase of carbon conversion while volatile matter and fixed carbon were nearly the same.

Table 5-7 : Chemical Characteristics of AC under different carbon conversion

Carbon conversion	Moisture (%[a]ad)	Proximate(wt% db)			Ultimate analysis (wt% db)		AAEM content(% db)				AC yield
		FC[b]	VM[c]	Ash	C	H	Na[d]	K[d]	Mg[d]	Ca[d]	
5.5	1.7	84.9	11	4.1	84.47	0.93	0.1669	0.4962	0.2472	0.8989	12.1
16.9	2.0	84.8	10.6	4.6	84.84	1.47	0.1735	0.5009	0.2642	0.9497	11.3

[a]Air dried, [b]Fixed carbon（FC）, [c]Volatile matter (VM), [d] Analysed by IC; (slow heating at 10 K/min, holding 15min pyrolysis at 750℃).

- ***FTIR spectrum***

FTIR spectroscopy was initially applied in order to identify the functional groups at the surface of biochar and AC. For AC under different carbon conversion from 5.5%~50% via steam gasification of biochar obtained from 750℃ pyrolysis, there were no obvious observable peaks in FTIR spectrum. This indicated that the chemical structure of the surface of activated carbon was similar and there was only small amount of functional groups on the surface of AC.

5.2.5 Effect of Acid Treatment of Wood on Biochar Structure in Steam Gasification

AAEM may catalyze reactions and thus shorten gasification time. Treatment with acid washing or water washing of biomass can remove inorganic matter partially or

completely thus affecting gasification reaction rates and corresponding evolved gas during gasification. To get the basic idea of the effect of AAEM on the structure of mallee biochar, acid washed wood particles were also applied to prepare AC. Figure 5-10 presents nitrogen isotherms of activated carbon obtained under different gasification time and temperature via steam gasification of acid washed biomass. It clearly demonstrates that extend gasification time and higher gasification temperature favor the development of pore. At lower relative pressure, the volume of AC obtained with 240 min gasification at 750℃ and at 850℃ with 50 min gasification increased quickly indicating the presence of amount of micropore. The hysteresis increases with the extension of gasification time due to the presence of mesopore. It also confirmed the data in Table 5-8 where long enough gasification time led to higher value of SBET and Vd. The increase of AHPW indicated the development of mesopore. Figure 5-11 is pore size distribution (PSD) of AC obtained through QSDFT model[212] provided by Quanta chrome software.

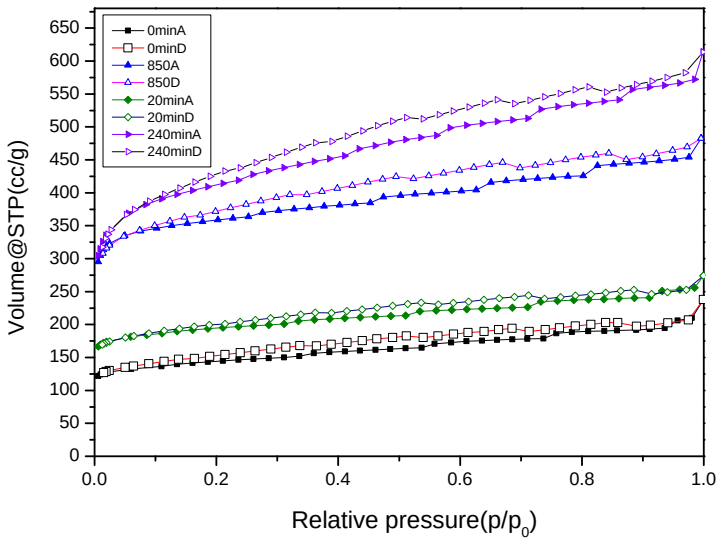

Figure 5-10: Nitrogen adsorption and desorption isotherms at 77K of AC form acid washed biomass at different time and temperature (A means adsorption, D means desorption; the same shape of symbol means the same sample while open one means desorption curves and solid one means adsorption curves); ×minA(D) means adsorption(desorption) curve of AC obtained with ×min gasification at 750℃; 850A (D) means adsorption(desorption) curve of AC obtained at 850℃with 55min gasification.

It can be seen in Figure 5-11 that biochar and AC obtained with 20min gasification time showed similar pore size distribution with majority of micropore and minority of mesopore. With the increase of gasification time to 240 min, mesopore developed well with half pore size mainly below 25 Å. It showed that higher temperature 850℃ led to more developed porosity of AC.

As shown in Table 5-8, compared with acid washed wood biochar of 470 m^2/g, acid washed biochar showed much lower surface area of 32 m^2/g. It increased to 577 m^2/g when gasification time increased to 20min. But with gasification time of 75 min, the BET surface area decreased only to 515 m^2/g. This behavior suggested the disappearance of micropores which led to the decrease of surface area.

Table 5-8: Textural characteristics of AC prepared from acid washed biomass and acid washed biochar

Parameters(holding time 15min)				DR		
sample	Pyrolysis +gasification(℃)	Gasification time(min)	SBET (m^2/g)	AHPW(A)	V_d(cc/g)	Total volume (cc/g)
Acid washing Mallee wood	750	0	470	5.63	0.21	0.37
	750	20	589	5.97	0.29	0.42
	750	240	1313	8.83	0.64	0.95
	850	55	1101	6.94	0.56	0.75
Acid washing biochar	Acid-washed biochar	0	32	20.40	0.01	0.07
	750	20	577	7.66	0.27	0.44
	750	75	515	7.65	0.25	0.41

SBET apparent surface area (m^2/g); Vd pore volume from DR plot (cc/g)

Average half pore width from DR plot (A); Total volume obtained at p/p_0=0.9998(cc/g).

Figure 5-12 presents the pore size distribution of activated carbon from acid washed biochar. It shows that AC obtained via 75min gasification time consisted of a majority of mesopores. Although activated carbon obtained from acid washed wood AC and acid washed biochar with 20 min displayed similar BET surface area of around 590 m^2/g, they had different pore size distribution. Acid washed biochar showed much wider mesopore size distribution.

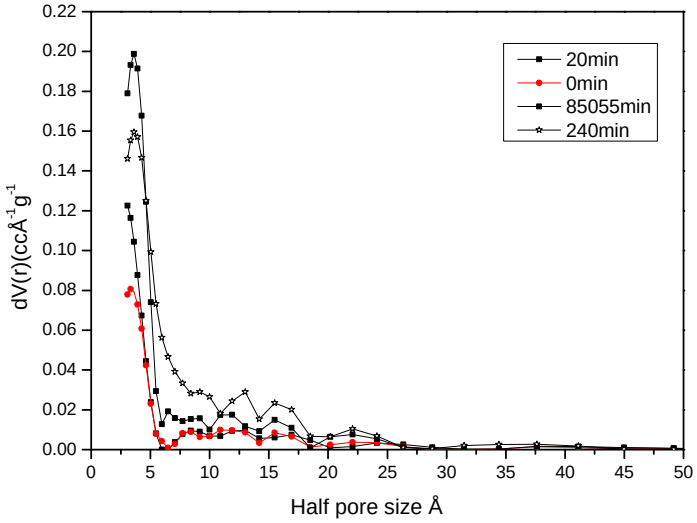

Figure 5-11: Pore size distribution by QSDFT for AC from acid washed wood biomass (×min means AC obtained with ×min gasification time at 750℃, 85055min means AC obtained at 850℃ with 55min gasification time)

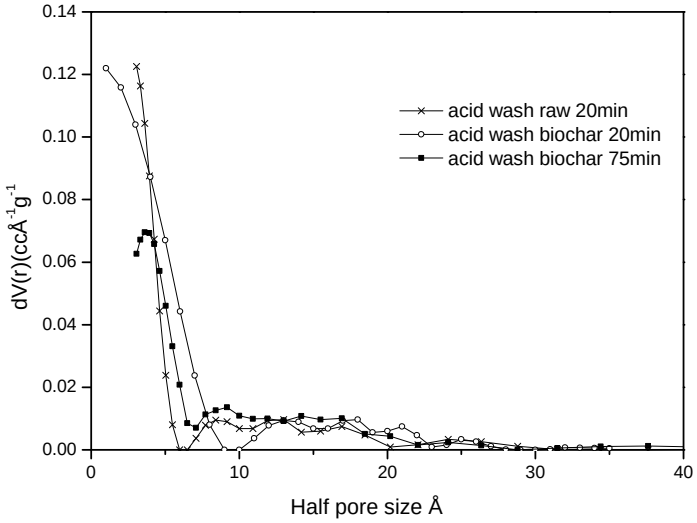

Figure 5-12: Pore size distribution by QSDFT for AC from acid washed wood biochar (x min means gasification time)

5.3 Steam Gasification of Mallee Biochar at Low Carbon Conversion

In this chapter, pyrolysis/gasification of mallee biochar was carried out at short low-temperature pyrolysis time and minimal conversion of the char for AC preparation during steam gasification. Under current experiments, pyrolysis temperature and steam gasification temperature were the same at 750℃ to simulate a continuous process.[213] This temperature 750℃ was chosen for four reasons: (1) AC with reasonable surface area was obtained at 750℃ with 5 min gasification (see Table 5-9); (2) according to TGA, most volatile matter were removed above 700℃; (3) this temperature is high enough for both gasification by steam or by carbon dioxide which will be presented in Chapter 7; (4) to guarantee reaction was under chemical reaction control.

Biochar was prepared at 750℃ with 15min holding time and 10 K/min heating rate. Due to the higher surface area obtained from fast biochar and for the purpose of comparison, the specific reactivity of fast biochar was also investigated. Table 5-9 gives the properties of mallee wood used in this chapter.

Table 5-9: Properties of mallee wood used in the present study

Proximate analysis, wt% db			Ultimate analysis, wt% daf				
M[a], % ad	Ash, db	VM[b], % db	FC[c], % db	C	H	N	S	O*
5.3	0.4	80.7	18.9	49.0	6.7	0.19	0.02	44.1

Inorganic species (wt% db)									
Element	Na	K	Mg	Ca	Cl	P	N	Al	Si
(wt%)	0.0212	0.0744	0.0364	0.1236	0.0323	0.0182	0.191	0.0025	0.0026

[a] moisture; [b] volatile matter; [c] fixed carbon; TP[d] pyrolysis temperature ,*by difference.

5.3.1 Chemical Reaction Control during Steam Gasification at Low Carbon Conversion

- ***Steam gasification of leaf, bark, and wood biochar at 850℃***

Moderate gasification temperature should be chosen to make sure steam gasification is under chemical reaction control. Steam gasification temperature 850℃ is a common temperature for activated carbon production. Therefore, steam gasification of three mallee biomass, namely leaf, bark, and wood were firstly carried out at 850℃. Figure 5-13 shows curves of carbon conversion of leaf, bark, and wood biochar as function of time.

It can be seen that leaf biochar showed highest reaction rate followed by bark biochar. Carbon conversion of leaf biochar reached nearly 100% at around 12 min, while bark biochar reached around 80% with similar gasification time. In contrast, wood biochar showed the lowest reaction rate. This is consistent with the order of AAEM content of three biomass components namely leaf > bark > wood. Figure 5-14 gives specific reactivity of leaf, bark, and wood biochar as a function of carbon conversion. As expected, the specific reactivity of leaf and bark increased dramatically with the increase of carbon conversion followed by a decrease. The decrease of specific reactivity of leaf and bark char was the consequence of depletion of carbon at higher carbon conversion where less carbon was available. While for wood biochar, the specific reactivity increased slightly in the course of gasification. Both Figures 5-13 and 5-14 gave the evidence that the rate of steam gasification of leaf and bark at temperature 850℃ was so fast as to probably lead to heat resistance. Therefore lower temperature 750℃ was applied.

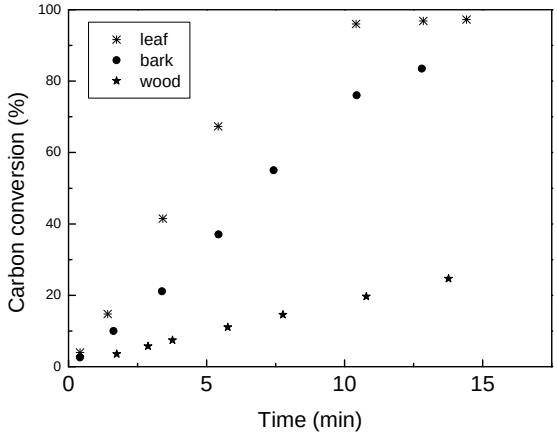

Figure 5-13: Carbon conversion of leaf, bark, and wood biochar as function of time during steam gasification at 850℃

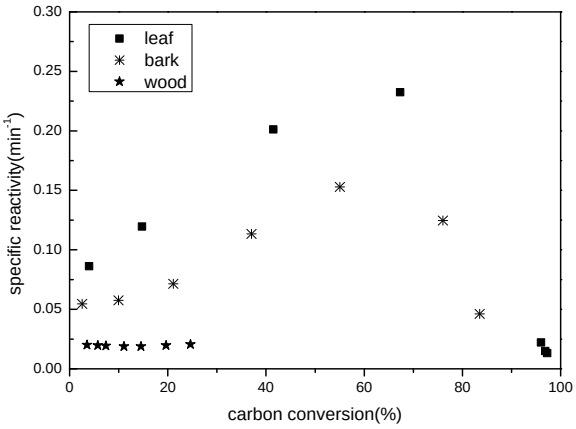

Figure 5-14: Specific reactivity of leaf, bark, and wood biochar as function of carbon conversion during steam gasification at 850℃

- ***Steam gasification of wood biochar at 750 ℃***

Figure 5-15 presents the curve of the specific reactivity against carbon conversion and Figure 5-16 gives the steam concentration during the course of steam gasification. It can be seen from Figure 5-15 that specific reactivities of AC were similar under different steam partial pressure (1.0L/min argon+0.074mL/min steam, 1.5L/min argon +0.114mL/min steam, and 1.5L/min argon+0.215ml/min steam). The specific reactivity overlaps at above 4% carbon conversion. From Figure 5-16 the consumption of steam was less than 1%. Therefore these confirmed that current reaction was under chemical reaction control. Such a conclusion was also supported

by the data of AAEM content of AC obtained under different steam partial pressure as shown in Table 5-10. The results show the AAEM contents of three AC were similar. The relative standard errors of Na is ±3.66 %, K±4.18 %, those of Mg and Ca are ±4.32% and ±7.66%, respectively.

Apart from the above evidence, the textural characteristics of AC under different steam partial pressure were also provided in Table 5-11. It is very clear that the results were very similar. The value of total volume, BET surface area, and Vd were around 0.41 cc/g, 600 m^2/g, and 0.28cc/g respectively. Such results suggested that there were no differences of AC caused by the change of steam partial pressure.

Table 5-10: AAEM content(% daf) of AC obtained under different steam partial pressure

Argon flow rate +steam flow rate	Na	K	Mg	Ca
1.5+0.215	0.1618	0.4719	0.2531	1.0079
1.5+0.113	0.1584	0.4838	0.2571	0.9638
1.0++0.074	0.1506	0.4456	0.2368	0.8662

Pyrolysis holding time 15min, AC 15min , at 750℃, symbol x +xx means x L/min argon+ xxml/min steam, eg, 1.5+0.215 means 1.5L/min Argon +0.215ml/min steam .

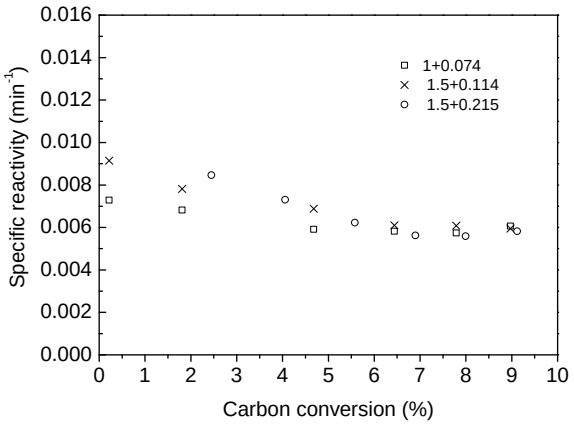

Figure 5-15: Specifice reactivity of gasification with various steam partial pressure and (symbol x +xx means x L/min argon+ xxml/min steam)

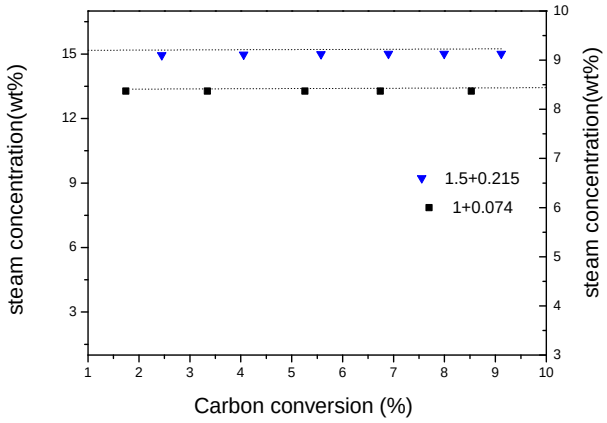

Figure 5-16: Steam concentration as the function of carbon conversion

Table 5-11: Characteristics of AC Obtained at the different steam partial pressure

Parameters	SBET	DR		Total volume
	(m^2/g)	AHPW(Å)	Vd (cc/g)	(cc/g)
3+0.215	600	6.87	0.29	0.41
1.5+0.215	596	7.36	0.26	0.43
1.5+0.113	598	7.26	0.28	0.41
1.0+0.074	593	7.11	0.27	0.41

SBET: surface area (m^2/g) based on Stephen Brunauer, Paul Hugh Emmett, and Edward Teller equation SBET; DR: Dubinin-Radushkevich equation; Total volume obtained at p/p_0=0.9998(cc/g); Vd: micropore volume from DR plot (cc/g) ; AHPW: average half pore width from DR plot (Å) Conditions : pyrolysis holding time 15min, AC 15min , x + xx means x L/min Argon +xx ml/min steam; pyrolysis holding 15min +gasification15min at 750℃).

5.3.2 Biochar Reactivity and Instantaneous Gas Produced During Steam Gasification

The curves of specific reactivity and steam concentration as a function of carbon conversion of slow biochar and fast biochar are shown in Figure 5-17. The specific reactivity of fast biochar was analyzed together with that of slow biochar. Meanwhile, the specific reactivity above 10 % carbon conversion of slow biochar was also provided to make the tendency of specific reactivity clearly. It is shown that steam consumption during gasification of slow biochar was slight so that the steam partial pressure kept constant. On the contrary, the consumption of steam gasification of fast biochar was much higher.

In the case of the reactivity, gasification rate depends on concentration of active sites, ease of accessibility of the active sites to the reactant gas and presence of inorganic impurities[214] acting as catalyst.[215] Such factors can be alerted through the pyrolysis process and subsequent gasification. For instance, the severity of pyrolysis effects the loss of catalytic activity as the consequence of sintering, formation of intercalation compounds or vaporization.[216] The increase of the density of catalytic contents is the consequence of consumption of the carbon material during the course of gasification.[134] However, the conclusions of the influence of heating rate on the reactivity are controversial. Samaras observed that slow coal char showed higher reactivity during CO_2 gasification. [207] However it was also observed rapid biochar showed higher reactivity which is the consequence of rapid heating rate: (1) less deposited pyrolytic carbon which provides lesser active reaction sites; (2) yield of defective carbon micro crystallites containing higher concentration of active sites. [217]

It can be seen that the results under current experimental conditions were in agreement with the latter, namely, the fast biochar had a higher specific reactivity peak at around 0.07(min^{-1}) than that of slow pyrolysis biochar at around 0.02 (min^{-1}). The reason may be due to two aspects namely pore size distribution and the catalysts of inherent inorganic matters. The surface of mesopores and macropores may provide more active sites compared with micropores which may not contribute to the gasification. That means the higher surface area lead by mesopores and macropores are better indicators to higher reactivity than total surface area. [218,219] The second cause of it may lie in the catalytic effect of inherent alkali and alkaline earth metallic (AAEM) species. As shown in Table 4-4, FB had higher concentrations of ash than SB. AAEM may disperse on the asperities of the surface of FB thus catalyzing steam gasification.

Unlike the continuous decrease of specific reactivity of fast biochar with the increase of carbon conversion, the reactivity of slow biochar decreased initially when carbon conversion below around 10%, then it increased afterwards. The possible

reason was that in the initial stage of steam gasification, an amount of AAEM catalyst dispersing on the surface of slow biochar led to higher density of reactive sites within the biochar. Therefore, these catalysts contacted well with steam thus speeding up the reaction. Due to the removal of a proportion of very reactive carbon materials in the biochar, the specific reactivity started to decrease. With the increase of carbon conversion, some carbon atoms on the surface of AC were removed leaving new catalytic active sites. Specific reactivity started to increase but it did not reach the altitude of the initial reactivity.

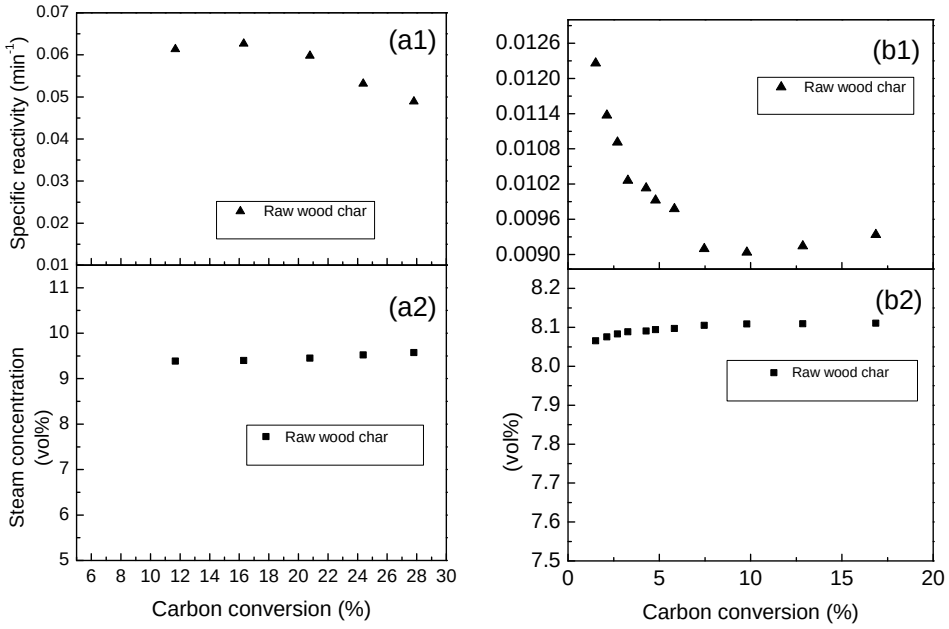

Figure 5-17: Biochar specific reactivity (a1)(b1)and steam concentration as(a2)(b2) a function of carbon conversion during biochar steam gasification. (a) FB at750 ^{o}C; inlet steam concentration 10 vol% (b) SB at 750 ^{o}C; inlet steam concentration: 8.2 vol %.

Efforts were then made to study the gas evolution during biochar steam gasification, with the specific gas formation rates being presented in Figure 5-18. It is clearly seen in the figure that the formation rates of H_2, CO and CO_2 decreases with conversion initially which was consistent with the reactivity data presented in Figure 5-17. Fast biochar showed much higher gas formation than that of slow biochar. Furthermore, it should be noted that the formation of CH_4 is thermodynamically

negligible under the reaction conditions. Therefore, the overall reaction can be written as:

$$(X+1)C+(2X+1)H_2O \rightarrow CO+XCO_2+(2X+1)H_2 \quad (5\text{-}1)$$

Where X = CO_2/CO is determined by was-gas-shift reaction

$$CO+H_2O \rightarrow CO_2+H_2 \quad (5\text{-}2)$$

$$Keq=\frac{p_{co_2}\,p_{H_2}}{p_{co}\;p_{H_2O}} \quad (5\text{-}3)$$

Where, p is partial pressure. So the ratio of H_2/CO and CO_2/CO at equilibrium can be calculated by equation $\frac{P_{CO_2}}{P_{CO}}=Keq\frac{p_{H_2O}}{p_{H_2}}$, $\frac{P_{H_2}}{P_{CO}}=Keq\frac{p_{H_2O}}{p_{CO_2}}$.[161]

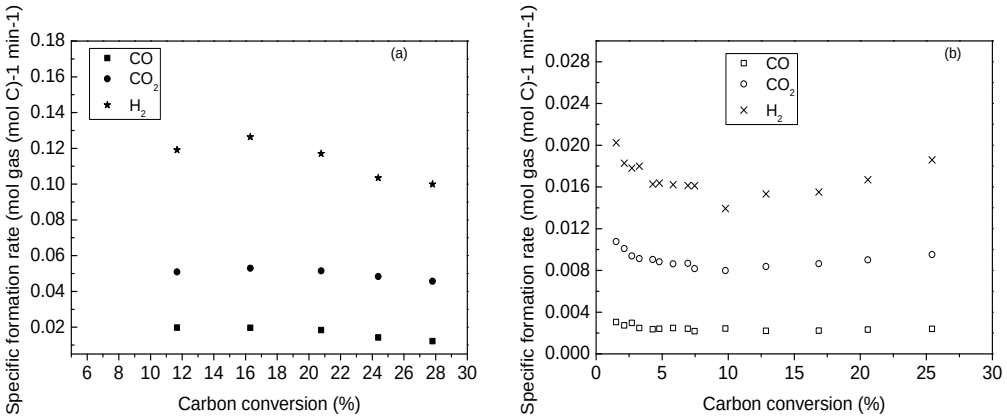

Figure 5-18: Specific gas formation during gasification of biochar:
(a) fast biochar (b) slow biochar

Figure 5-19 presents the actual ratios of H_2/CO and CO_2/CO based on the experimental data, benchmarking against the equilibrium ratios calculated under the same steam gasification conditions. It is obvious that the actual ratio of CO_2/CO is lower than the equilibrium values, suggesting that the primary product is CO and the formation of CO_2 is more likely from water-gas-shift reaction.

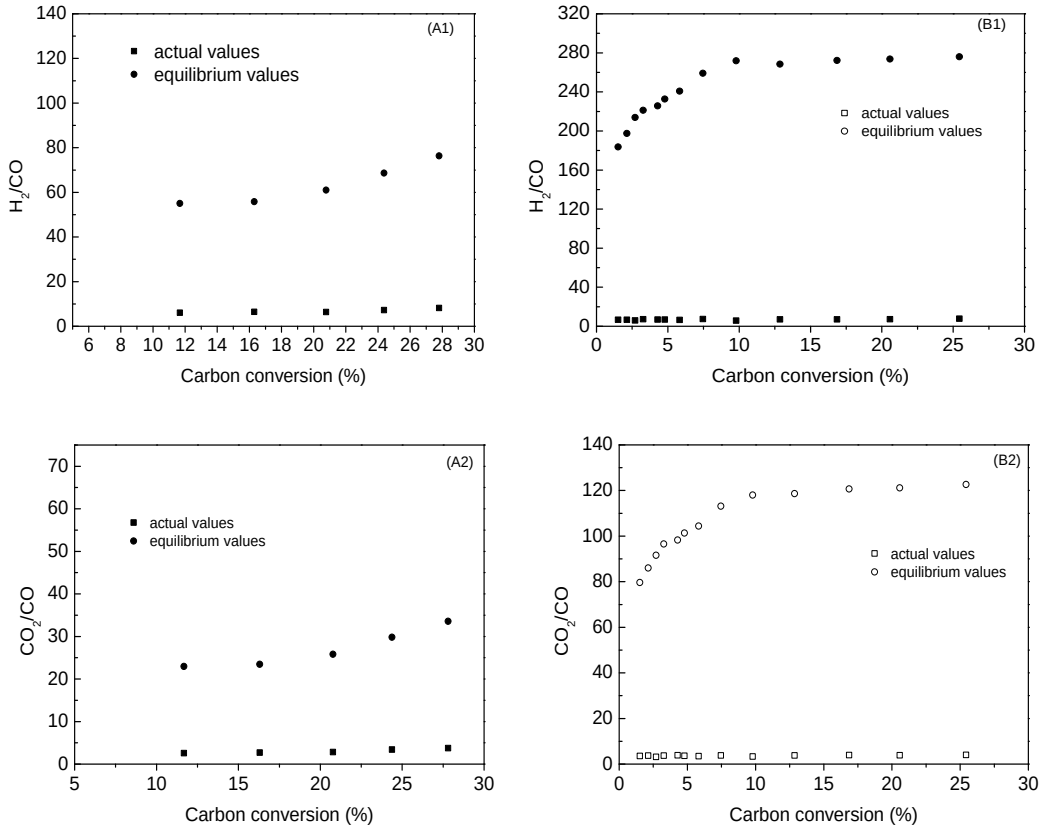

Figure 5-19: Comparison between the actual and theoretical equilibrium ratios of H_2/CO: (A1) fast biochar , (A2) slow biochar; CO_2/CO: (B1) fast biochar; (B2) slow biochar.

5.3.3 Reasons of Higher Reactivity of Mallee Wood Particle in Gasification

Biochar obtained at 750℃ shows high reactivity leading to a reasonable surface area at 526m^2/g even within a short gasification time of 5min. The possible reason for the phenomena is of interest. To understand the effect of topography of biochar on the reactivity, the images obtained by the combination of FIBSEM, BSE, and EDS are shown in Figures 5-20 and 5-21.

In Figure 5-20 shows morphology of wood biochar and the EDS results of bright points on the surface of wood biochar. Images (b) and (e) are biochar images. Images (a), (d), (c), and (f) demonstrated magnified local area with arrow indicting the designated place. According to these images, two phenomena were obvious. Firstly, the surface of biochar was rough with porosity. The porosity consisted of distinct

macropores. Secondly, metals (such as Na, Mg, Ca detected as bright spots) distributed around the mesopore were easy to be observed in both SEM images and BSE images. Catalysts on large pores were also observed by Pasotr[192] and Hurt. [220] There was evidence that the reaction primarily took place outside the microporous catalyst on network on the surfaces of larger pores.[220] Moreover, according to the unaltered surface of some areas of activated carbon, a selective gasification process takes place. [168]

Figure 5-21 illustrates the morphology of AC which was obtained under 5min steam gasification. Figures 5-22, 5-23, and 5-24 illustrate the EDS results of bright points and certain area of the surface of AC. It was obvious a great amount of bright points are on the surface of AC. Through the EDS result, they are mainly AAEM (Na, K, Ca, and Mg). Being consistent with the AAEM content, the higher intensity of Ca and Mg was observed. This morphology gave more evidence of mallee biochar having higher reactivity which could be used to produce AC with relatively higher surface area within shorter gasification time.

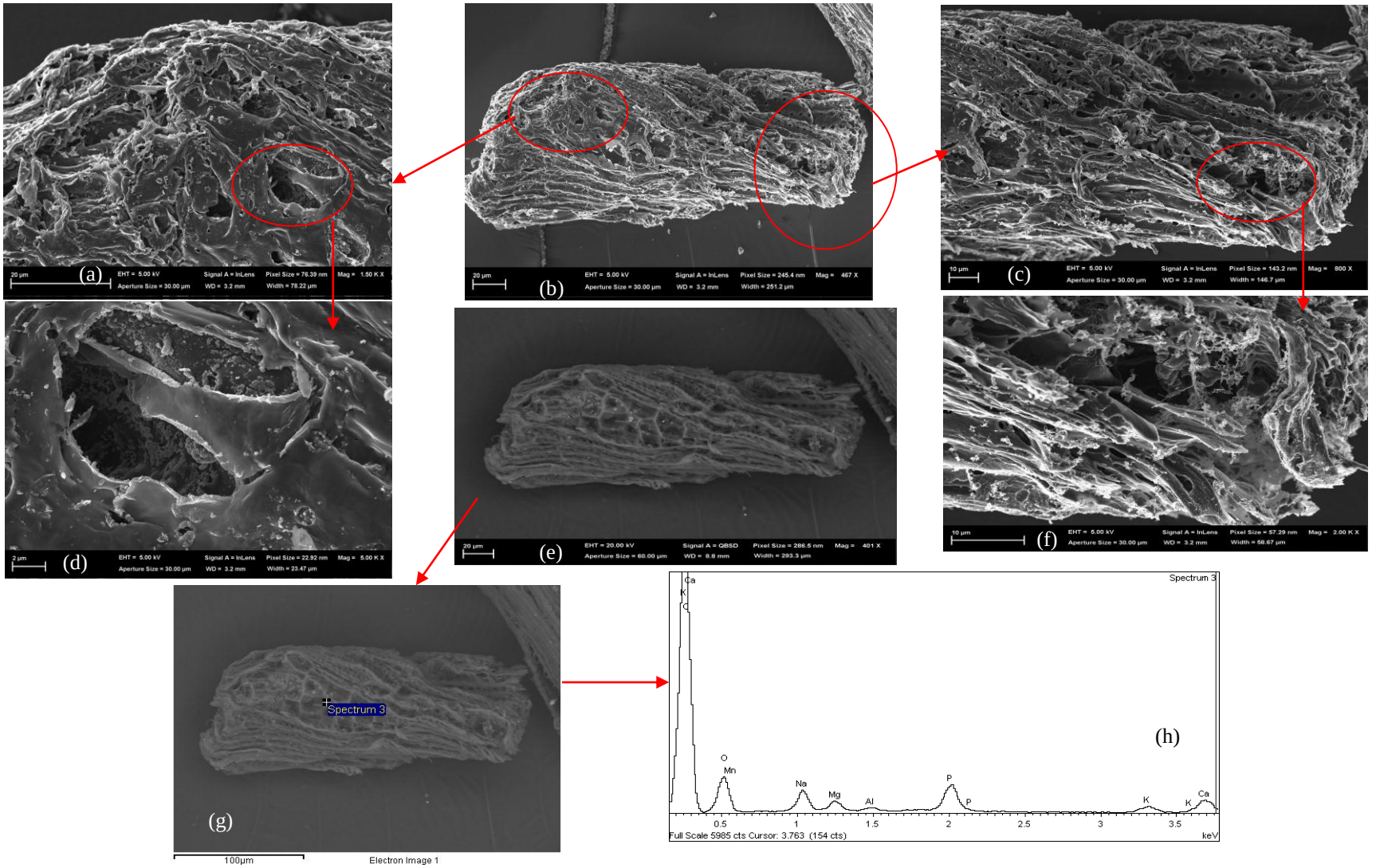

Figure 5-20: Morphology of wood biochar : (a) magnification of left red circle of (b); (b) SEM images of wood biochar; (c) magnification of right red circle of (b); (d) magnification of red circle of (a);(e) BSEM image of wood biochar ; (f) magnification of red circle of (c); (g) BSEM image of wood biochar with EDS ; (h)the EDS results of bright points on the surface of wood biochar.

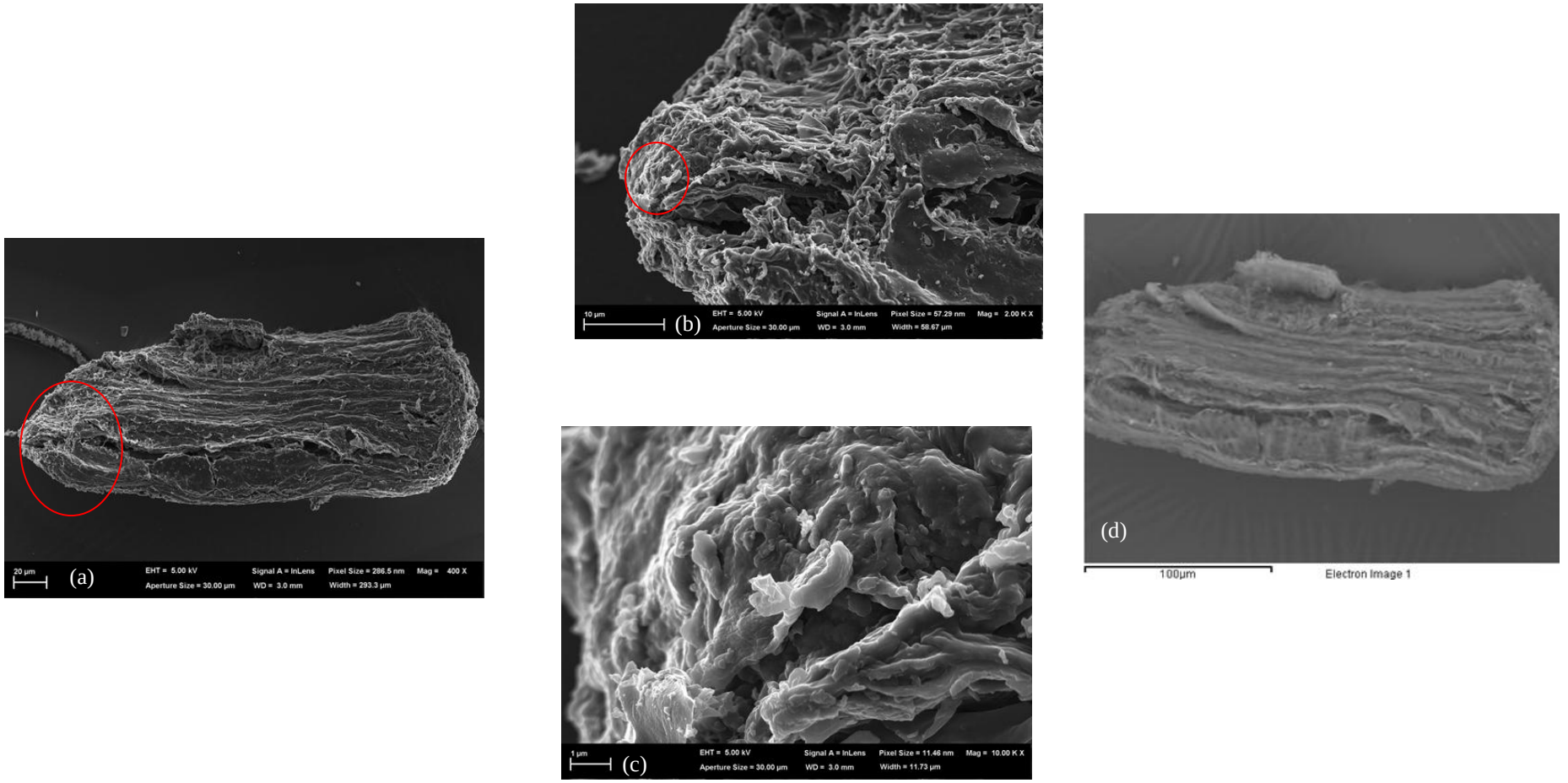

Figure 5-21: Morphology of AC under different magnification (a) SEM image of AC (obtained with 5min gasification); (b)magification of red circle of (a); (c) magnification of red circle of (b); (d) BSEM of AC.

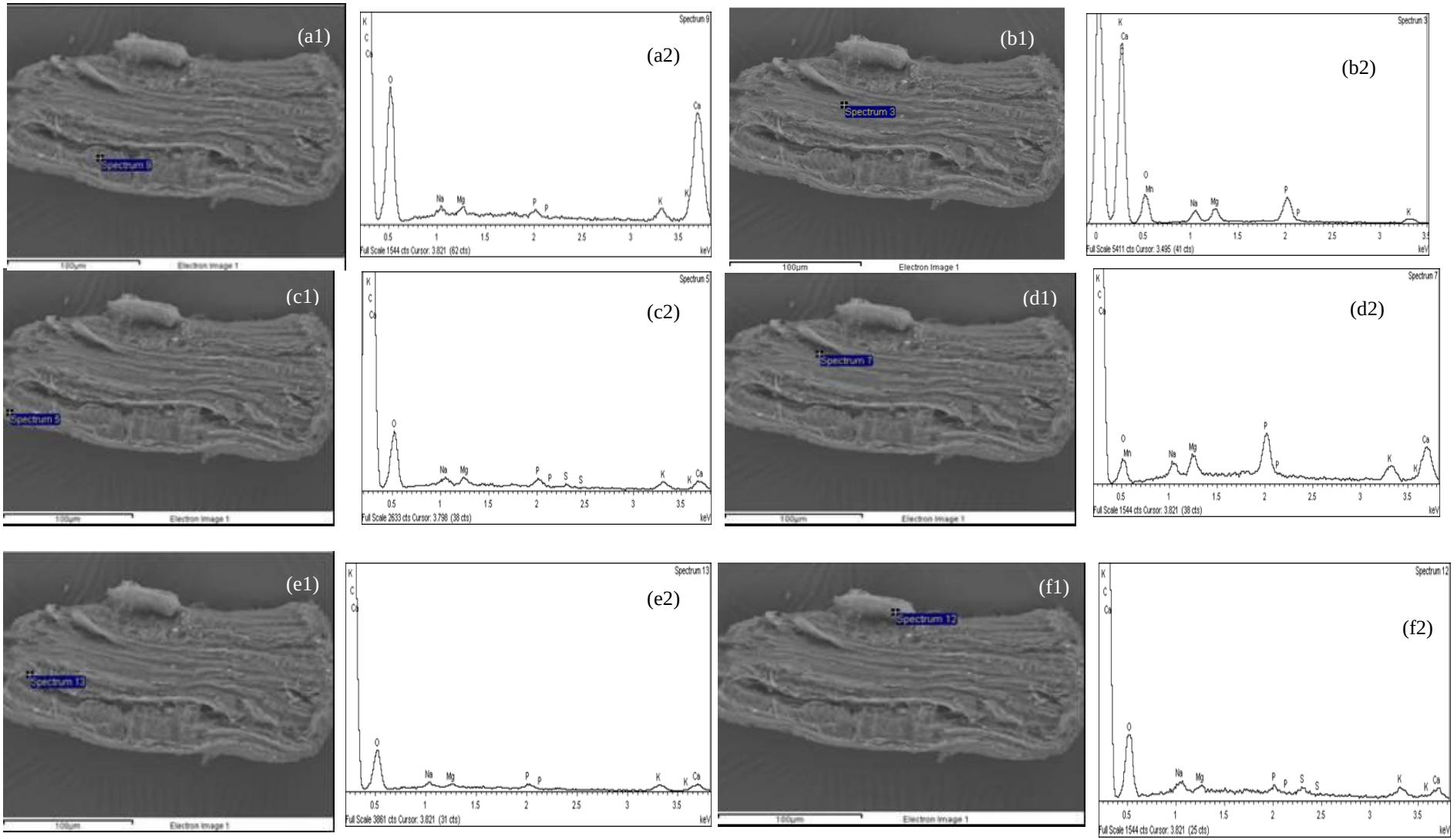

Figure 5-22: Morphology of AC (5min gasification) and the EDS results of bright points on the surface of AC: (×1) means FIBSEM, (×2) means EDS results (×character from a to f)

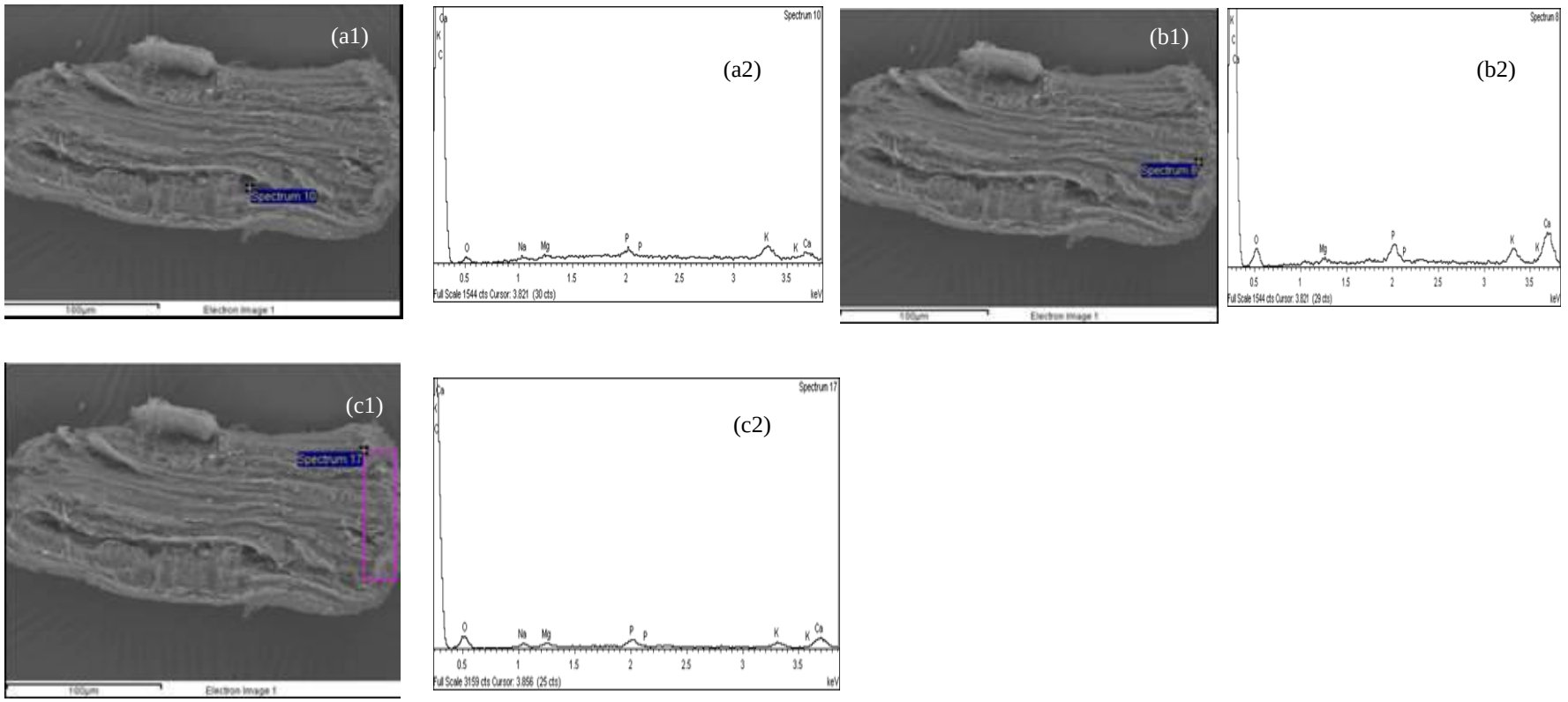

Figure 5-23: Morphology of AC (5min gasification) and the EDS results of bright points / area on the surface of AC: (×1) means BSEM, (×2) means EDS results (×character from a to c)

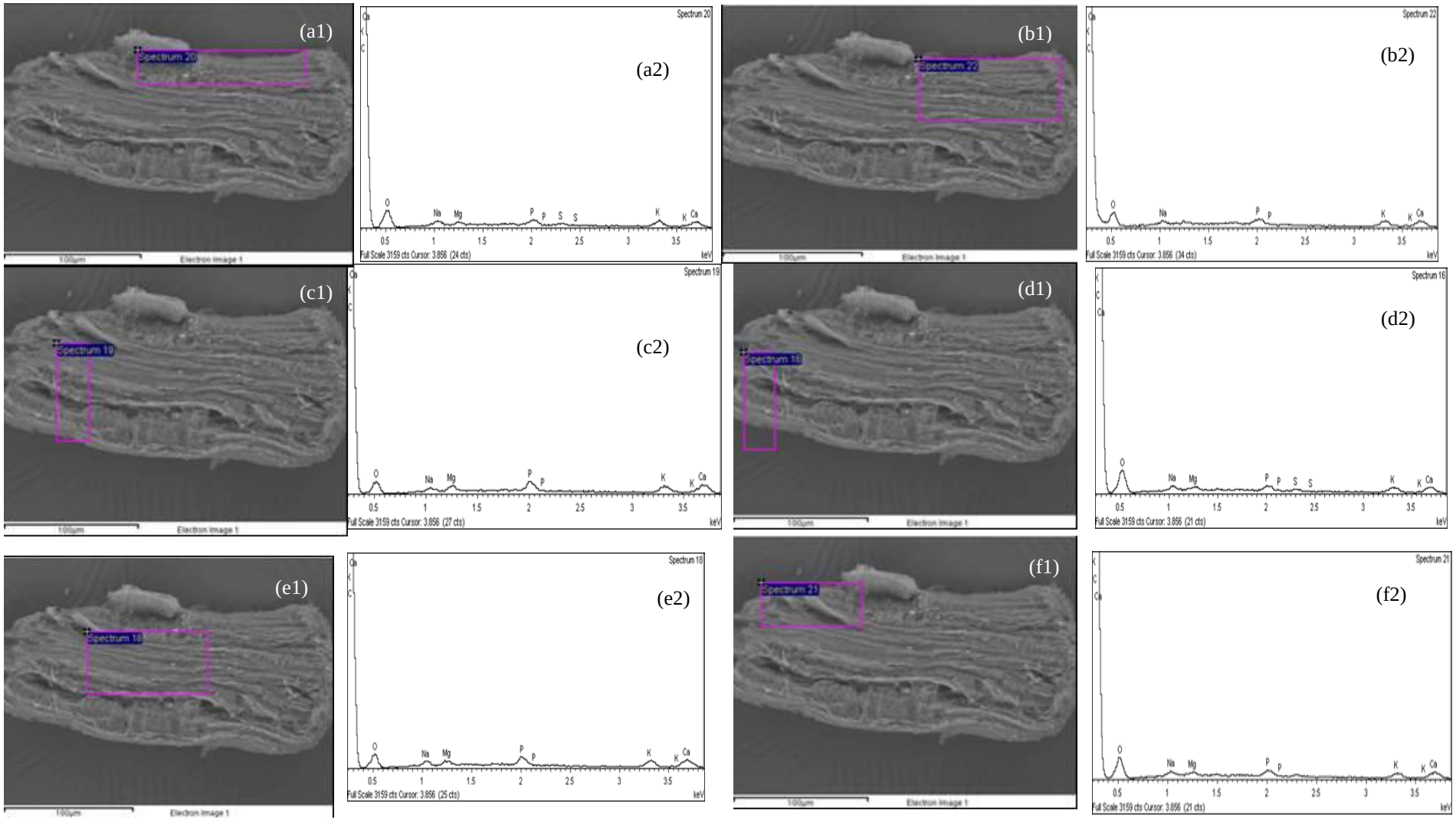

Figure 5-24: Morphology of AC (5min gasification) and the EDS results of area on the surface of AC: (×1) means BSEM, (×2) means EDS results (×character from a to f)

5.3.4 Evolution of Mallee Biochar Structure at Low Carbon Conversion

- ***Pore structure***

Figure 5-25 presents the N_2 adsorption-desorption isotherm of the biochar produced from Mallee wood pyrolysis at 540 ℃ and the AC produced from the biochar after steam gasification for 5 min at 750 ℃. Figure 5-25 clearly shows that the adsorption capability has been increased substantially after steam gasification of the biochar. The adsorption capacity of AC increased to >100 cc/g, suggesting that the AC has abundant micropores. It shows that hysteresis loop appears after steam gasification, indicating the presence of meospores in AC. As shown in Table 5-12, the BET surface of the biochar increased substantially from 19 m^2/g to 435 m^2/g after gasification.

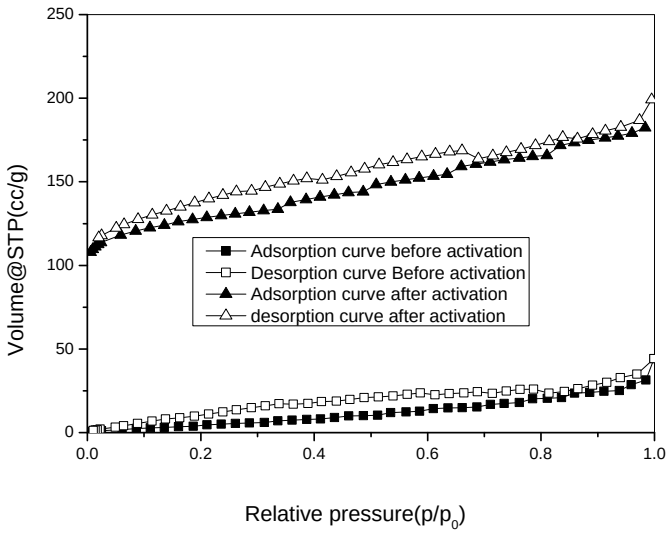

Figure 5-25: N_2 adsorption-desorption isotherm at 77K of biochar and AC produced from steam gasification of the biochar (biochar produced at 540℃; 10 K/min; 15 mins holding time; AC at 750℃, 5min gasification time).

Practically, a minimal conversion of the biochar is desired during steam gasification in order to maximize the productivity of AC. A series of experiments were then carried out to study the properties of biochar in steam gasification with various

carbon conversions for gasification 2~5%. Figure 5-26 and Figure 5-27 present the adsorption-desorption isotherm and the BET surface area of various AC produced, respectively. For the purpose of comparison, isotherms of higher conversion above 5% were also shown in Figure 5-26. Figure 5-26 clearly shows that the adsorption curves of all ACs similar suggesting that the ACs consist of a wide range of micro-, meso- and macro-pores, as also evident by the data listed in Table 5-13.

Table 5-12: Characteristics of raw biochar and AC prepared from steam gasification of the biochar

Samples	SBET (m^2/g)	DR		Total volume (cc/g)
		V_d(cc/g)	AHPW(Å)	
Biochar produced from mallee wood (540 ℃; 10 K/min; 15 mins holding)	19	0.01	22.81	0.07
Activated Carbon (750 ℃; 5 min steam gasification)	435	0.19	6.48	0.19

SBET: surface area (m^2/g) based on Stephen Brunauer, Paul Hugh Emmett, and Edward Teller equation SBET; DR: Dubinin-Radushkevich equation; Total volume obtained at p/p0=0.9998(cc/g); Vd: micropore volume from DR plot (cc/g) ; AHPW: average half pore width from DR plot (Å).

It is also clear that the adsorption ability generally increases with biochar conversion but only in the early stage up to ~5% carbon conversion. Longer time of gasification led to only limited further increase in opening more pores and generating more surface area within the biochar, as shown in Table 5-13. Therefore, the data clearly suggest that only a short period of steam gasification was needed to produce AC from the biochar. In this case, a very low carbon conversion of ~5% was required to produce ACs with an SBET surface area of 526 m^2/g.

Table 5-13 gives the texture characteristics of AC under low carbon conversion. It seemed that the BET surface did not change at the carbon conversion range of 2.1% and 4.3%. It is also supported by nearly constant values of AHPW, Vd, and total volume over the same carbon conversion range. Such observation is also confirmed by the Figure 5-28. As shown in Figure 5-28, the QSDFT curves were very similar and micropores made an important contribution to the overall pore structure. [163]

Table 5-13: Characteristics of AC obtained at the different level of carbon conversion

Carbon Conversion (%)	SBET (m^2/g)	DR AHPW(Å)	DR Vd (cc/g)	Total volume (cc/g)
2.1	423	5.81	0.21	0.31
2.7	425	6.04	0.20	0.34
3.3	439	6.09	0.20	0.33
3.8	452	6.05	0.22	0.34
4.3	454	5.81	0.21	0.31
5.5	526	7.53	0.24	0.42
12.9	572	7.47	0.27	0.43

SBET: surface area (m^2/g) based on Stephen Brunauer, Paul Hugh Emmett, and Edward Teller equation SBET; DR: Dubinin-Radushkevich equation; Total volume obtained at p/p_0=0.9998(cc/g); Vd: micropore volume from DR plot (cc/g) ; AHPW: average half pore width from DR plot (Å) .

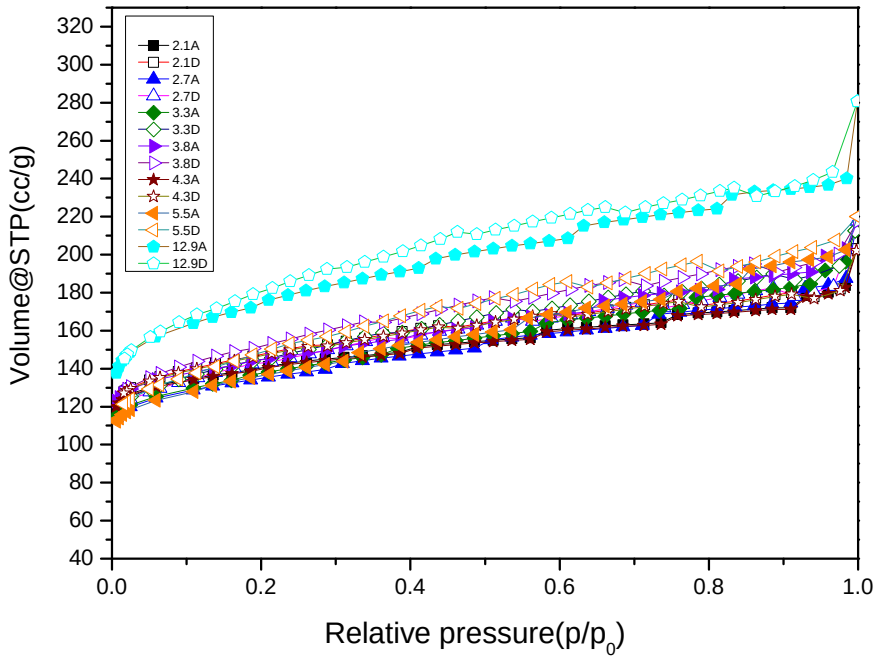

Figure 5-26: N_2 adsorption-desorption isotherm at 77K of AC produced from biochar via steam gasification with various carbon conversion (A means adsorption, D means desorption; the same shape of symbol means the same sample while open one means desorption curves and solid one means adsorption curves); ×A (D) means adsorption (desorption) curve of AC obtained at × carbon conversion at 750℃).

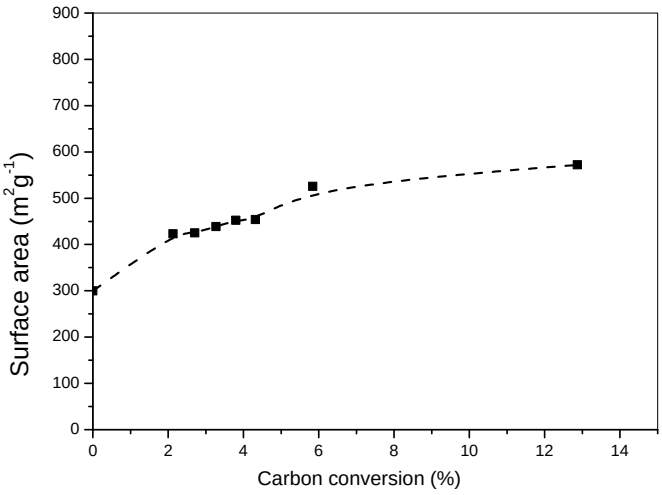

Figure 5-27: Surface areas as the function of carbon conversion during the course of steam gasification

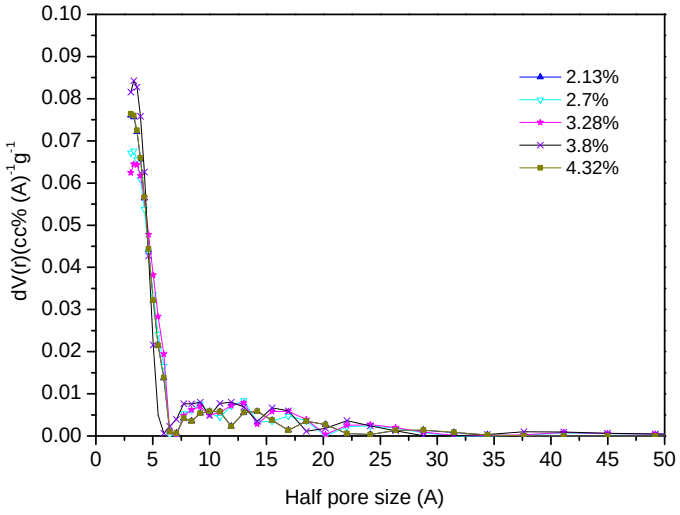

Figure 5- 28: Pore size distribution by QSDFT for AC under low carbon conversion (× %)(wood biochar at 750℃ with 15 min holding time, steam gasification at 750℃)

- ***Chemical composition of AC***

Table 5-14 shows elemental analysis and proximate analysis of AC obtained under different carbon conversion. Generally, under low carbon conversion, the chemical composition of AC was nearly the same as expected.

Table 5-14: Properties of AC under different carbon conversion

Carbon conversion	Moisture (%[a]ad)	Proximate (wt% db)			Ultimate analysis (wt% db)			AAEM content(% daf)			
		FC[b]	VM[c]	Ash	C	H	N	Na[d]	K[d]	Mg[d]	Ca[d]
Raw sample	3.7	16.8	82.7	0.5	45.88	6.38	0.74	0.0234	0.0591	0.0336	0.128
0	5.4	84.9	11.7	3.4	84.77	1.42	0.48	0.1515	0.4222	0.2235	0.8831
2.1	3.0	85.6	10.4	4.0	83.46	3.02	0.45	0.1658	0.4768	0.2429	0.8680
3.8	1.5	85.3	10.5	4.2	83.10	2.09	0.27	0.1682	0.4676	0.2403	0.8743
5.5	1.7	84.9	11.0	4.1	84.47	0.93	3.15	0.1669	0.4962	0.2472	0.8989

[a]air dired, [b]Fixed carbon（FC）, [c]Volatile matter(VM), [d] Analysed by IC

- ***Evolution of intrinsic gasification reactivity***

Specificity of biochar was normalized by surface area to understand the effect of carbon structure on the specific reactivity. This value could be treated as intrinsic reactivity of biochar. [132, 221-224] Figure 5-29 shows the reactivity per unit pore surface area of wood biochar and retention of AAEM contents (Na, K, Mg, and Ca). It can be seen that the reactivity per unit pore surface area decreased with increase of carbon conversion. The peak of the curve was the consequence of "fresh" active sites sand well dispersed AAEM on the biochar as discussed above. AAEM retention was nearly the same when the carbon conversion is below 15%.

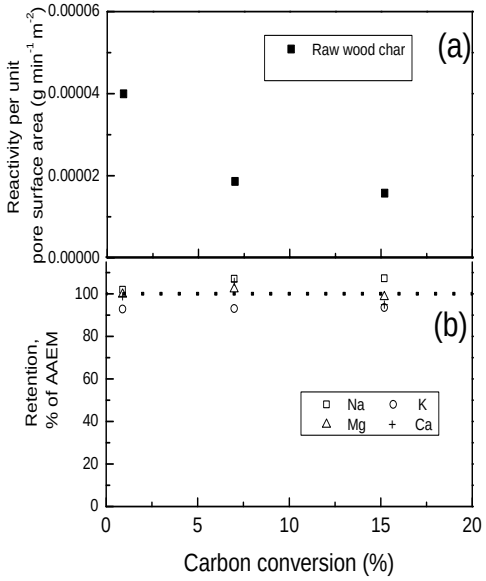

Figure 5-29: Reactivity per unit pore surface area of wood biochar (a) and retention of AAEM contents of Na, K, Mg, and Ca (b)

- ***FTIR spectrum***

For AC obtained from steam gasification of 750℃ at low carbon conversion, there were no obvious observable peaks in FTIR spectrum. This indicated only small amount of function groups existed on the surface of AC.

- ***Raman spectrum***

Raman spectrums were obtained to get the structure of AC. D band represents highly ordered materials aromatic rings, aromatics with no less than 6 rings, and defects in carbon graphic structure while ($Gr+Vr+V_l$) band represents amorphous carbon structure, aromatics with 3-5 rings, and methylene or methyl.[178] As expected, the structures of AC obtained under low carbon conversion were similar due to low carbon conversion at 750℃ steam gasification. Figure 5-30 shows the D band, ($G_r+V_r+V_l$), and their ratio as a function of carbon conversion. It can be seen from Figure 5-30, as expected, D band changed slightly. It meant the ordered structure of biochar was not developed at lower carbon conversion. ($G_r+V_r+V_l$) band showed a slight increase at 13% carbon conversion which may be caused by the continuous pyrolysis of biochar. The ratio of ($G_r+V_r+V_l$) and D kept nearly the same before 10% carbon conversion then followed by a slight increase after 10% carbon conversion.

Figure 5-31 gives the peak area of S band against carbon conversion. S band represents Caromatic-Calky, aromatic (aliphatic) ether, C-C on hydro aromatic rings, and C-H on aromatic rings. [178] The values of S band were nearly the same.

Figure 5-32 shows the peak area of D and G/D. G band represents the graphic structure, aromatic ring quadrant breathing, and alkene C=C. [178] G band kept almost stable below 10% carbon conversion but decreased slightly after 10% carbon conversion. This decrease suggested after 10% carbon conversion biochar structure started changed gradually.

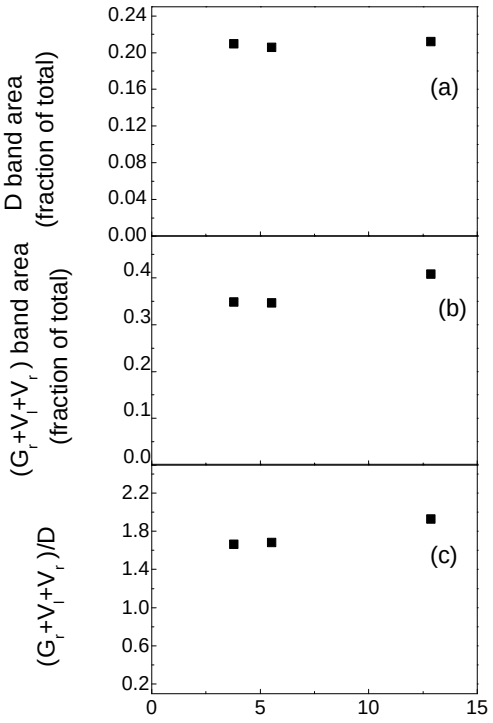

Figure 5-30: Peak area of D band (a) and (Gr+Vr+Vf) band (b), and ratio of (Gr+Vr+Vf)/D (c), as a function of carbon conversion

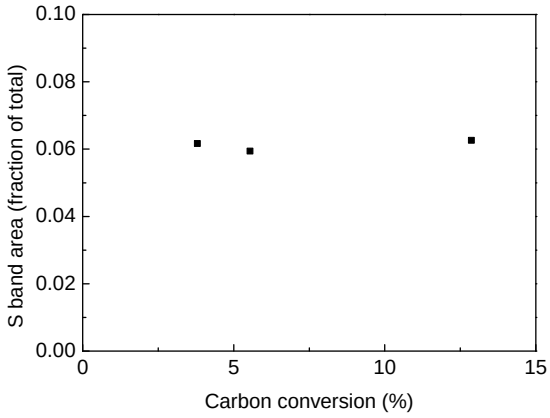

Figure 5-31: Peak area of S band as a function of carbon conversion

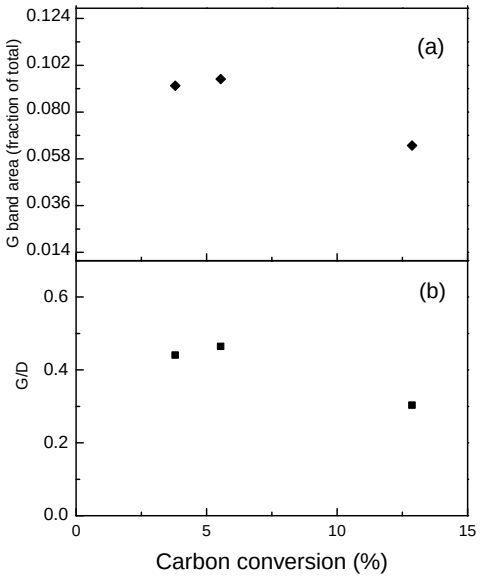

Figure 5-32: G band area (a) and the ratio of G/D (b) as function of carbon conversion

5.4 Conclusions

The results of operating parameters which influence pyrolysis/gasification are as follows:

(1) Temperature is an important parameter to both pyrolysis and steam gasification. Increasing pyrolysis /gasification temperature had a positive effect on the surface area; however, the effect became less significant for temperatures above 700℃. At temperatures of 700℃ and 750℃, AC with reasonably high surface area at 481m^2/g and 526 m^2/g were obtained after only 5 min gasification time. Thus 750℃ was chosen for AC preparation in this study.

(2) For 40 min steam gasification, AC obtained from both slow pyrolysis biochar and fast pyrolysis biochar showed higher BET surface at 943 m^2/g and 991m^2/g respectively. Thus both slow and fast pyrolysis biochar could be suitable feedstock

for activated carbon preparation.

(3) Under current experimental conditions, larger particle size led to low surface area of AC. Results showed at 750℃,for biochar obtained via pyrolysis of 150~250μm particle with 15min holding time, and increasing carbon conversion to 50% led to higher surface area of 819 m^2/g. However, for low carbon conversion 5.5% (5min) and 16.9% (15min) resulted in 526 m^2/g, 600 m^2/g respectively.

(4) Biochar obtained from acid washed biomass showed much higher surface area 470 m^2/g than that of raw biomass at 270 m^2/g biochar. After 20min steam gasification, the surface area of acid washed biomass biochar increased to 589 m^2/g.

The mechanism of pyrolysis/gasification under low carbon conversion was investigated in depth. The results are:

(1) During steam gasification, the biochar specific reactivity initially decreased with conversions. Based on the syngas compositions during the steam gasification, the primary product is probably CO.

(2) Specific reactivity decreased initially when carbon conversion below around 10%, then it increased afterwards. The possible reason for that is the dispersion of inherent AAEM catalyst changes with the carbon conversion. With the increase of carbon conversion, the surface area of AC increased.

(3) Form the morphology of biochar and AC, a great amount of AAEM content dispersed on the surface of biochar and AC. These images explained the possible reason for higher specific reactivity of mallee wood biochar. Higher reactivity of mallee biochar is beneficial to produce AC for shorter gasification time but with relatively higher surface area as consequence.

CHAPTER6 TRANSFORMATION OF INHERENT OXYGEN IN BIOCHAR DURING STEAM

6.1 Introduction

Physical gasification process involves two steps known as pyrolysis and gasification. Biochar produced from pyrolysis is subjected to gasification process using gasification agent such as steam, carbon dioxide, air, oxygen or a mixture of them. Most of literatures published are based on physical gasification process. Apart from characteristics of AC, they mainly focused, from the view of statistical thermodynamics, on the relationship between char yield and operating parameters, the relationship between thermodynamic variables and pore size distribution of AC, the relationship between thermodynamic variables, and adsorption ability of AC, catalytic effect of metal matter on the gasification.[20, 207,186]

However, the gas transformation pathway of biochar in gasification process (such as oxygen) was not mentioned much until now. It is well known that during the production process of AC via pyrolysis and steam gasification, oxygen is highly relative to the gas formation of CO, CO_2, and H_2. A good understanding of evolution of gas is of vital importance to investigate the oxygen transformation in the course of steam gasification of mallee biochar.

The purpose of this chapter is to investigate the oxygen transformation in pyrolysis/steam gasification of mallee biomass basing on the principle of conservation of energy and mass, and to establish the relationship between pyrolysis and stream gasification via the pathway and amount of oxygen transformation obtained.

In the steam gasification, the gas formations are mainly from the following reactions.

$C + H_2O \rightarrow H_2 + CO$ △H=+118.628kJ /mol (6-1)

$CO + H_2O \rightarrow H_2 + CO_2$ △H= -43.514kJ /mol (6-2)

The molar ratio of H_2 and ($CO+CO_2$) can be represented by *q:*

$q = H_2/(CO+CO_2)$ (6-3)

For the purpose of obtaining the value range of *q*, two extreme assumptions of reaction (6-1) and reaction (6-2) could be taken. One assumption is that if only equation (6-1) takes place, the value of q_{min} will be 1. The other assumption is both equation (6-1) and equations (6-2) occur completely, so the value of q_{max} will be 2. Generally, both reactions occur but the intensity of reaction is different so that $1 < q < 2$. In this way, the value of q can somehow indicate the process of steam gasification. However, during the steam gasification of acid washed mallee wood, $q < 1$ is an unusual phenomena. From the mathematical view, the possible reason is either the decrease of H or the increase of ($CO+CO_2$).

From reactions (6-2) and (6-3), the mole ratio of H_2 and CO should be at least 1. Therefore, the cause of $q<1$ is the increase of the fraction of ($CO+CO_2$), in other word, there is an existence of increase of oxygen content and $q<1$ is an indicator index.

In this study, the temperature of pyrolysis/gasification is 750℃. The pyrolysis holding time was 15min and steam gasification time was 30 min. The properties of AB550-750 are shown in Table 6-1.

Table 6-1: Characteristics of biomass, biochar and AC prepared

[a] Sample	Moisture	Proximate(wt% db)			Ultimate analysis(wt% daf)				SBET
		FC[b]	VM[c]	Ash	C	H	N	O*	
	(% ad)								(m^2/g)
AB550-750	-	89.6	10.4	-	90.49	0.97	0.39	8.15	562
AP550-750	-	88.8	11.2	-	91.35	0.72	0.43	7.5	517
AAC550-750	-	90.7	9.3	-	93.74	0.73	0.49	5.04	570

[a], "AB550-750" means acid washed biomass biochar obtained at 550℃ pyrolysis then heat up to 750℃ , "AP550-750" means biochar obtained using the same procedure applied as "AAC550-750" without steam introduced; "AAC 550-750" " means AC obtained via the steam gasification of AB 550-750; [b]Fixed carbon （FC）, [c]Volatile matter(VM), O* by difference.

6.2 Pathway of Oxygen Transformation

• ***Phenomena of oxygen transformation***

Figure 6-1 shows the results of experiments of oxygen transformation phenomena. It presents the curve of the value of *q* against steam gasification time with standard deviation.

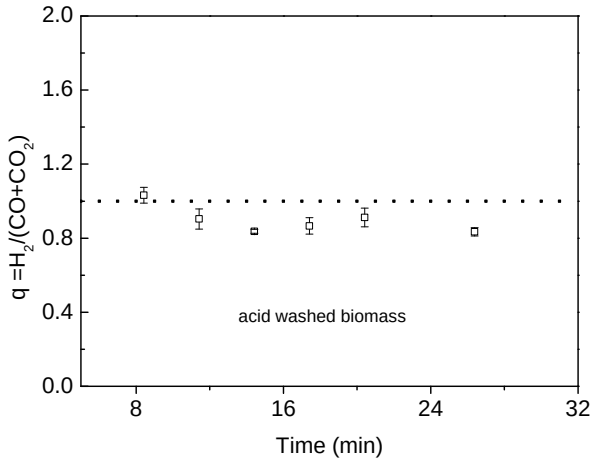

Figure 6-1: *q*, the ratio of H_2/ ($CO+CO_2$), as function of time for steam gasification of acid washed wood

It can be seen clearly the ratio of *q* dropped below 1 and decreased slightly to stay at around 0.8, after around 9 min gasification. In the early stage of steam gasification, *q* was slightly higher than 1. It indicated that both reactions (6-1) and（6-2）occurred and reaction (6-1) was the main reaction. This phenomenon lasted only a short time.

After 9 min, the increase of production of CO and CO_2 which is higher than the increase of H led to a *q* value of around 0.8. Based on the above discussion, the existence of oxygen transformation was evident as *q* was below 1.

- ***Pathway of oxygen transformation***

In the experimental system used, there were three possible sources of oxygen: steam introduced during steam gasification, attribution of oxygen from mallee biochar, and the leakage of air from outside the reactor system. The possibility in the leakage of system was eliminated according to the results of gas leakage test. To check the gas leakage in the reactor system, two methods were used initially. One was pumping inert gas into the sealed reactor system to a fixed pressure value and keeping it for 5 min to observe the change of inert gas pressure. Another was to check the quantity of gas generated in the reaction. Therefore, graphite was used as a sample under the pyrolysis condition. Because there is no oxygen in graphite, theoretically, no gas should be evolved in pyrolysis experiments. The results of experiments show there was no pressure decrease found by monitoring the pressure level in a sealed system. There was no evolved gas detected too. Thus oxygen could have come from the other two possible oxygen sources namely steam or /and mallee biochar.

Oxygen in this case was released mainly in the form of CO, CO_2. The analysis of the evolution of CO and CO_2 could provide an estimation of the amount of surface oxygen and functional groups on the carbons. [120] Therefore, on the one hand, one can view the pathway of oxygen transformation via the analysis of evolved gas (CO/CO_2) during the steam gasification of mallee biochar; on the other hand, according to the molar ratio of H and O based on reactions (1) and (2), one can determine the pathway of oxygen migration via the analysis of the amount of H produced in pyrolysis and steam gasification.

Figures 6-2, 6-3, and 6-4 present the curves of specific gas formation of CO, CO_2 and H_2 against time respectively. It is obvious that the same gases of CO, CO_2 and H_2

occurred during both the pyrolysis and steam gasification steps. In Figures 6-2 and 6-3, the specific gas formation of CO and H_2 in steam gasification was around 5 times and 4 times higher than that in pyrolysis. That means the amount of H_2 and CO in steam gasification was much higher compared with the amount of H and CO formed in pyrolysis. Therefore, the production of H_2 and CO was mainly from steam gasification. Our previous study showed CO was the primary gas.[7] So CO_2 formation was mainly from water-gas shift reaction (6-2).

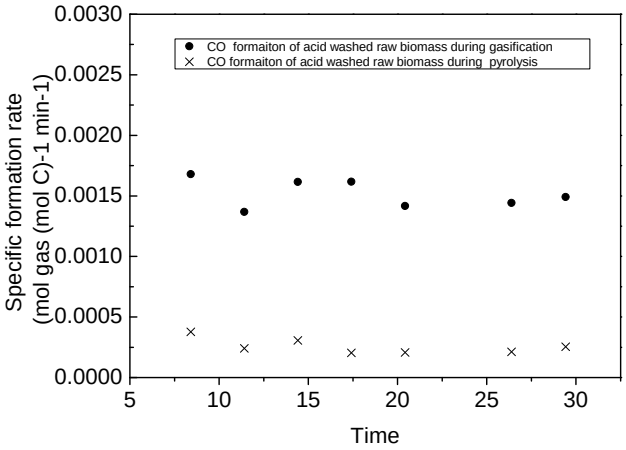

Figure 6-2**:** Specific formation of CO in steam gasification and pyrolysis as a function of time

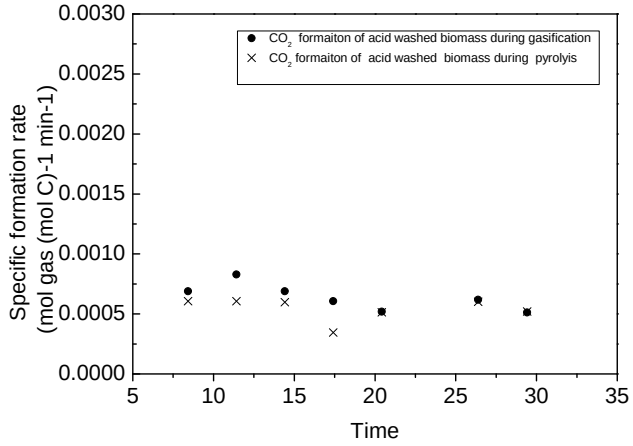

Figure 6-3: Specific formation of CO_2 in steam gasification and pyrolysis as a function of time

However in Figure 6-3, the value of the specific gas formation of CO_2 in pyrolysis is

nearly the same as that in steam gasification. This finding suggests that under current experimental conditions, the water-gas shift reaction (6-2) did not develop well. Therefore, only small amount of CO_2 resulted from reaction (6-2). It is possible that the oxygen was mainly migrating from mallee biochar in the form of CO_2 or/and CO rather than from steam. To further justify this suggestion, oxygen balance was carried out in Chapter 6.3

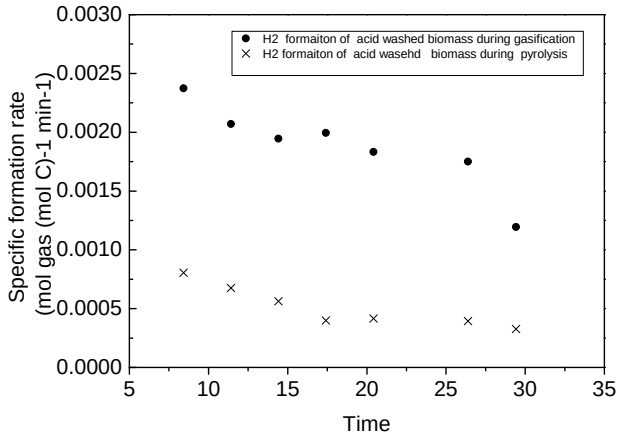

Figure 6-4: Specific formation of H_2 in steam gasification and pyrolysis as a function of time

6.3 Determination of Oxygen Transformation from Biochar during Pyrolysis/ Steam Gasification

To further clarify the observed results, oxygen balance was carried out.

During steam gasification, H was not only originating from steam but also from pyrolysis as shown in Figure 6-4. However the assumption that all H originated from steam meant that the consumption of steam was maximized namely the maximized oxygen can be obtained from steam. Therefore, the real mole of H_2 collected（Q_h）can be used to get the theoretical value of the amount of oxygen（Q_o）. According to the mole ratio of H and O in H_2O as 2:1, the total mole of oxygen obtained from steam will be half the total mole of H（Qh）.

The actual consumed oxygen amount (Q_b) can be calculated from the total mole of

CO and CO_2 produced. If $Q_b<Q_o$, oxygen from steam alone was not sufficient for steam gasification. Otherwise, steam would not limit the gasification process. However, as shown in Figure 6-5, steam concentration was virtually nearly constant during the course of the gasification process at around 15.2%. That meant excessive steam was passed through the reactor. As a result, it can be concluded that some oxygen must have originated from mallee biochar if $Q_b<Q_o$.

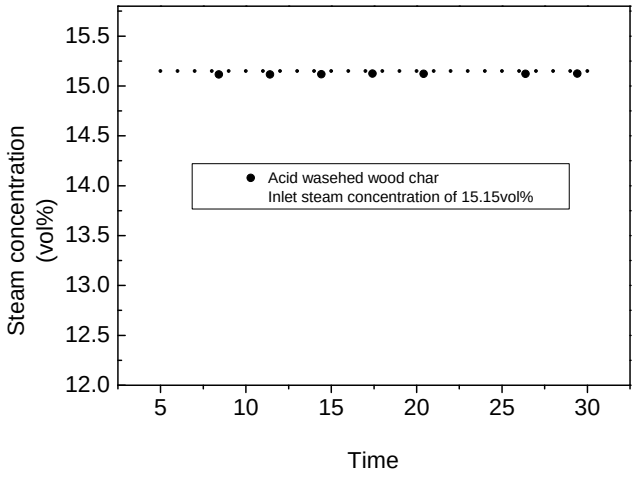

Figure 6-5: Biochar steam concentration as a function of carbon conversion during steam gasification: acid washed biomass

From the elemental analysis of biochar, the total moles of oxygen that can be transformed from biochar can be estimated.

In this experiment, total mole of H （Qh）is 1.311E-03 mole. Based on the above calculation, the maximum oxygen amount （Qo）which can be obtained from steam is 6.56E-04 mole. According to the total mole of CO and CO_2 collected the real amount of oxygen consumption（Qb）is 7.63E-04 mole. Obviously, the result is Qb>Qo. That means steam did not provide enough oxygen for reaction so that the oxygen (1.07E-04 mol) had to migrate from mallee biochar. The oxygen content of biochar has been analyzed in order to get the total mole of oxygen (Q) from mallee biochar. The value of Q is 5.07 E-04. Thus the release rate is about 21%.

Table 6-2: Characteristics of biochar and AC

Sample	Proximate(wt% db)			Ultimate analysis(wt% daf)				Biochar/AC	Oxygen
	FC[b]	VM[c]	Ash	C	H	N	O*	Yield/ [d]	Retention [e](%)
AB550-750	89.6	10.4	-	90.49	0.97	0.39	8.15	0.110	100
AAC550-750	90.7	9.3	-	92.74	0.73	0.49	6.04	0.110	74

[b]Fixed carbon（FC）, [c] Volatile matter(VM), O * by difference ;[d] based on biomass; [e] based on bio char AB 550-750.

The above results show the possible transformation of oxygen through the calculation of the amount of evolved gas. Similar results can be verified by comparing the oxygen content between AC and mallee biochar. Table 6-2 gives the oxygen content of biochar and AC. Assuming the oxygen content of mallee biochar as 100%, the calculated oxygen retention of 74% can be obtained when oxygen content of AC was divided by oxygen content of biochar. It indicated that 26% oxygen was released from biochar. This data is slightly higher than that obtained from the calculation from gas. The reason is that the original assumption that all H originating from steam which led to a higher calculated oxygen content part. Correspondingly, the calculated oxygen from biochar became lower.

6.4 Oxygen Transformation and Biochar Functional Group

The pathway of oxygen transformation from biochar and from steam was partially quantified above. In this section, further discussion of oxygen migration based on the chemical structure of mallee biochar was conducted.

The mallee biomass consisted of cellulose, hemicellulose, and lignin.[225] The glycosidic linkage of cellulose start to break quickly at 300 ℃, and bio-oil and gas are released. With increase of temperature, volatile matter was released and carbon was formed due to further thermal decomposition of media product. Both cellulose and hemicellulose behave similarly that they decompose at lower decomposition temperature where hydrogen bond is broken between 150~270℃. However, the decomposition of lignin covers a wider temperature range. The basic unit of lignin is

phenyl propane with abundant methoxy group and hydroxy group, and small amount of carbonyl group and carboxyl group.[226, 227, 235, 236] All of the functional groups usually are active in a reaction.

Lignin starts to thermally decompose at 260℃.The breakage of aliphatic hydroxyl in side chain leads to the evolution of H_2O and small molecular volatiles. At 410℃, some kinds of ether bonds start to decompose with the gas released mostly in the form of CO_2. With the increase of temperature, decomposition becomes more complicated. In this paper, steam gasification was carried out at 750℃; the main reactions were depolymerisation of lignin polymer, polymerization of unsaturated chain aliphatic hydrocarbon, alcohols, aldehydes, and ring-opening of the benzene. Pyrolysis products of acid hydrolysis of lignin at 780℃ consisted of various functional groups such as hydroxyl, methoxyl, and methoxy phenol. [228]

In the range of 550℃-800℃， gaseous products of lignin can be divided into two categories : one is stable micro molecular gases such as acetic acid, phenol, benzene, and the other are unstable products such as1-hydroxyl, 2-2 acyl toluene, methoxyl, dimethyl oxygen radicals phenol, 3-hydroxyl. These products containing methoxy phenol were further pyrolyzed and final product CO_2 was released.

There were 8 kinds of ether bonds existing in the aromatic rings, structures linking to aromatic rings, or the benzene alkylation ethers. Among them, β-O-4 alkyl (see Figure 6-6) aromatic ether is a main connection type which is mainly derived from the phenolic hydroxyl group of guaiacyl and syringyl units. The breakage of ether bonds take place above 700℃ [228] which is main one of sources of CO production. Another source of CO is the reduction of CO_2 at higher temperature in gasification. Thus CO is the main gas evolved in the gasification of mallee biochar which increase with the increase of temperature.

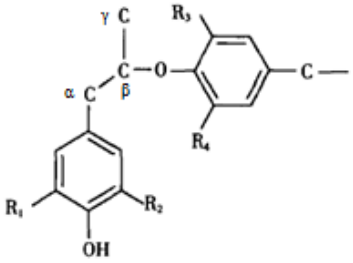

Figure 6-6: β-O-4 in lignin[229]

6.5 Effect of Oxygen Transformation on the Structure of AC

Figure 6-7 gives the pore size distribution of AB550-750, AP550-750, and AAC550-750. Figure 6-8 presents the FIB-SEM images of these three samples. As for AAC550-750, although the surface area was 570m^2/g, and similar to that of AB550-750, the pore structure is different as shown in Figure 6-7, more micropores developed and the fraction of mesopore decreased. Since pyrolysis didnot lead to the development of micropores (see the curve of AP550-750 in Figure 6-7), it should be steam gasification leading to the development of micropore. From Figure 6-8, it can be seen that biochar AB550-750 shows developed wide pore size distribution where there are amount of both micropores and mesopores. The surface area was 562m^2/g. Half pore size (A) of mesopores were at the range of 5~25A. Figure 6-8 (a) illustrates its FIB-SEM image. It is obvious that it keeps the skeleton of biochar. Comparatively, the micropore and mesopore of AP550-750 decreased slightly. The surface area decreased to 517m^2/g. It is likely to be the cause of the collapse of some mesopores during the extension of pyrolysis time. Figure 6-8 (b) shows the surface topography of AP550-750 which is similar to AB550-750. Such similarity of surface of AB550-750 and AP550-750 coincides with the value of both BET surface area. Figure 6-8 (c) shows the surface morphology of AAC550-750 is different from the other two. The surface has lost its original structure.

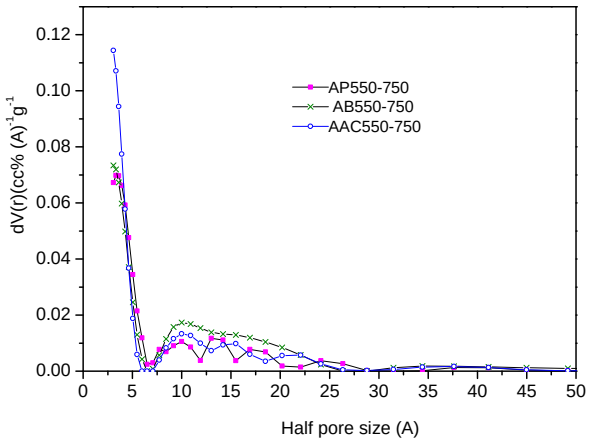

Figure 6-7: Pore size distribution of AB550-750, AP550-750, and AAC550-750 by QSDFT

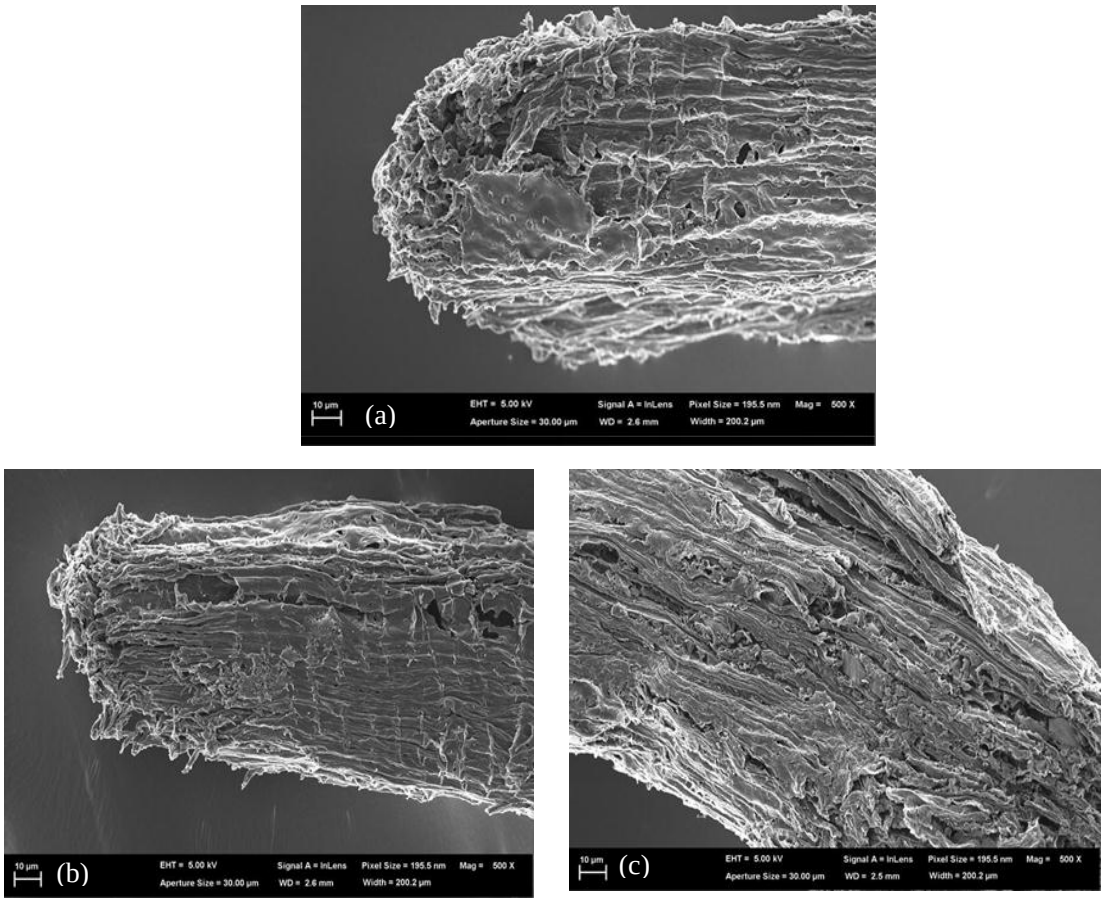

Figure 6-8: FIBSEM-images: (a) AB550-750; (b) AP550-750; (c) AAC550-750.

6.6 Conclusions

This chapter analyzed the oxygen transformation to obtain the attribution of oxygen of biochar to steam gasification.

(1) The oxygen in the evolved gases was mostly provided by steam and partly from biochar. In other words, the oxygen of biochar was also released.

(2) The value of the amount of oxygen transformation was obtained from two methods. One was from the calculation of evolved gases; the other was calculated based on the oxygen content of biochar. The oxygen transformation from biochar was about 20%.

(3) This chapter indicated that the oxygen migrated is probably from the breakage of C-O band and decomposition of methoxy group on side chain of lignin.

(4) It was observed that the oxygen migration impact on the surface area was only slight. However, pore size distribution was changed leading to increase of micropores.

CHAPTER 7 MECHANISM STUDY OF CARBON DIOXIDE GASIFICATION OF MALLEE BIOCHAR

7.1 Introduction

CO_2 (aerodynamic diameter 0.33nm) and steam (aerodynamic diameter 0.27~0.32nm) are two common gases used as gasification agents for AC production. Although carbon dioxide is not used as much as steam industrially, it is the preferred agent used at laboratory level due to its relatively slow reaction and being easy to control.[230] CO_2 is a greenhouse gas and it can be usefully used as a gasification agent. Von[231] put forward Langmuir–Hinshel rate expression (equation 7-1) could be used to describe gasification rate.

$$r_m = \frac{k_a p_n}{1 + k_b p_n + k_c p_m} \qquad (7\text{-}1)$$

Where P_n, P_m, n=CO_2, m=CO

Carbon dioxide gasification reaction is an endothermic reaction. Usually, temperature of CO_2 gasification is about 850℃~1000℃ and is higher than that of steam gasification at around 750℃~1000 ℃. Figure 7-1 presents the composition of the equilibrium mixture as a function of temperature. It is obvious that an increase of temperature favors the reaction. Adopting a lower temperature at 750 ℃ led to a slower reaction rate allowing a better control of the gasification process. [232]

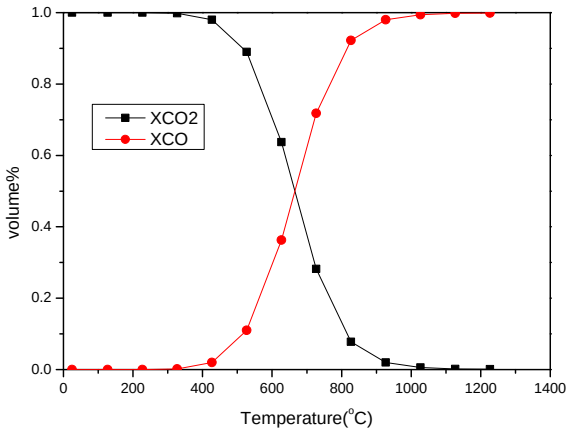

Figure 7-1:Composition of the equilibrium mixture of CO_2 and CO as a function of temperature[233]

The gasification mechanisms of steam and carbon dioxide are different. As discussed in Chapter 2.6.4， it is believed that CO_2 plays a role to widen micropores in the late stage and steam widen micropores in the early stage. [234] The effect of steam gasification was prominent resulting in more macropores and mesopores than that of CO_2 gasification.[90] However, kinetic studies of CO_2 gasification of waste biomass fuels and the effect of mineral matter on specific reactivity are limited.[16, 134, 235]

Thus this chapter aims to understand the evolution of carbon structure and specific reactivity during gasification and the influence of inorganic species on CO_2 gasification. Therefore, the behaviour of raw wood particle in pyrolysis/CO_2 gasification was studied. Apart from that, the roles of CO_2 and H_2O in the evolution of pore structure were analyzed.

7.2 Chemical Reaction Control during CO_2 Gasification

To investigate the mechanism of the reaction between carbon and carbon dioxide, the reaction should be controlled in the regime of chemical reaction control so that the CO_2 gas concentration is consistent and gasification takes place uniformly inside the particle. It was reported that smaller char particle sizes (<300 μm) and lower temperatures (below about 1000 ℃) will normally make the reaction of C-CO_2

reaction in the regime of chemical reaction control. [236,237] The reaction takes place nearly uniformly throughout the interior surfaces of the char particles.[236,237] However , smaller pulverized char particles (<100 μm) and high temperatures (>1100 ℃) lead to pore diffusion.[238]

Initially, a series of experiments were designed to prove the reaction was run in chemical reaction control. Such experiments were done by Vlad Curteanu in our research team (unpublished data). The experimental conditions included temperature 750℃, two rates between CO_2 and argon, and two sample sizes were used in tests: (1) sample size 100 μm ~250μm, CO_2 at 0.19L/min diluted in 2.33L/min argon; (2) sample size 106~150μm CO_2 at 0.093L/min diluted in 1.166L/min argon; (3) sample size 106~150μm CO_2 at 0.19L/min diluted in 2.33L/min argon. Encinar[21] found that for the particle size about 500μm and temperature below 1000℃ the gasification was reaction controlling. According to this result, the gasification under the flow rate of 3L/min of argon was chemical reaction control reaction.

As discussed in Chapter 5.3, inherent of oxygen of biochar transformed during steam gasification. To make the results comparable between steam gasification and CO_2 gasification, biochar used for CO_2 gasification should experience the same thermal decomposition history. Therefore, the same pyrolysis process as that used for steam gasification namely 750℃ and gas flow rate 3L/min were applied in this paper. The experimental work was carried out at atmospheric pressure.

7.3 Biochar Reactivity during CO_2 Gasification

7.3.1 Process of CO_2 Gasification

During the process of gasification, the process of pyrolysis occurs concurrently. Two possible mechanisms of the reaction between carbon and carbon dioxide were put forward. One is the interface reaction through adsorption,[239] the other is interface

reaction without the effect of adsorption.[240] Ergun suggested a reasonable reaction mechanism: (1) certain carbon atoms can obtain oxygen atoms from CO_2 molecule reducing CO_2 to CO and form an occupied site. The reaction is reversible. CO can remove the oxygen from occupied sites to form CO_2 and C_f (surface active site of biochar). [239] This process is shown in reaction (7-2).

$$C_f + CO_2 \Leftrightarrow C_f(O) + CO \quad (7\text{-}2)$$

(2) A carbon originating from occupied sites transfers from solid phase to gas phase:

$$C_f(O) \rightarrow C_f + CO \quad (7\text{-}3)$$

C_f is surface active site of biochar. This is the slowest step of the reactions. Feng suggested the interface reaction was completed by collision of CO_2 and carbon. [240]

The rate of interface reaction through adsorption was lower while the reaction without adsorption was quicker. The effect of adsorption disappeared in faster gasification stage.[241] Chen believed that besides $C_f(O)$, new compound $C_f(O)C(O)$ was formed. This structure was less stable than $C_f(O)$ and decomposed at lower temperature easily. [242]

7.3.2 Variables Affecting the Specific Reactivity of CO_2 Gasification

Gasification rate heavily depends on the concentration of active sites and their accessibility to the reactant gas, as well as inorganic impurities.[214,215]

- ***Interface reaction gasification energy***

As discussed above, chemical adsorption is concurrent with gasification. The adsorption rate may increase initially then decrease till disappear with the increase of carbon conversion.

Adsorption take place at the edge of microcrystal due to the higher adsorption ability of carbon atom or vacancy resulted from desorption of CO.[241] As for the pure graphite (99.999%) the activated energy of adsorption was 23.7~40.2KJ mol^{-1} which was much lower than the gasification energy of interface reaction through adsorption 183.5~213.5KJ mol^{-1}. [241] Therefore, gasification rate is controlled by interface reaction through adsorption.With the consumption of adsorption sites, interface reaction plays a dominant role. The gasification energy of interface reaction was 142.2 $KJ.mol^{-1}$~187.4 $KJ.mol^{-1}$ which is lower than the activated energy of interface reaction through adsorption at 183.3 $KJ.mol^{-1}$ ~213.5 $KJ.mol^{-1}$.[241] Therefore, the gasification is controlled by interface reaction.

- ***Temperature***

Temperature is one of the most important factors influencing the rate of chemical reaction. Theoretically, increase of temperature will accelerate the reaction between carbon and carbon dioxide. As discussed in Chapter 2.6.4, higher temperature is required for the reaction between carbon and carbon dioxide than that in steam gasification.

Figure 7-2 shows the curves of specific reactivity as a function of carbon conversion of raw biomass biochar at 750℃ and 850℃. Both curves decrease initially then increase afterwards. One of the reasons for this phenomenon was due to the catalytic effects of catalysts (AAEM as shown in Table 7-1) in the biochar (described in Chapter 5.3.3). These catalysts were easy to contact with CO_2; therefore, the initial rate of the reaction of carbon and carbon dioxide was higher. Another reason is the higher adsorption ability of carbon atom on the edge of microcrystal and vacancy resulted from desorption of CO. At this stage, the interface reaction through adsorption played a dominate role. With the process going, proportion of these very reactive carbons and vacancies decreased gradually, so that the specific reactivity starts to decrease. However, new catalytic active sites were left as the consequence of

removal of carbon atoms and reaction was at the interface, thus specific reactivity started to increase.

Table 7-1: Properties AC under different carbon conversions

Carbon conversion % (gasification time min)	AAEM content(%db) Na[b]	K[b]	Mg[b]	Ca[b]
[a1]1(1)	0.1807	0.5018	0.2697	1.0359
[a1]7(5)	0.1875	0.4963	0.2729	1.0923
[a1]15(13)	0.2049	0.5445	0.2869	1.0708
[a1]26(30)	0.2451	0.5927	0.3603	1.3693
[a1]41(58)	0.2652	0.7671	0.3538	1.2833
[a2]11(5)	0.2026	0.6209	0.3067	1.3038
[a2]59 (30)	0.4030	1.2929	0.4631	1.8940

a1:750℃+750℃ means both temperature of pyrolysis and gasification were 750℃;

a2 850℃+850℃; [b]Analysed by IC.

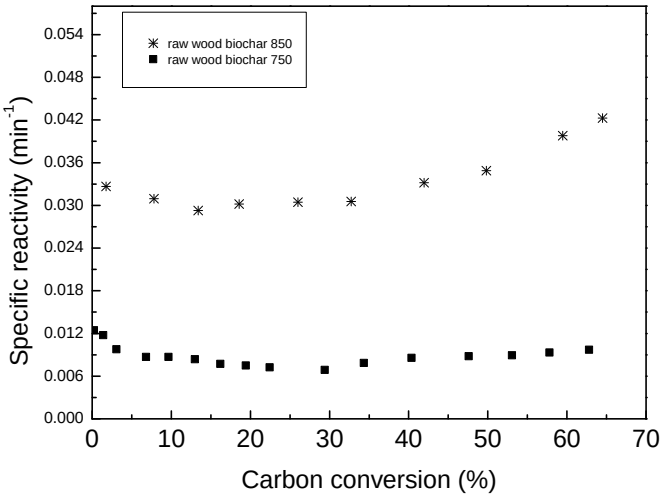

Figure 7-2**:** Specific gasification reactivity of raw biochar as a function of carbon conversion for CO_2 gasification at 750℃ and 850℃ with CO_2 concentration of 7.6%

It is obvious that at higher temperature at 850℃, as expected, the specific reactivity increased.[243] There is a relatively higher value 0.033min^{-1} of specific reactivity and a steeper increase at higher carbon conversion compared with the curve at 750℃ with

specific reactivity at 0.012min^{-1}. The possible reason was higher ash content of biochar obtained at 850℃ which will be discussed in Chapter 7.4.1.

AAEM content

Figure 7-3 shows the curves of specific reactivity as a function of carbon conversion of raw biomass biochar and acid washed biochar at 750℃. The curve of raw biochar decreases initially till 30% carbon conversion then increases afterwards. The shape of curve indicates the catalytic effect is not saturated. [10] In contrast, the curve of acid washed biochar decreased slightly in the initial stage until about 8% carbon conversion, then increased afterwards and remained nearly stable during the course of CO_2 gasification. Generally speaking, acid washed biochar showed much lower specific reactivity, as expected. These results suggest the important catalytic effect of inorganic matter. The AAEM content of AC obtained via CO_2 gasification at 750℃ and 850℃ are shown in Table 7-1. From Table 7-1, the AAEM content of AC at 750℃ presents the higher content of potassium and calcium, and the order of content of AAEM is Ca> K >Mg> Na. Generally, AAEM content increases slightly before 15% carbon conversion followed by a quicker increase to 26% carbon conversion. Figure 7-2 also shows the increase of specific reactivity started at around 29% indicating more intensive catalytic effect of AAEM due to the increase of rate between AAEM and carbon.

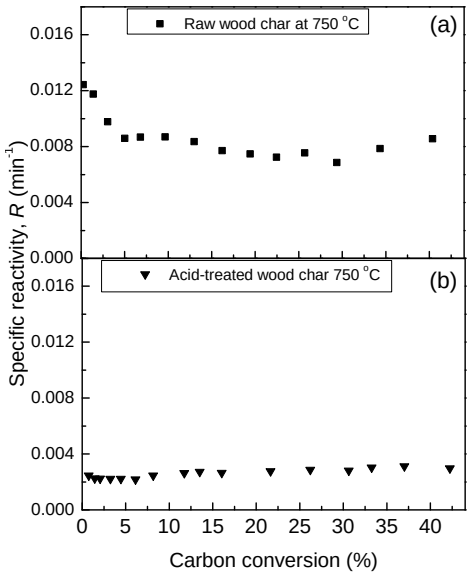

Figure 7-3: Specific gasification reactivity of raw wood char (a) and acid washed biochar (b) as a function of carbon conversion for CO_2 gasification at 750℃

7.3.3 Evolution of Intrinsic Gasification Reactivity

The above specific reactivity is based on the "overall " reactivity of all active sites. To obtain the effect of carbon structure on the specific reactivity, the specificity of biochar was normalized by surface area as shown in Figure 7-4. It was believed for highly disordered carbon material the surface area could be approximately the number of active sites. [244,245,246, 247]

Specific reactivity per unit pore surface area ($g.min^{-1}m^{-2}$) of wood biochar could be treated as intrinsic reactivity of biochar. [132, 221-224] Figure 7-4 described the reactivity per unit pore surface area of wood biochar and retention of AAEM contents (Na, K, Mg, and Ca). It shows the reactivity per unit pore surface area decreased rapidly below 15% carbon conversion but remained unchanged per unit pore surface area at higher carbon conversion. The initial peak of reactivity per unit pore surface area is attributed to the "fresh" active site and vacancy. The slight change of reactivity per unit pore surface area with carbon conversion suggested carbon structure changed

slightly with the increase of carbon conversion at the current carbon conversion range. The figure also shows the AAEM retention during the course of CO_2 gasification. It can be seen the AAEM retention was virtually right through all the carbon conversion (up to 40% carbon conversion). It proves again the activate sites attribute more to the specific reactivity. Despite of slight decrease of Mg and Ca (as shown in Table 7-1), the specific reactivity still increased during the course of gasification. Therefore, it may be deduced that K and Na play more important catalytic roles.

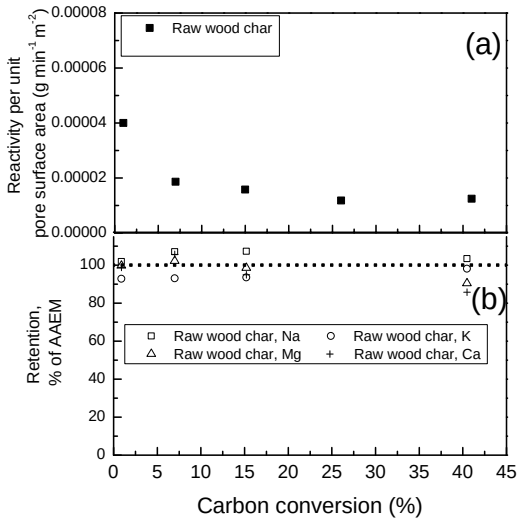

Figure 7-4: Reactivity per unit pore surface area of wood biochar (a) and retention of AAEM contents (Na, K, Mg, and Ca) (b); (750℃ pyrolysis, holding 15min and CO_2 gasification at 750℃).

7.3.4 Mallee Leaf Biochar Reactivity during CO_2 Gasification

Figure 7-5 gives the curve of specific reactivity against carbon conversion of leaf biochar at 750℃. It can be seen that the shape of the curve is different for the curve of wood biochar (see Figure 7-2). Unlike the curve of wood biochar, the specific reactivity of leaf biochar increases continuously with the increase of carbon conversion. As expected, leaf biochar has higher specific reactivity as the consequence of higher ash content of biochar (see Table 5-1). The ash content of leaf

biochar is 14.9% which is three times higher than that of wood char. Therefore the catalytic effect of AAEM played a dominate role and the effect of adsorption can be ignored. Therefore, it should be noted the important role played by the inorganics in the char reactivity.

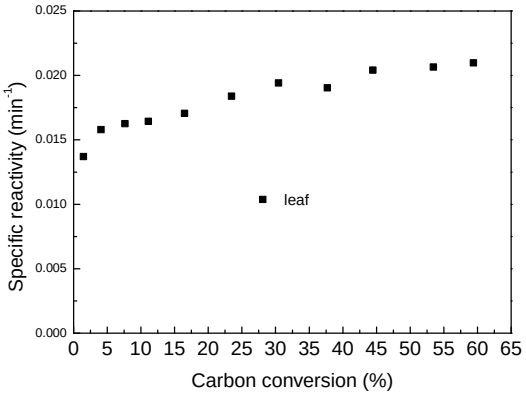

Figure 7-5: Specific gasification reactivity against carbon conversion of leaf at 750℃

7.4 Evolution of Mallee Biochar Structure during CO_2 Gasification

7.4.1 Evolution of Chemical Composition of Biochar

AC produced under different carbon conversions were collected and analyzed to obtain the evolution of their chemical compositions. Table 7-2 shows elemental analyses and proximate analysis of AC. Generally, moisture and ash contents are nearly the same while fixed carbon content decreases slightly. During the gasification both incorporation and elimination of carbon atom is happening with one dominating.[165] In Table 7-2, the increase of the gasification time from 1 to 58 min at temperature 750℃ led to the decrease of the carbon content of AC from 87.3% to 83.5%. However, hydrogen content increased with the process of gasification from 0.55% to 1.14%. Such decrease of carbon content is attributed to the increase of consumption of carbon resulting in correspondent increases of the fraction of the nitrogen and oxygen contents. Another reason for it could be the more oxygen introduced from CO_2 into AC during the course of CO_2 gasification could have led to

higher content of oxygen.[50,118,124] The two-site surface complex structure could be lactone-type as shown in Figure 7-6.[124]

Table 7-2: Proximate properties of AC obtained under different carbon conversion

Carbon conversion% (gasification time min)	Moisture (% ad)	Proximate(wt% db)			Ultimate analysis (wt% daf)		
		FC[b]	VM[c]	Ash	C	H	N
[a1] 1 (1)	3.7	79.0	16.2	4.8	87.35	0.55	1.05
[a1] 7 (5)	3.6	77.4	17.7	4.9	86.70	0.70	0.77
[a1] 15 (13)	3.7	76.9	17.4	5.4	85.39	0.76	0.68
[a1] 26 (30)	3.8	75.8	19.3	4.9	84.29	0.62	0.42
[a1] 41 (58)	3.5	75.7	19.7	4.6	83.51	1.14	0.99
[a2] 11(5)	2.00	80.9	13.6	5.5	81.2	0.7	0.4
[a2] 59 (30)	2.91	77.5	13.0	9.5	78.7	0.4	0.4

[a1] 750+750 AC obtained by the pyrolysis and CO_2 gasification at 750℃; [a2] 850+850 AC obtained by the pyrolysis and CO_2 gasification at 850℃; [b]Fixed carbon（FC）, [c]Volatile matter(VM).

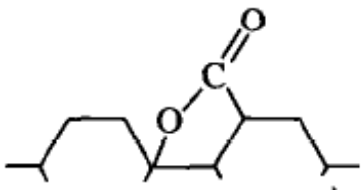

Figure 7-6: Examples of oxygen functional groups on carbon surfaces[124]

The results in Table 7-2 also show the reaction of carbon and carbon dioxide occurring at both temperature 750 ℃ and 850℃. After 30 min gasification, the carbon content of AC was 84.29 % at 750 ℃ decreased to 78.7% at 850 ℃. Their carbon conversions were 59 % at 850 ℃ and only 26% carbon conversion was obtained at 750 ℃.

As shown in Table 7-2, the ash content of AC obtained at 850℃ was generally higher than that of AC obtained at 750℃. As for AC obtained at 750℃ with 41%

carbon conversion and 850℃ with 59% carbon conversion, their ash contents were 4.6% and 9.5 % respectively.

To further understand the pore structure evolution of AC with the CO_2 gasification, Raman spectroscopy and FTIR were used to obtain structural information of AC.

- ***FTIR spectrum***

FTIR was applied to obtain the function groups of AC. Results shown there were no obvious observable peaks in FTIR spectrum of AC obtained from CO_2 gasification at 750℃. This indicated only small amount of functional groups existed on the surface of AC.

- ***Raman spectrum***

Figure 7-7 shows the D band, (Gr+Vr+Vl), and their ratio as a function of carbon conversion. Raman band assignment was summarized in Table 3-4.[178] It can be seen from Figure 7-7, D band decreased slightly when carbon conversion was lower than 7%. A slight increase was also observed for D band from 0.19 to 0.22 with the increase of carbon conversion from 7% to 41%. Meanwhile, (Gr+Vr+Vl) band kept nearly stable. The increase of D bands indicated the development of the ordered structure during the course of CO_2 gasification. As expected, the ratio of (Gr+Vr+Vl) to D decreased, although, slightly from 2.0 to 1.8 with increase of carbon conversion demonstrating the evolution of ordered structure of biochar.

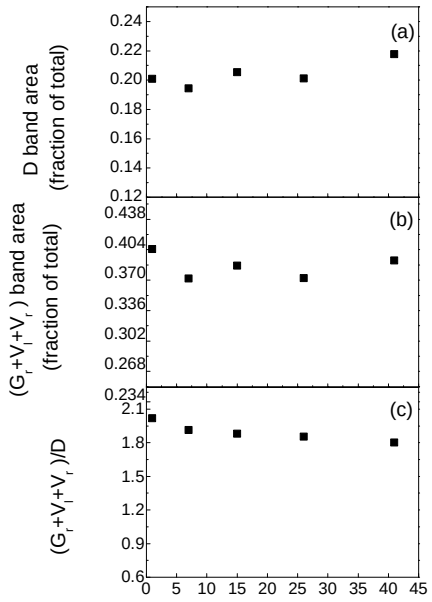

Figure 7-7: Peak area of D band (a) and (Gr+Vr+Vf) band (b), and ratio of (Gr+Vr+Vf)/D (c) as a function of carbon conversion

S band, another important band of biochar, represents $C_{aromatic}$-C_{alky}, aromatic (aliphatic) ether, C-C on hydro aromatic rings, and C-H on aromatic rings. Figure 7-8 gives the peak area of S band against carbon conversion. There is a general decrease of S band with the process of CO_2 gasification. The significant decrease in the initial stage is likely attributed to the pyrolysis of biochar.

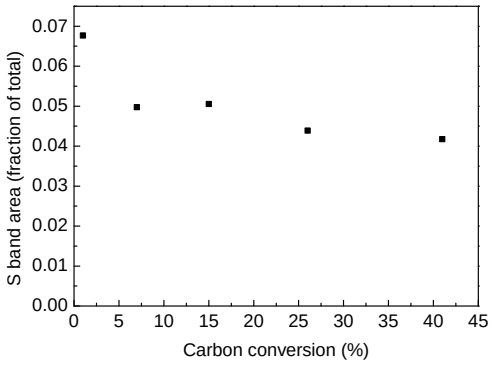

Figure 7-8: Peak area of S band as a function of carbon conversion

G band represents the graphite structure, aromatic ring quadrant breathing, and alkene C=C. Figure 7-9 shows the peak area of D and G/D. G band increased from 0.09 at carbon conversion 1% to 0.11 at carbon conversion 7%. After that, G band

decreased and increased again from 0.08 to 0.11 with the increase of carbon conversion from 15 to 41%. Similarly, the rate of G/D increased from 0.45 to 0.59 followed by a decrease to 0.39 then increased to 0.53. The tendency of G/D after 10% carbon conversion is similar with others.[248]

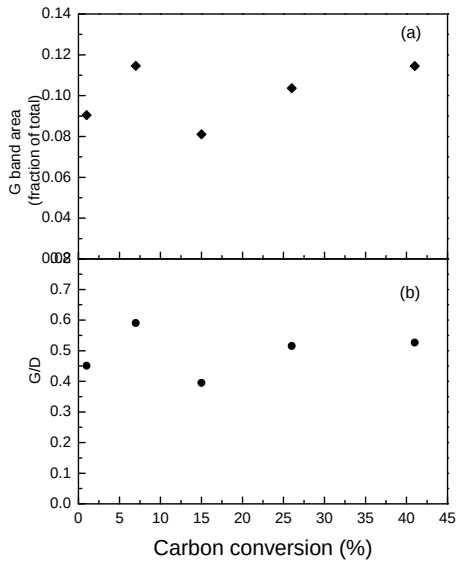

Figure 7-9: G band area (a) and the ratio of G/D (b) as a function of carbon conversion

7.4.2 Evolution of Surface Structure of Biochar

To investigate the evolution of pore structure, CO_2 gasification experiments with various conversion levels were carried out. Figures 7-10(a) and 7-10(b) show the adsorption-desorption isotherms of AC obtained at 750℃ and 850℃ respectively. It is clearly visible that the porosity developed well as indicated in Table 7-3. Figure 7-11 presents BET surface area of AC produced. Similar to the isotherm obtained under steam gasification of biochar, all isotherm of AC are of the same type. The knees of the isotherm are broader, and the plateaus are steep. It is obvious that hysteresis loops were present (see Figure 7-10).

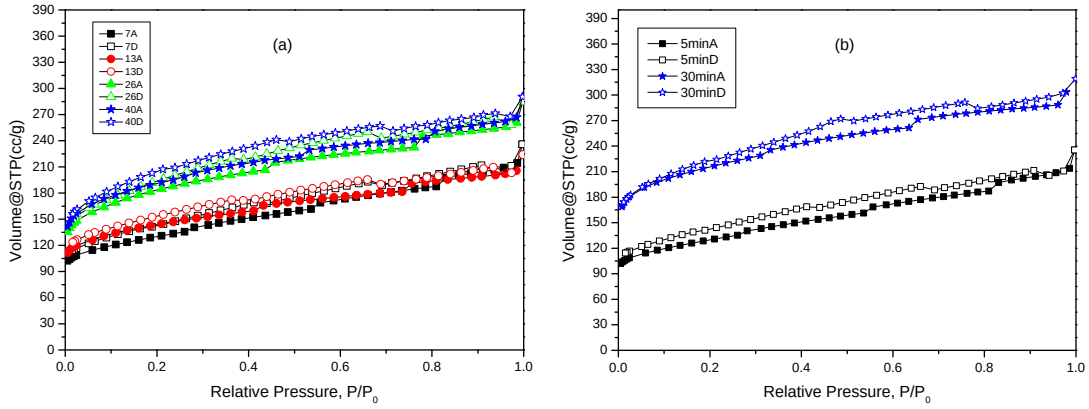

Figure 7-10: N_2 adsorption-desorption isotherm at 77K of AC produced from biochar via CO_2 gasification with various carbon conversion (a) 750℃, (b) 850℃

(A means adsorption, D means desorption; the same shape of symbol means the same sample while open one means desorption curves and solid one means adsorption curves); ×A(D) means adsorption(desorption) curve of AC obtained with × carbon conversion or × gasification time

Under current experimental conditions, surface area of AC increased firstly with increase of carbon conversion, however, it decreased with further increase of carbon conversion. This is shown in Table 7-3 and Figure 7-11, surface area of AC increased from 584 m^2/g to 639 m^2/g after 30min CO_2 gasification but followed by decrease back to 581m^2/g with around 80min gasification. It suggested that there is an optimum gasification time and further gasification may have a negative effect on the evolution of pore structure. Table 7-3 shows the increase of both Vd and SBET indicating the development of pore structure with increasing carbon conversion. The micropore volume increased from 0.1cc/g to 0.29 cc/g when the carbon conversion increased from 1% to 41%. The continuous increase of percentage of micropore occurred during the course of CO_2 gasification. On the other hand, the value of the mesopore changed slightly. The increase of both micropores and mesopores indicate the occurrence of widening micropores and creating new micropores. [249] The opening up of closed micropores and the enlargement of opened micropores are the consequence of the gasification which removes carbon atoms from the interior of the particle.[168] Table 7-4 also shows activated carbon obtained with shorter gasification

time 30 min at higher temperature 850℃ had lower the average pore diameter of 7.98Å, higher micropore volume of 0.32 cc/g, and higher total volume of 0.49 cc/g compared with that of AC obtained at 750℃ with 60 min gasification whose corresponding values were 8.28Å, 0.29 cc/g, and 0.45cc/g. It suggested that higher temperatures favored exothermic reducing reactions and pore development.

It is believed the value of pore size and pore size distribution is one of the most important parameters which can describe the nature of adsorbate.[250] During the adsorption process of AC, pore size distribution determines the accessibility of adsorbent to the surface of adsorbate.[251] Therefore, Figure 7-12 presents the pore size distribution by the quenching solid density function theory (QSDFT).

As shown in Table 7-3, there is no obvious change of surface area at similar carbon conversion for gasification temperatures of 750℃ and 850℃. However, the average pore diameter calculated from DR decreased slightly from 7.61Å to 7.39Å with the increase of temperature. This result suggested that pore deepening may be the predominant mechanism at high temperatures.[91]

Table 7-3: Characteristics of AC obtained at the different level of carbon conversion

Carbon Conversion (%)(TIME)	SBET (m^2/g)	DR		Total volume (cc/g)
		AHPW(Å)	Vd (cc/g)	
[a1]1(1)	285	10.33	0.10	0.31
[a1]7(5)	427	7.39	0.19	0.36
[a1]15(13)	446	7.61	0.21	0.35
[a1]26(30)	584	8.27	0.27	0.44
[a1]41(58)	639	8.68	0.29	0.45
[a2]11(5)	422	7.39	0.19	0.36
[a2]59 (30)	670/697	7.98	0.32	0.49

a1 750+750 AC obtained by the pyrolysis and CO_2 gasification at 750℃; a2 850+850 AC obtained by the pyrolysis and CO_2 gasification at 850℃; SBET: surface area (m^2/g) based on Stephen Brunauer, Paul Hugh Emmett, and Edward Teller equation SBET; DR: Dubinin-Radushkevich equation; Total volume obtained at p/p_0=0.9998(cc/g); Vd: micropore volume from DR plot (cc/g) ; AHPW: average half pore width from DR plot (Å).

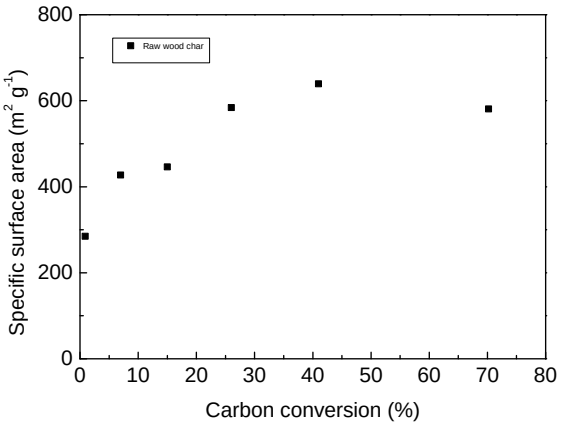

Figure 7-11: Surface areas as the function of carbon conversion during the course of carbon dioxide gasification (750℃ pyrolysis holding 15min, 750℃ CO_2 gasification)

It can be seen in Figure 7-12 that the peak points occurring at around 2.5 Å half pore width clearly indicating the fact that micropores made an important contribution to the overall pore structure.[163] However, longer gasification time led to the decrease of the BET surface area. The decrease of surface area was due to the widening[252] and eventual collapse of pore walls ,[235] and a shrinkage of the carbon structure as well.[192]

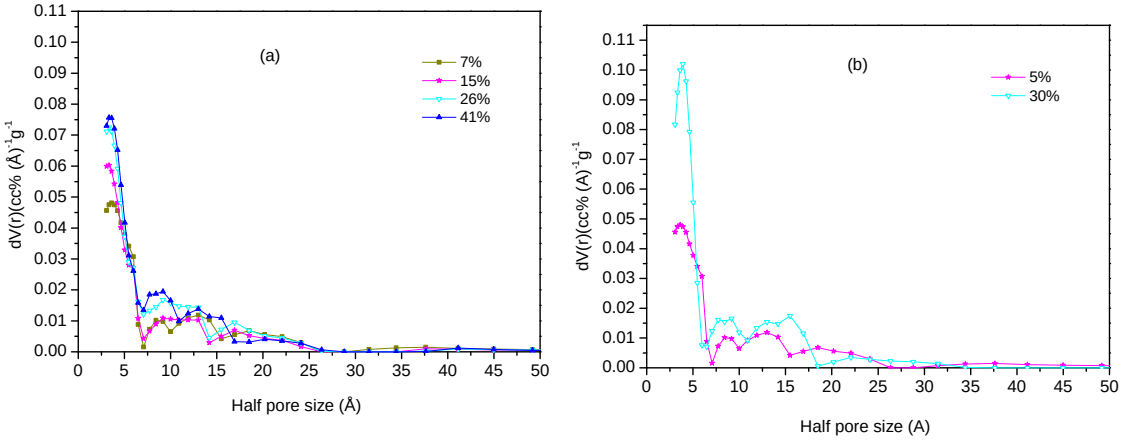

Figure 7-12: Pore size distribution by QSDFT for AC under low carbon conversion (× %) ((a) 750℃ pyrolysis holding 15min, 750℃ CO_2 gasification (b) 850℃pyrolysis holding 15min, 850℃CO_2 gasification)

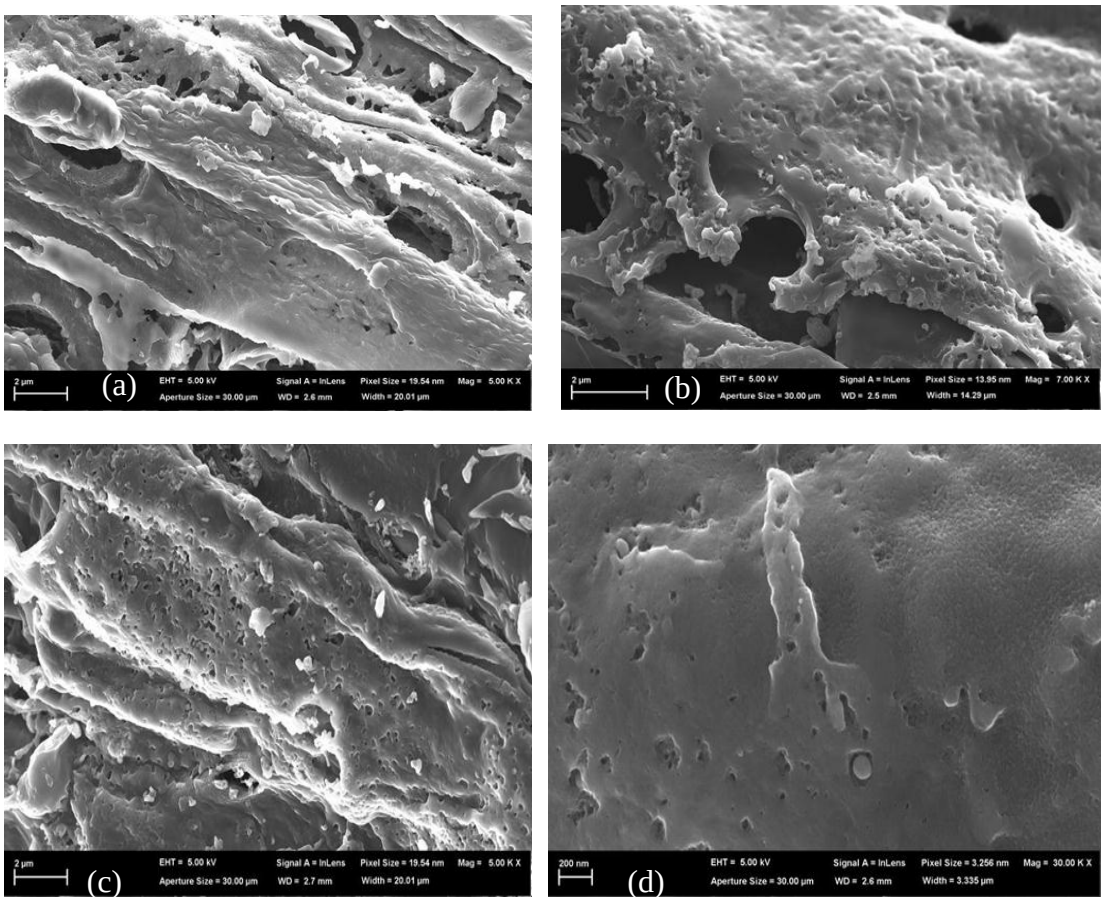

Figure 7-13: Morphology of AC images of AC obtained under different carbon conversions at 750℃ CO_2 gasification: (a) 1% (b) 7% (c) 15% (d) 41%

7.5 Gas Evolved during CO_2 Gasification

During CO_2 gasification at 750℃, pyrolysis took place concurrently. However, CO is the main product from the reaction of carbon dioxide and carbon. Due to the low concentration of H_2 and CO_2 produced from pyrolysis, only the evolution of CO was discussed in this chapter.

Figure 7-14 presents the carbon monoxide concentration of leaf biochar at 750℃ and wood biochar at 750 ℃ during CO_2 gasification. Both curves showed dramatically increases of CO in the initial stage but decrease afterwards. This shape of curve is similar with the pyrolysis/gasification of olive bagasse.[21] Chapter 5.3.3

described the well dispersed AAEM on the biochar. The catalyst effect of AAEM favoured the reaction of carbon and carbon dioxide. Therefore there is a peak production rate in the initial stage. In the case of leaf, CO decreased gently after its peak. This was the consequence of higher AAEM content of leaf biochar. The reaction was in the fast gasification stage.

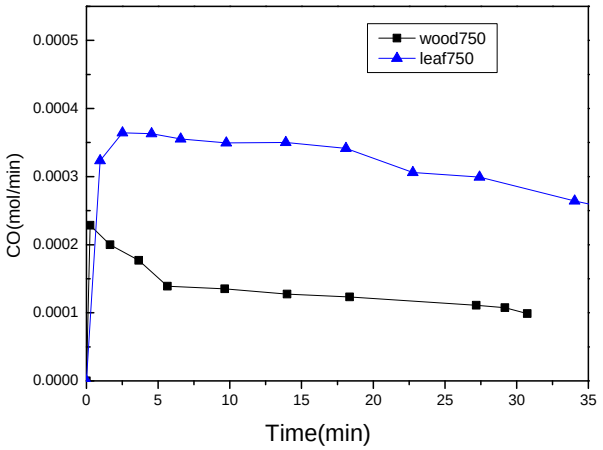

Figure 7-14: Carbon monoxide production rate during gasification of leaf biochar and wood biochar at 750 ℃; leaf (wood) 750 means AC obtained via pyrolysis and gasificaion of leaf (wood) at 750℃.

7.6 Comparison of Mechanisms of Steam and CO_2 Gasification

7.6.1 Specific Reactivity

Figure 7-15 presents specific gasification reactivities as a function of carbon conversion with CO_2 and steam gasification at 750℃. It can be seen that the specific reactivity obtained using different gasification agent were similar at low carbon conversions up to 10%. The specific reactivity of CO_2 gasification was lower than H_2O gasification at higher carbon conversion. The difference between both curves became more significant with increase of carbon conversion. The curve of steam

gasification started to increase from around 10% carbon conversion while the curve of CO_2 gasification started to increase only from around 27% carbon conversion.

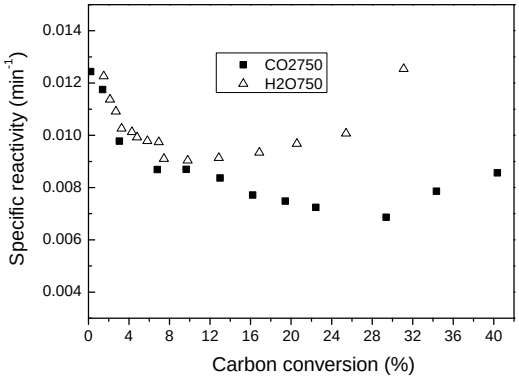

Figure 7-15: Specific gasification reactivity as a function of carbon conversion for CO_2 gasification and steam gasification at 750℃; symbol CO_2 (H_2O) 750 means AC obtained via pyrolysis and CO_2 (H_2O) gasificaion at 750℃.

As discussed in Chapter 5.3.3, the active sites and well dispersive AAEM on the surface of biochar led to good contacts between carbon and gasification agents. Higher specific reactivity of both CO_2 and steam gasification were obtained at the early stage of gasification. With the consumption of active sites, there were less active sites available resulting in decrease of the specific reactivity. With the progress of gasification, new active sites could be available as a result of depletion of carbon and the ratio between AAEM and carbon increase. Therefore specific reactivity started to increase again. Unlike steam gasification, CO_2 gasification experienced a longer decreasing period and the specific reactivity increased relatively slowly after turning around at 27% carbon conversion. At higher carbon conversions, lower reactivity of carbon dioxide could be due to three reasons: (1)750℃ is relatively lower for CO_2 gasification; (2) the diffusion effect caused by the bigger size of carbon dioxide molecule[91] which is difficult to enter into 1.5nm pore; (3) more stable oxygen groups were formed during carbon dioxide gasification

than that in steam gasification, these groups can remain longer on the carbon surface during thus leading to the lower reactivity.[98]

7.6.2 Evolution of Surface of Biochar

Figure7-16 presents the surface area as function of carbon conversion during the course of steam gasification and carbon dioxide gasification. One can see at similar carbon conversion steam gasification led to higher BET surface area than CO_2 gasification especially under higher carbon conversion. For instance, when carbon conversion is 7%, the BET surface area obtained under CO_2 gasification and H_2O gasification are 427 m^2/g and 526m^2/g, while at around 30% carbon conversion the value is 584 m^2/g and 785 m^2/g.

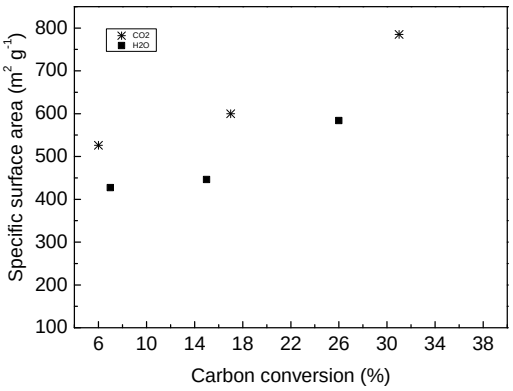

Figure 7-16: Surface areas as the function of carbon conversion during the course of steam gasification and carbon dioxide gasification

Figure 7-17 shows the pore size distribution by QSDFT for AC via CO_2 and H_2O gasification at different carbon conversions. It shows that both CO_2 and steam gasification led to a large volume of micropore by continuously creating new micropores when carbon conversion was below around 30%. When steam gasification carbon conversions were 6%, 17%, and 31%, the peaks of curves were 0.086, 0.102, and 0.115 cc $(Å)^{-1}$ g^{-1} respectively. While for CO_2 gasification carbon conversions were 7%, 15%, and 26%, the peaks were 0.048, 0.06, and 0.073 cc $(Å)^{-1}$. It suggests steam gasification produced a higher portion of micropore compared with

carbon dioxide. As shown in Figure 7-17 (b), both CO_2 and steam gasification gave rise to larger increase of mesopores. The main fraction of mesopore was at the range of 2nm~5nm. Generally, steam gasification resulted in more mesopores than CO_2 gasification at similar carbon conversions. It suggested that the role of steam was widening of the micropores. Under current experimental condition, CO_2 gasification did not result in more micropores than that in steam gasification. It is the consequence of relatively lower temperature of 750℃ for CO_2 gasification. Finally the decrease of micropore was due to the breaking through of pore walls.[253, 254] There are two reasons for the above phenomena. The first reason is that CO_2 gasification required higher temperature than steam gasification. In other words, 750℃ was not high enough for faster CO_2 gasification. The second reason is that steam could enter into 0.6nm pores easily. This is why steam gasification favoured the development of mesopores.

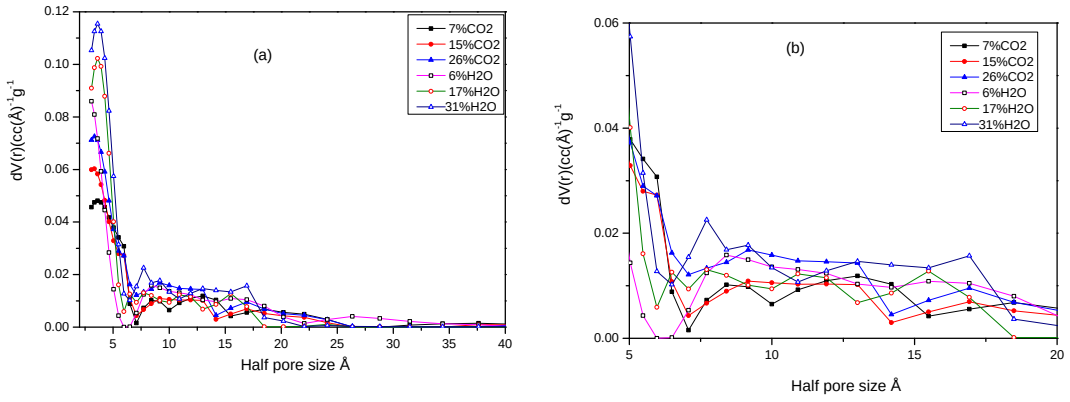

Figure 7-17: Pore size distribution by QSDFT for AC via CO_2 and H_2O gasification at different carbon conversion (open note means steam gasification, close note means CO_2 gasification (× %)) (b) is magnified area of part curve (a).

7.6.3 Raman Spectrum

The curves of D band area of both steam and carbon dioxide gasification show the same shape namely an initial decrease followed by an increase with increase of carbon conversion. The decrease of D band area is likely due to the molecular

fragments of lignin. With increase of gasification, more aromatics with no less than 6 rings were formed resulting in the increase of D band. AC obtained from steam gasification had lower ($Gr+Vr+V_f$) band and higher D bands. It proved that steam gasification developed better than CO_2 gasification. Generally steam gasification of biochar has higher S band area than that of CO_2 gasification biochar. It gives the evidence that the steam gasification led to higher specific reactivity of biochar. As for G band, steam gasification gave rise to a slightly lower value. However, the ratio of G/D of biochar from both steam and carbon dioxide gasification was similar.

7.7 Conclusion

In this chapter, the mechanism of CO_2 gasification of raw wood biochar and leaf biochar were researched. Additionally, acid washed biochar was applied to understand the catalytic effect of AAEM in CO_2 gasification. Experiments were carried out under chemical reaction control and at 1 atmospheric pressure. The following conclusions can be drawn:

(1) The majority of AAEM remains due to insignificant volatilization in the course of CO_2 gasification.

(2) The specific reactivity of wood biochar decreased initially and then increased with increase of carbon conversion. The curve of leaf at 750℃ kept increasing and was much higher than that of wood biochar during the course of CO_2 gasification. This is mainly due to the effect of higher AAEM content in the leaf.

(3) At 750 ℃, steam gasification showed higher specific reactivity compared with CO_2 gasification. Steam gasification led to higher values of micropores and mesopores than that resulting from CO_2 gasification. Both CO_2 and H_2O led to the development of predominant micropores.

(4) According to the spectrum of FTIR and Raman, there are small amounts of functional group of AC. The kind of surface group changed slightly with different gasification agents.

CHAPTER 8 CONLCUSIONS AND RECOMMENDATIONS

8.1 Introduction

This chapter summarizes the key results of this PhD study. Thermal decomposition behaviour of three mallee components (leaf, bark, and wood) was investigated. Biochar obtained can be either act as carbon sequestration and soil amendments or be further gasified to produce activated carbon. Partial gasification was then carried out to improve the properties of biochars and understand gasification reaction mechanism, particularly at low conversion levels. Finally, based on the main results, some recommendations are provided for future work.

8.2 Conclusions

Pyrolysis and gasification of biomass were carried out in a fixed/fluidized bed reactor. Biomass used in this research includes raw mallee biomass (leaf, bark, and wood), acid washed mallee wood, and acid washed mallee wood biochar.

8.2.1 Pyrolysis Characteristics of Mallee Biomass

(1) Leaf and bark biochar is likely to be good soil conditioner and for recycling nutrients in biomass due to their high ash content. Wood biochar had the highest carbon content and lowest ash content which are good for activated carbon production. Experiments were carried out to investigate the effect of various operating parameters (e.g. particle size, temperature, heating rate, and holding time) on mallee biomass pyrolysis. It was found that a low temperatures (<500℃) and large particle size (1 mm ~2mm) favours biochar yield, with 1h holding time appearing to be enough for pyrolysis above 500℃.

(2) Temperature and heating rate had dramatic effect on the structure of biochar. The surface area of biochar obtained at 350℃~600℃ showed low surface areas (less than 50m^2/g). Slowing-heating biochar (SB) kept botanical structure; however, fast-heating biochar (FB) showed obvious asperities and melting surface. FB (above 350℃) had higher content of K, Mg, and Ca as well as higher content of H and O indicating more active sites.

(3) Biochar can be used for potential applications of soil amendment. The addition of biochar to soil can sequestrate CO_2 in atmosphere into the form of biochar in soil and also potentially recycling the inherent inorganic nutrients in biochar.

8.2.2 Mechanism Study of Steam Gasification of Biochar

- ***Effect of parameters on steam gasification***

(1) Both types of AC obtained from SB and FB of wood with 40min steam gasification showed higher BET surface at 943 m^2/g and 991m^2/g respectively. Thus both SB and FB had a potential to be feedstock of activated carbon preparation.

(2) For 150~250 μm sample particle, the surface area of the partially-gasified wood biochar (with 15min holding time) increased to 526 m^2/g even with only 5 min steam gasification (corresponding to a carbon conversion of 5.5 %) at 750℃. Higher carbon conversion led to higher surface area. For example, increasing carbon conversion of raw wood biochar from 5.5% to 50.0 % resulted in the increase of surface area from 526m^2/g to 819m^2/g.

(3) The raw-wood biochar has lower surface area of 270 m^2/g than that of acid-washed-wood biochar of 470 m^2/g; although, they have similar biochar yield. However, the surface area of biochar which was obtained by acid washing wood biochar showed much lower surface area of 32m^2/g.

- ***Steam gasification at low carbon conversion levels***

(1) FB showed much higher specific reactivity and gas formation than that of slow biochar at carbon conversion of below 10%. Based on syngas compositions during steam gasification, CO appeared to be more likely the primary product while CO_2 was probably derived from water-gas-shift reaction.

(2) FIBSEM images gave one possible reason for higher reactivity of mallee wood. AAEM dispersed well on the surface of biochar especially around macropores of biochar. Higher reactivity of mallee biochar meant AC with higher surface area could be obtained within a shorter gasification time.

- ***Transformation of inherent oxygen in biochar during steam gasification***

(1) Steam provided the major oxygen source during steam gasification, but some inherent oxygen of biochar (around 20%) also took part in the evolution of gaseous products especially in the initial stage of steam gasification. These indicated the existence of abundant heteroatoms of biochar and the inherent oxygen can play an important role in the steam gasification.

8.2.3 CO_2 Gasification of Mallee Biochar

(1) Different optimal parameters are required to tune biochar pore structure under H_2O gasification and CO_2. At 750℃, the specific reactivity of steam gasification was similar to that of CO_2 gasification at below 15% carbon conversion but it became higher with increase of carbon conversion. Both CO_2 gasification and H_2O gasification at 750℃ led to the development of predominant micropores. However, AC with H_2O gasification showed higher surface area and larger fraction of micropores and mesopores. CO_2 gasification led to a slower increase in the BET surface area. An optimum time of about 60 min was required to obtain the maximum of BET surface area of AC.

(2) Based on the Raman spectrum, D band of activated carbon via gasification of steam and carbon dioxide showed the same tendency, namely, initial decrease but followed subsequent increase.

(3) Unlike steam gasification, the carbon content of AC decreased with the increase of carbon conversion. The reason for that is likely to be that H_2O gasification mainly takes place on the active sites of biochar while CO_2 gasification takes place through the formation of oxygen complex. Oxygen was transformed form CO_2 and formed bigger oxygen complex which was transformed to fixed carbon through decarburization.

8.3 Recommendations

Based on the above conclusions, the suggestions of future research are as follows:

(1) Steam and CO_2 gasification appear to follow different reaction pathways. It is desired to carry out future work to investigate the fundamental mechanism governing these, under both non-catalytic and catalytic reaction conditions.

(2) In this study, controlling pore size of AC can be realized vis partial gasification. However, further study is required to examine the actual performance of AC in gas treatment or/and water treatment for the benefits of practical applications.

(3) Mechanical properties are key consideration for applying biochar or its upgraded product for AC application. Therefore, future work is certainly required to test the strength of AC. If necessary, efforts should be taken to consider pelletizing with/without adding binding agents in order to achieve optimised objectives.

(4) The use of biochar for soil applications are also important consideration. This study has shown that a small fraction of partial gasification can significantly improve the biochar properties. However, further work is required to investigate into the overall recyclability of inherent nutrient species in biochar and carry out the actual

experiments to obtain use data.

(5) Future work is also required to investigate the leachability and leaching of various inherent nutrient species in biochar under various conditions. Particularly, efforts should be taken to understand how partial gasification of biochars can effect these important aspects of biochars prepared under different conditions.

REFERENCES

1. Dave, N.; Do, T.; Palfreyman, D.; Feron, P. H. M., Impact of liquid absorption process development on the costs of post-combustion capture in Australian coal-fired power stations. *Chemical Engineering Research and Design* **2011,** 89, (9), 1625-1638.
2. IEA, "World Energy Outlook 2009", OECD/IEA, 2009.
3. Wu, H.; Fu, Q.; Giles, R.; Bartle, J., Production of Mallee Biomass in Western Australia: Energy Balance Analysis†. *Energy & Fuels* **2007,** 22, (1), 190-198.
4. Ridley, A. M.; Pannell, D. J., The role of plants and plant-based research and development in managing dryland salinity in Australia. *Australian Journal of Experimental Agriculture* **2005,** 45, (11), 1341-1355.
5. Yu, Y.; Bartle, J.; Li, C.-Z.; Wu, H., Mallee Biomass as a Key Bioenergy Source in Western Australia: Importance of Biomass Supply Chain. *Energy & Fuels* **2009,** 23, (6), 3290-3299.
6. Garcia-Perez, M.; Wang, X. S.; Shen, J.; Rhodes, M. J.; Tian, F.; Lee, W.-J.; Wu, H.; Li, C.-Z., Fast Pyrolysis of Oil Mallee Woody Biomass: Effect of Temperature on the Yield and Quality of Pyrolysis Products. *Industrial & Engineering Chemistry Research* **2008,** 47, (6), 1846-1854.
7. Wu, H.; Yip, K.; Tian, F.; Xie, Z.; Li, C.-Z., Evolution of Char Structure during the Steam Gasification of Biochars Produced from the Pyrolysis of Various Mallee Biomass Components. *Industrial & Engineering Chemistry Research* **2009,** 48, (23), 10431-10438.
8. Abdullah, H.; Wu, H., Biochar as a Fuel: 1. Properties and Grindability of Biochars Produced from the Pyrolysis of Mallee Wood under Slow-Heating Conditions. *Energy & Fuels* **2009,** 23, (8), 4174-4181.
9. Abdullah, H.; Mediaswanti, K. A.; Wu, H., Biochar as a Fuel: 2. Significant Differences in Fuel Quality and Ash Properties of Biochars from Various Biomass Components of Mallee Trees. *Energy & Fuels* **2010,** 24, (3), 1972-1979.
10. Khan, A. A.; de Jong, W.; Jansens, P. J.; Spliethoff, H., Biomass combustion in fluidized bed boilers: Potential problems and remedies. *Fuel Processing Technology* **2009,** 90, (1), 21-50.
11. Yip, K.; Xu, M.; Li, C.-Z.; Jiang, S. P.; Wu, H., Biochar as a Fuel: 3. Mechanistic Understanding on Biochar Thermal Annealing at Mild Temperatures and Its Effect on Biochar Reactivity. *Energy & Fuels* **2010,** 25, (1), 406-414.
12. Garcia-Perez, M., Fast pyrolysis of oil mallee woody biomass: effect of temperature on the yield and quality of pyrolysis products. *Industrial & engineering chemistry research* **2008,** 47, (6), 1846.
13. Garcia-Perez, M., Effects of Temperature on the Formation of Lignin-Derived Oligomers during the Fast Pyrolysis of Mallee Woody Biomass. *Energy & fuels* **2008,** 22, (3), 2022-2032.
14. Jun Shen; Xiao-Shan Wanga; Manuel Garcia-Pereza; Mouranta, D.; Rhodesa, M. J.; Chun-Zhu Lia, Effects of particle size on the fast pyrolysis of oil mallee woody biomass. *Fuel* **2009,** 88, (10), 1810-1817.
15. Patnukao, P.; Pavasant, P., Activated carbon from Eucalyptus camaldulensis Dehn bark using phosphoric acid activation. *Bioresource Technology* **2008,** 99, (17), 8540-8543.
16. Arriagada, R., Steam and carbon dioxide activation of Eucalyptus globulus charcoal. *Journal of chemical technology and biotechnology* **1994,** 60, (4), 427-433.

17. Encinar, J. M., Catalysed and uncatalysed steam gasification of eucalyptus char: influence of variables and kinetic study. *Fuel and Energy Abstracts* **2002,** 43, (4), 267-267.

18. Tancredi, N.; Cordero, T.; Rodriguez-Mirasol, J.; Rodriuez, J. J., CO_2 gasification of eucalyptus wood chars. *Fuel* **1996,** 75, (13), 1505-1508.

19. Pimenta, A. S.; Vital, B. R.; Bayona, J. M.; Alzaga, R., Characterisation of polycyclic aromatic hydrocarbons in liquid products from pyrolysis of Eucalyptus grandis by supercritical fluid extraction and GC/MS determination. *Fuel* **1998,** 77, (11), 1133-1139.

20. Tancredi, N.; Corderoa, T.; Rodríguez-Mirasola, J.; Rodrígueza, J. J., Activated carbons from Uruguayan eucalyptus wood. *Fuel* **1996,** 75, (15), 1701-1706.

21. Encinar, J. M.; Beltrán, F. J.; Ramiro, A.; González, J. F., Pyrolysis/gasification of agricultural residues by carbon dioxide in the presence of different additives: influence of variables. *Fuel Processing Technology* **1998,** 55, (3), 219-233.

22. Bell, S. J.; Barton, A. F. M.; Stocker, L. J., Agriculture for health and profit in Western Australia: The Western Oil Mallee Project. *Ecosystem Health* **2001,** 7, (2), 116-121.

23. Wu, H.; Fu, Q.; Giles, R.; Bartle, J., Production of Mallee Biomass in Western Australia: Energy Balance Analysis. *Energy Fuels* **2008,** 22, (1), 190-198.

24. Bartle, J.; Cooper, D.; Olsen, G.; Carslake, J., Acacia species as large scale crop plants in the Western Australian weatbelt. *Conserv. Sci. West. Aust.* **2002,** 4, 96.

25. Bartle, J.; Olsen, G.; Don, C.; Trevor, H., Scale of Biomass Productionfrom New Woody Crops for Salinity Control in Dryland Agriculture in Australia. *Int.J.Global Energy Issues* **2007,** 27, (2), 115-137.

26. Yu, Y.; Bartle, J.; Li, C. Z.; Wu, H., Mallee Biomass as a Key Bioenergy Source in Western Australia: Importance of Biomass Supply Chain. *Energy Fuels* **2009,** 23, (6), 3290-3299.

27. Yu, Y.; Wu, H., Bioslurry as a Fuel. 2. Life-Cycle Energy and Carbon Footprints of Bioslurry Fuels from Mallee Biomass in Western Australia. *Energy & Fuels* **2010,** 24, 5660-5668.

28. Bartle, J. R.; Abadi, A., Toward Sustainable Production of Second Generation Bioenergy Feedstocks. *Energy Fuels* **2010,** 24, (1), 2-9.

29. Bartle, J., Scale of biomass production from new woody crops for salinity control in dryland agriculture in Australia. *International journal of global energy issues* **2007,** 27, (2), 115.

30. Olsen, G.; Cooper, D.; Huxtable, D.; Carslake, J.; Bartle, J., DeVeloping multiple purpose species for large scale reVegetation, search project final report (nht project 973849); Department of Conservation and Land Management: Perth, Western Australia, 2004.

31. Maciejewska, A.; Veringa, H.; Sanders, J.; Peteves, S. D. *Co-firing of Biomass with Coal: Constraints and Role of Biomass Pre-treatment.*; DG JRC Institute for Energy: 2006.

32. Esteban, L. S.; Carrasco, J. E., Evaluation of different strategies for pulverization of forest biomasses. *Powder Technology* **2006,** 166, (3), 139-151.

33. Bridgewater, A. V., Biomass Fast Pyrolysis. *Thermal Science* **2004,** 8, (2), 21-49.

34. Czernik, S.; Bridgewater, A. V., Overview of Applications of Biomass Fast Pyrolysis Oil. *Energy & Fuels* **2004,** 18, 590-598.

35. Mohan, D.; Pittman, C. U.; Steele, P. H., Pyrolysis of Wood and Biomass For Bio Oil: A Critical Review. *Energy& Fuels* **2006,** 20, 846-889.

36. Garcia-Perez, M.; Chaala, A.; Pakdel, H.; Kretschmer, D.; Rodrigue, D.; Roy, C., Vacuum Pyrolysis of Softwood and Hardwood Biomass Comparison between Products Yields and Bio oil Properties. *J.Anal.Appl.Pyrolysis* **2007,** 78, 104-116.

37. Mulligan, C. J.; Strezov, L.; Strezov, V., Thermal Decomposition of Wheat Straw and Mallee Residue Under Pyrolysis Conditions. *Energy & Fuels* **2010,** 24, 46.

38. Garcia-Perez, M.; Chaala, A.; Pakdel, H.; Kretschmer, D.; Rodrigue, D.; Roy, C., Multiphase Structure of Bio oils. *Energy & Fuels* **2006,** 20, 364-375.

39. Garcia-Perez, M.; Wang, X. S.; Shen, J.; Rhodes, M. J.; Tian, F.; Lee, W.; Wu, H.; Li, C., Fast pyrolysis of oil mallee wood biomass: effect of temperature on the yield and quality of pyrolysis products. *Ind. Eng. Chem. Res.* **2008,** 47, 1846-1854.

40. Abdullah, H.; Mediaswanti, K. A.; Wu, H., Biochar as a Fuel:2. Significant Differences in Fuel Quality and Ash Properties of Biochars from Various Biomass Components of Mallee Trees. *Energy & Fuels* **2010,** 24, (3), 1972-1979.

41. Lehmann, J., Bio-Energy in the Black. *Frontiers in Ecology and the Environment* **2007,** 5, (7), 381-387.

42. Cazetta, A. L.; Vargas, A. M. M.; Nogami, E. M.; Kunita, M. H.; Guilherme, M. R.; Martins, A. C.; Silva, T. L.; Moraes, J. C. G.; Almeida, V. C., NaOH-activated carbon of high surface area produced from coconut shell: Kinetics and equilibrium studies from the methylene blue adsorption. *Chemical Engineering Journal* 174, (1), 117-125.

43. Alam, M. Z.; Ameem, E. S.; Muyibi, S. A.; Kabbashi, N. A., The factors affecting the performance of activated carbon prepared from oil palm empty fruit bunches for adsorption of phenol. *Chemical Engineering Journal* **2009,** 155, (1-2), 191-198.

44. Awwad, N. S.; Gad, H. M. H.; Ahmad, M. I.; Aly, H. F., Sorption of lanthanum and erbium from aqueous solution by activated carbon prepared from rice husk. *Colloids and Surfaces B: Biointerfaces* 81, (2), 593-599.

45. Schroder, E.; Thomauske, K.; Weber, C.; Hornung, A.; Tumiatti, V., Experiments on the generation of activated carbon from biomass. *Journal of Analytical and Applied Pyrolysis* **2007,** 79, (1-2), 106-111.

46. Marsh, H.; Rodríguez-Reinoso, F., Chapter 2 - Activated Carbon (Origins). In *Activated Carbon*, Elsevier Science Ltd: Oxford, 2006; p 71.

47. IUPAC. Compendium of Chemical Terminology. In 2 ed.; McNaught, A. D.; Wilkinson., A.; Publications, B. S., Eds. Blackwell Scientific Publications: Oxford, 1997.

48. Sing KSw, E. D., Haul RA, Moscou L, Pierotti RA, Rouuquerol J,Siemieniewska T., Reporting physisorption data for gas/solid systems with special reference to the determination of surface area and porosity,. *Pure Appl Chem* **1985,** 57, (4), 603-619.

49. GU, L. L. k., Effects of high temperature treatment on activated carbon pore structure. *Chemistry and Industty of Forest Products* **1999,** 19, (3), 37-40.

50. Lua, A. C.; Guo, J., Preparation and characterization of activated carbons from oil-palm stones for gas-phase adsorption. *Colloids and Surfaces A: Physicochemical and Engineering Aspects* **2001,** 179, (2-3), 151-162.

51. Yanzhen, F., Chemistry Of Active Carbon. *Coal Conversion* **2000,** 23, (4), 26-30.

52. S. H. Yoon, S. S. J. J., A study on the effect of heat treatment on functional groups of pitch based activated carbon fiber using FT-IR. *Carbon* **1997,** 35, 1739-1743.

53. Fuels, I. E. Torrefied wood - green coal. http://www.integrofuels.com/green.html

54. Gonzalez, J. C.; Gonzalez, M. T.; Molina-Sabio, M.; Rodriguez-Reinoso, F.; Sepulveda-Escribano, A., Porosity of activated carbons prepared from different lignocellulosic materials. *Carbon* **1995,** 33, (8), 1175-1177.

55. Jagtoyen, M.; Derbyshire, F., Activated carbons from yellow poplar and white oak by H3PO4 activation. *Carbon* **1998,** 36, (7-8), 1085-1097.

56. Lillo-Ródenas, M. A.; Marco-Lozar, J. P.; Cazorla-Amorós, D.; Linares-Solano, A., Activated carbons prepared by pyrolysis of mixtures of carbon precursor/alkaline hydroxide. *Journal of Analytical and Applied Pyrolysis* **2007,** 80, (1), 166-174.

57. Heschel, W.; Klose, E., On the suitability of agricultural by-products for the manufacture of granular activated carbon. *Fuel* **1995,** 74, (12), 1786-1791.

58. Hong, I.; Jiang, H.; Park, Y.-D.; Kim, J.-Y.; Ha, B.-H., Metal dispersed activated carbon fibers and their application for removal of SOx. *Chemical Physics Letters* **2002,** 366, (5–6), 572-577.

59. Moreno-Castilla, C.; Maldonado-Hódar, F. J., Carbon aerogels for catalysis applications: An overview. *Carbon* **2005,** 43, (3), 455-465.

60. Raveendran, K.; Ganesh, A.; Khilar, K. C., Influence of mineral matter on biomass pyrolysis characteristics. *Fuel* **1995,** 74, (12), 1812-1822.

61. Carrott, P. J. M.; Suhas; Carrott, M. M. L. R.; Guerrero, C. I.; Delgado, L. A., Reactivity and porosity development during pyrolysis and physical activation in CO2 or steam of kraft and hydrolytic lignins. *Journal of Analytical and Applied Pyrolysis* **2008,** 82, (2), 264-271.

62. Şentorun-Shalaby, Ç. d.; Uçak-Astarlıogˇlu., M. G.; Çigdem; Sarıcı, Preparation and characterization of activated carbons by one-step steam pyrolysis/activation from apricot stones. *Microporous and mesoporous materials* **2006,** 88, (1-3), 126-134.

63. Ahmad, T.; Awan, I. A.; Nisar, J.; Ahmad, I., Influence of inherent minerals and pyrolysis temperature on the yield of pyrolysates of some Pakistani coals. *Energy Conversion and Management* **2009,** 50, (5), 1163-1171.

64. Afrane, G.; Achaw, O.-W., Effect of the concentration of inherent mineral elements on the adsorption capacity of coconut shell-based activated carbons. *Bioresource Technology* **2008,** 99, (14), 6678-6682.

65. Nowicki, P., Siberian anthracite as a precursor material for microporous activated carbons. *Fuel* **2008,** 87, (10-11), 2037.

66. Srinivasakannan, C., Production of activated carbon from rubber wood sawdust. *Biomass & bioenergy* **2004,** 27, (1), 89.

67. Kawano, T., Preparation of activated carbon from petroleum coke by KOH chemical activation for adsorption heat pump. *Applied thermal engineering* **2008,** 28, (8-9), 865.

68. Bagheri, N., Preparation of high surface area activated carbon from corn by chemical activation using potassium hydroxide. *Chemical engineering research and design* **2009,** 87, (8), 1059.

69. Bagheri, N.; Abedi, J., Preparation of high surface area activated carbon from corn by chemical activation using potassium hydroxide. *Chemical Engineering Research and Design* **2009,** 87, (8), 1059-1064.

70. Nowicki, P.; Pietrzak, R.; Wachowska, H., Siberian anthracite as a precursor material for microporous activated carbons. *Fuel* **2008,** 87, (10-11), 2037-2040.

71. zhang, Y., Development of new thechnology in xyloid activated carbon by sulphuric acid method. *Journal of chemical industry of forest products* **2001,** 35, (2), 18-19.

72. Li, W.; Yang, K.; Peng, J.; Zhang, L.; Guo, S.; Xia, H., Effects of carbonization temperatures on characteristics of porosity in coconut shell chars and activated carbons derived from carbonized coconut shell chars. *Industrial Crops and Products* **2008,** 28, (2), 190-198.

73. Budinova, T.; Gergova, K.; Petrov, N.; Minkova, V., A study of the process of pyrolysis in a

water-vapor stream of activated carbons, prepared from agricultural by-products by some physico-chemical methods. *Thermochimica Acta* **1994,** 244, 267-276.

74. Kawano, T.; Kubota, M.; Onyango, M. S.; Watanabe, F.; Matsuda, H., Preparation of activated carbon from petroleum coke by KOH chemical activation for adsorption heat pump. *Applied Thermal Engineering* **2008,** 28, (8-9), 865-871.

75. Lua, A. C.; Lau, F. Y.; Guo, J., Influence of pyrolysis conditions on pore development of oil-palm-shell activated carbons. *Journal of Analytical and Applied Pyrolysis* **2006,** 76, 96-102.

76. López-González, d. D.; Martínez-Vilchez, F.; Rodríguez-Reinoso, F., Preparation and characterization of active carbons from olive stones. *Carbon* **1980,** 18, (6), 413-418.

77. Basu, P., . In *Biomass Gasification and Pyrolysis ,Practical Design and Theory*, p 72.

78. http://en.wikipedia.org/wiki/Activated_carbon

79. Shafizadeh, F.; Bradbury, A. G. W.; DeGroot, W. F.; Aanerud, T. W., Role of inorganic additives in the smoldering combustion of cotton cellulose. *Industrial & Engineering Chemistry Product Research and Development* **1982,** 21, (1), 97-101.

80. Marsh, H.; Rodríguez-Reinoso, F., *Activated Carbon*. CPI Antony Rowe, Great Britain, Eastbourne, 2006.

81. Franklin, R. E., The interpretation of diffuse X-ray diagrams of carbon. *Acta crystallographica* **1950,** 3, (2), 107-121.

82. Franklin, R. E., The structure of graphitic carbons. *Acta crystallographica* **1951,** 4, (3), 253-261.

83. Stoeckli, H. F., Microporous carbons and their characterization: The present state of the art. *Carbon* **1990,** 28, (1), 1-6.

84. Rodríguez-Reinoso, F.; Molina-Sabio, M., Textural and chemical characterization of microporous carbons. *Advances in Colloid and Interface Science* **1998,** 76–77, (0), 271-294.

85. Leofanti, G.; Padovan, M.; Tozzola, G.; Venturelli, B., Surface area and pore texture of catalysts. *Catalysis Today* **1998,** 41, (1–3), 207-219.

86. Blazewicz, S.; Swiatkowski, A.; Trznadel, B. J., The influence of heat treatment on activated carbon structure and porosity. *Carbon* **1999,** 37, (4), 693-700.

87. Yu, M.; Hu, X.; Wang, K.; yin, H., Preparation of Activated Carbon with High Specific Surface Area from Bamboo by Potassium Hydroxide. *Journal of ZHEJINANG Forestry Science and Tchenology* **2006,** 26, (3).

88. JIANG, M. s., Micromechanism of carbonization for thinning wood of Chinese fir. *Journal of Fujian College of Forestry* **2005,** 42, 112-116.

89. Centeno, T. A.; Marbán, G.; Fuertes, A. B., Importance of micropore size distribution on adsorption at low adsorbate concentrations. *Carbon* **2003,** 41, (4), 843-846.

90. Lua, A. C.; Guo, J., Activated carbon prepared from oil palm stone by one-step CO2 activation for gaseous pollutant removal. *Carbon* **2000,** 38, (7), 1089-1097.

91. Wigmans, T., Industrial aspects of production and use of activated carbons. *Carbon* **1989,** 27, (1), 13-22.

92. Chang, C.-F.; Chang, C.-Y.; Tsai, W.-T., Effects of Burn-off and Activation Temperature on Preparation of Activated Carbon from Corn Cob Agrowaste by CO2 and Steam. *Journal of Colloid and Interface Science* **2000,** 232, (1), 45-49.

93. Turney, C. S. M.; Wheeler, D.; Chivas, A. R., Carbon isotope fractionation in wood during carbonization. *Geochimica et Cosmochimica Acta* **2006,** 70, (4), 960-964.

94. 00/02274 Structure properties, and reactivity of solid fuels. *Fuel and Energy Abstracts* **2000,** 41,

(5), 260-261.

95. Standish, N.; Tanjung, A. F. A., Gasification of single wood charcoal particles in CO2. *Fuel* **1988,** 67, (5), 666-672.

96. Encinar, J. M., Gonzalez, J.F., Rodriguez, J.J., and Ramiro, M.J., Catalysed and Uncatalysed Steam Gasification of Eucalyptus Char: Influence of Variables and Kinetic Study. *Fuel* **2001,** 80, 2025-2036.

97. Henrich, E.; Bürkle, S.; Meza-Renken, Z. I.; Rumpel, S., Combustion and gasification kinetics of pyrolysis chars from waste and biomass. *Journal of Analytical and Applied Pyrolysis* **1999,** 49, (1-2), 221-241.

98. Molina-Sabio, M.; Gonzalez, M. T.; Rodriguez-Reinoso, F.; Sepúlveda-Escribano, A., Effect of steam and carbon dioxide activation in the micropore size distribution of activated carbon. *Carbon* **1996,** 34, (4), 505-509.

99. Zevenhoven-Onderwater, M., Ash-forming Matter in Biomass Fuels. *Ph.D. Thesis, Department of Chemical Engineering, Åbo Akademi University, Åbo/Turku, Finland* **2002**.

100. Dayton, D. C.; French, R. J.; Milne, T. A., Direct Observation of Alkali Vapor Release during Biomass Combustion and Gasification. 1. Application of Molecular Beam/Mass Spectrometry to Switchgrass Combustion. *Energy & Fuels* **1995,** 9, (5), 855-865.

101. Ruiz, B. a.; Parra, J.; Alvarez, T.; Fuertes, A. B.; Pajares, J. A.; Pis, J., Active carbons from semianthracites. *Applied Catalysis A: General* **1993,** 98, (2), 115-123.

102. van Lith, S. C.; Jensen, P. A.; Frandsen, F. J.; Glarborg, P., Release to the Gas Phase of Inorganic Elements during Wood Combustion. Part 2: Influence of Fuel Composition. *Energy & Fuels* **2008,** 22, (3), 1598-1609.

103. Franceschi, V. R.; Horner, H. T., Jr., Calcium Oxalate Crystals in Plants. *Botanical Review* **1980,** 46, (4), 361-427.

104. Hawley, M. C.; Boyd, M.; Anderson, C.; DeVera, A., Gasification of wood char and effects of intraparticle transport. *Fuel* **1983,** 62, (2), 213-216.

105. Jensen, A.; Dam-Johansen, K.; Wójtowicz, M. A.; Serio, M. A., TG-FTIR Study of the Influence of Potassium Chloride on Wheat Straw Pyrolysis. *Energy & Fuels* **1998,** 12, (5), 929-938.

106. Keown, D. M.; Favas, G.; Hayashi, J.-i.; Li, C.-Z., Volatilisation of alkali and alkaline earth metallic species during the pyrolysis of biomass: differences between sugar cane bagasse and cane trash. *Bioresource Technology* **2005,** 96, (14), 1570-1577.

107. Olsson, J. G.; Jäglid, U.; Pettersson, J. B. C.; Hald, P., Alkali Metal Emission during Pyrolysis of Biomass. *Energy & Fuels* **1997,** 11, (4), 779-784.

108. Knudsen, J. N.; Jensen, P. A.; Dam-Johansen, K., Transformation and Release to the Gas Phase of Cl, K, and S during Combustion of Annual Biomass. *Energy & Fuels* **2004,** 18, (5), 1385-1399.

109. Quyn, D. M.; Wu, H.; Bhattacharya, S. P.; Li, C.-Z., Volatilisation and catalytic effects of alkali and alkaline earth metallic species during the pyrolysis and gasification of Victorian brown coal. Part II. Effects of chemical form and valence. *Fuel* **2002,** 81, (2), 151-158.

110. Wu, H.; Quyn, D. M.; Li, C.-Z., Volatilisation and catalytic effects of alkali and alkaline earth metallic species during the pyrolysis and gasification of Victorian brown coal. Part III. The importance of the interactions between volatiles and char at high temperature. *Fuel* **2002,** 81, (8), 1033-1039.

111. JUNCAN; GANG XIAO; XIOA XU; JIN, S. B., Functional groups evolvement and charcoal formaiton during lignin pyrolysis/carbonization. *Journal of SOUTHES UNIVERSITY* **2012,** 42, (1),

83-87.
112. Sharma, R. K., Characterization of chars from pyrolysis of lignin. *Fuel* **2004,** 83, (11-12), 1469-1482.
113. Longlong Ma; Chuangzhi Wu; Li sun, In *The Technology of Application of Biomass Gasification*, Chemical Industrial Press: China, 2003; p 49.
114. Smoliński, A., Coal char reactivity as a fuel selection criterion for coal-based hydrogen-rich gas production in the process of steam gasification. *Energy Conversion and Management* **2011,** 52, (1), 37-45.
115. Linxian Zhang; Rongjie Huang; Yi tian Fang; Yang, W., Study on reactivity of Chines anthracite chars gasificaiton -comparison of reactivity between steam and CO2 gasification. *Journal of Fuel Chemistry and Technology* **2006,** 34, (3), 265-269.
116. Xioahu Gu; Min Cao; Lanfu Wang; Zhang, A., CO2 Rasification Reactivity of Yima Coal Char at Elevated Temperature. *Coal Conversion* **2009,** 32, (3), 6-8.
117. Liu, X. The Analysis of Distributed Activation Energy Model for Coal Pyrolysis and the Simulation of Pressurized Gasification of Coal in Fixed-bed Gasifier. 2000.
118. Ko, T.-H.; chiranairadul, P.; Lu, C.-K.; Lin, C.-H., The effects of activation by carbon dioxide on the mechanical properties and structure of PAN-based activated carbon fibers. *Carbon* **1992,** 30, (4), 647-655.
119. Marsh, H.; Rodríguez-Reinoso, F., Activated Carbon. In *Activated Carbon*, First ed.; CPI Antony Rowe: Great Britain, Eastbourne, 2006; p 182.
120. Tremblay, G.; Vastola, F. J.; Walker Jr, P. L., Thermal desorption analysis of oxygen surface complexes on carbon. *Carbon* **1978,** 16, (1), 35-39.
121. Haynes, B. S.; Newbury, T. G., Oxyreactivity of carbon surface oxides. *Proceedings of the Combustion Institute* **2000,** 28, (2), 2197-2203.
122. Guerrero, M.; Ruiz, M. P.; Alzueta, M. U.; Bilbao, R.; Millera, A., Pyrolysis of eucalyptus at different heating rates: studies of char characterization and oxidative reactivity. *Journal of Analytical and Applied Pyrolysis* **2005,** 74, (1-2), 307-314.
123. Normand M, L., Heterogeneous kinetics of coal char gasification and combustion. *Progress in Energy and Combustion Science* **1978,** 4, (4), 221-270.
124. Barton, S. S.; Harrison, B. H., Acidic surface oxide structures on carbon and graphite—I. *Carbon* **1975,** 13, (4), 283-288.
125. Kapteijn, F.; Meijer, R.; Moulijn, J. A.; Cazorla-Amóros, D., On why do different carbons show different gasification rates: A transient isotopic CO2 gasification study. *Carbon* **1994,** 32, (7), 1223-1231.
126. Walker Jr, P. L., Production of activated carbons: Use of CO2 versus H2O as activating agent. *Carbon* **1996,** 34, (10), 1297-1299.
127. Di Blasi, C., Combustion and gasification rates of lignocellulosic chars. *Progress in Energy and Combustion Science* **2009,** 35, (2), 121-140.
128. Mitsuoka, K.; Hayashi, S.; Amano, H.; Kayahara, K.; Sasaoaka, E.; Uddin, M. A., Gasification of woody biomass char with CO2: The catalytic effects of K and Ca species on char gasification reactivity. *Fuel processing technology* 92, (1), 26-31.
129. Ollero, P.; Serrera, A.; Arjona, R.; Alcantarilla, S., The CO2 gasification kinetics of olive residue. *Biomass and Bioenergy* **2003,** 24, (2), 151-161.
130. Seo, D. K.; Lee, S. K.; Kang, M. W.; Hwang, J.; Yu, T.-U., Gasification reactivity of biomass

chars with CO_2. *Biomass and Bioenergy* 34, (12), 1946-1953.

131. Zhang, T.; Walawender, W. P.; Fan, L. T.; Fan, M.; Daugaard, D.; Brown, R. C., Preparation of activated carbon from forest and agricultural residues through CO2 activation. *Chemical Engineering Journal* **2004,** 105, (1-2), 53-59.

132. Roberts, D. G.; Harris, D. J., Char gasification in mixtures of CO2 and H2O: Competition and inhibition. *Fuel* **2007,** 86, (17-18), 2672-2678.

133. Zhu, Y.; Gao, J.; Li, Y.; Sun, F.; Gao, J.; Wu, S.; Qin, Y., Preparation of activated carbons for SO2 adsorption by CO_2 and steam activation. *Journal of the Taiwan Institute of Chemical Engineers* **2012,** 43, (1), 112-119.

134. Marquez-Montesinos, F.; Cordero, T.; RodrIguez-Mirasol, J.; RodrIguez, J. J., CO_2 and steam gasification of a grapefruit skin char. *Fuel* **2002,** 81, (4), 423-429.

135. Tancredi, N.; Cordero, T.; rodriguez -Mirasol, J.; J.Rodriguez, J., Activated carbons from Uruguayan eucalyptus wood. *Fuel* **1996,** 75, (15), 1701.

136. Johannes, L.; John, G.; Marco, R., Bio-char Sequestration in Terrestrial Ecosystems - A Review. *Mitigation and Adaptation Strategies for Global Change* **2006,** 11, (2), 395-419.

137. Skjemstad, J. O.; Janik, L. J.; Taylor, J. A., Non-living soil organic matter: what do we know about it? *Australian Journal of Experimental Agriculture* **1998,** 38, (7), 667-680.

138. Swift, R. S., Sequestration of carbon by soil. *Soil Science* **2001,** 166, (11), 858-871.

139. Krull, E. S.; Skjemstad, J. O.; Graetz, D.; Grice, K.; Dunning, W.; Cook, G.; Parr, J. F., 13C-depleted charcoal from C4 grasses and the role of occluded carbon in phytoliths. *Organic Geochemistry* **2003,** 34, (9), 1337-1352.

140. Marris, E., Putting the carbon back: Black is the new green. *Nature* **2006,** 442, (7103), 624-626.

141. Glaser, B.; Haumaier, L.; Guggenberger, G.; Zech, W., The 'Terra Preta' phenomenon: a model for sustainable agriculture in the humid tropics. *Naturwissenschaften* **2001,** 88, (1), 37-41.

142. Chun, Y.; Sheng, G.; Chiou, C. T.; Xing, B., Compositions and Sorptive Properties of Crop Residue-Derived Chars. *Environmental Science & Technology* **2004,** 38, (17), 4649-4655.

143. Rumpel, C.; Alexis, M.; Chabbi, A.; Chaplot, V.; Rasse, D. P.; Valentin, C.; Mariotti, A., Black carbon contribution to soil organic matter composition in tropical sloping land under slash and burn agriculture. *Geoderma* **2006,** 130, (1–2), 35-46.

144. Keiluweit, M.; Nico, P. S.; Johnson, M. G.; Kleber, M., Dynamic Molecular Structure of Plant Biomass-Derived Black Carbon (Biochar). *Environmental Science & Technology* **2010,** 44, (4), 1247-1253.

145. Asai, H.; Samson, B. K.; Stephan, H. M.; Songyikhangsuthor, K.; Homma, K.; Kiyono, Y.; Inoue, Y.; Shiraiwa, T.; Horie, T., Biochar amendment techniques for upland rice production in Northern Laos: 1. Soil physical properties, leaf SPAD and grain yield. *Field Crops Research* **2009,** 111, (1–2), 81-84.

146. Cao, X.; Harris, W., Properties of dairy-manure-derived biochar pertinent to its potential use in remediation. *Bioresource Technology* **2010,** 101, (14), 5222-5228.

147. Yuan, J.-H.; Xu, R.-K.; Zhang, H., The forms of alkalis in the biochar produced from crop residues at different temperatures. *Bioresource Technology* **2011,** 102, (3), 3488-3497.

148. Singh, B.; Singh, B. P.; Cowie, A. L., Characterisation and evaluation of biochars for their application as a soil amendment. *Soil Research* **2010,** 48, (7), 516-525.

149. Van Zwieten, L., Effects of biochar from slow pyrolysis of papermill waste on agronomic performance and soil fertility. *Plant and soil* **2010,** 327, (1-2), 235.

150. Özçimen, D.; Ersoy-Meriçboyu, A., Characterization of biochar and bio-oil samples obtained from carbonization of various biomass materials. *Renewable Energy* **2010,** 35, (6), 1319-1324.

151. Chan, K. Y.; Van Zwieten, L.; Meszaros, I.; Downie, A.; Joseph, S., Agronomic values of greenwaste biochar as a soil amendment. *Soil Research* **2007,** 45, (8), 629-634.

152. B.Glaser, B.; Lehmann, J.; Zech, W., Ameliorating physical and chemical properties of highly weathered soils in the tropics with charcoal-a review. *Biology and fertility of soils* **2002,** 35, (4), 219-230.

153. Oguntunde, P. G.; Abiodun, B. J.; Ajayi, A. E.; van de Giesen, N., Effects of charcoal production on soil physical properties in Ghana. *Journal of Plant Nutrition and Soil Science* **2008,** 171, (4), 591-596.

154. Warnock, D. D. Arbuscular Mycorrhizal Responses to Biochar in soils-potential Mechanisms of Intergraction and Observed Responses in Controlled Environments University of Oregon, Eugene, Oregon,, The University of Montana
Missoula, MT, 2009.

155. Kimetu, J. M.; Lehmann, J., Stability and stabilisation of biochar and green manure in soil with different organic carbon contents. *Soil Research* **2010,** 48, (7), 577-585.

156. Liang, B.; Lehmann, J.; Solomon, D.; Kinyangi, J.; et al., Black Carbon Increases Cation Exchange Capacity in Soils. *Soil Science Society of America Journal* **2006,** 70, (5), 1719-1730.

157. Zackrisson, O.; Nilsson, M.-C.; Wardle, D. A., Key Ecological Function of Charcoal from Wildfire in the Boreal Forest. *Oikos* **1996,** 77, (1), 10-19.

158. Kolb, S. E. F., Kevin J; Dornbush, Mathew E, Effect of Charcoal Quantity on Microbial Biomass and Activity in Temperate Soils. *Soil Science Society of America Journal* **2009,** 73, (4), 1173-1181.

159. Laird, D.; Fleming, P.; Wang, B.; Horton, R.; Karlen, D., Biochar impact on nutrient leaching from a Midwestern agricultural soil. *Geoderma* **2010,** 158, (3–4), 436-442.

160. Marco, A. R.; Johannes, L.; Juan, R.; Maria, H., Biological nitrogen fixation by common beans (Phaseolus vulgaris L.) increases with bio-char additions. *Biology and fertility of soils* **2007,** 43, (6), 699-708.

161. Yip, K.; Tian, F.; Hayashi, J.-i.; Wu, H., Effect of Alkali and Alkaline Earth Metallic Species on Biochar Reactivity and Syngas Compositions during Steam Gasification. *Energy & Fuels* **2010,** 24, (1), 173-181.

162. Chan, M. L., The oxidative reactivity of coal chars in relation to their structure. *Fuel* **1999,** 78, (13), 1539-1552.

163. Suuberg, E. M.; Aarna, I., Porosity development in carbons derived from scrap automobile tires. *Carbon* **2007,** 45, (9), 1719-1726.

164. ASTM Standard E871 - 82, 2006, " Standard Test Method for Moisture Analysis of Particulate Wood Fuels," ASTM International, West Conshohocken, PA, 2006, DOI: 10.1520/E0870-82R06, www.astm.org.

165. Pels, J. R.; Kapteijn, F.; Moulijn, J. A.; Zhu, Q.; Thomas, K. M., Evolution of nitrogen functionalities in carbonaceous materials during pyrolysis. *Carbon* **1995,** 33, (11), 1641-1653.

166. Wu, H., Removal and Recycling of Inherent Inorganic Nutrient Species in Mallee Biomass and Derived Biochars by Water Leaching. *Industrial & Engineering Chemistry Research* 50, (21), 12143.

167. Jasieńko-Hałat, M.; Kędzior, K., Comparison of molecular sieve properties in microporous chars from low-rank bituminous coal activated by steam and carbon dioxide. *Carbon* **2005,** 43, (5), 944-953.

168. Iley, M.; Marsh, H.; Reinoso, F. R., The adsorptive properties of carbonised olive stones. *Carbon* **1973,** 11, (6), 633-638.

169. González, J. F.; Román., S.; Encinar, J. M.; Martínez., G., Pyrolysis of various biomass residues and char utilization for the production of activated carbons. *Journal of Analytical and Applied Pyrolysis* **2009,** 85, (1-2), 134-141.

170. Jagtoyen, M.; Derbyshire, F., Some considerations of the origins of porosity in carbons from chemically activated wood. *Carbon* **1993,** 31, (7), 1185-1192.

171. *AUTOSORB AS-1, AS1Win GAS SORPTION SYSTEM OPERATION MANUAL*. 2008.

172. Neimark, A. V.; Lin, Y.; Ravikovitch, P. I.; Thommes, M., Quenched solid density functional theory and pore size analysis of micro-mesoporous carbons. *Carbon* **2009,** 47, (7), 1617-1628.

173. Ravikovitch, P. I.; Vishnyakov, A.; Russo, R.; Neimark, A. V., Unified Approach to Pore Size Characterization of Microporous Carbonaceous Materials from N2, Ar, and CO2 Adsorption Isotherms†. *Langmuir* **2000,** 16, (5), 2311-2320.

174. Silvestre-Alberoa, J.; Silvestre-Alberoa, A.; Rodríguez-Reinosoa, F.; Thommesb, M., Physical characterization of activated carbons with narrow microporosity by nitrogen (77.4 K), carbon dioxide (273 K) and argon (87.3 K) adsorption in combination with immersion calorimetry. *Carbon* **2012,** 50, (9), 3128-3133.

175. http://cmr.curtin.edu.au/facilities/sem.cfm

176. Dumont, M.; Chollon, G.; Dourges, M. A.; Pailler, R.; Bourrat, X.; Naslain, R.; Bruneel, J. L.; Couzi, M., Chemical, microstructural and thermal analyses of a naphthalene-derived mesophase pitch. *Carbon* **2002,** 40, (9), 1475-1486.

177. Qian, W.; Liu, T.; Wei, F.; Yuan, H., Quantitative Raman characterization of the mixed samples of the single and multi-wall carbon nanotubes. *Carbon* **2003,** 41, (9), 1851-1854.

178. Li, X.; Hayashi, J.-i.; Li, C.-Z., FT-Raman spectroscopic study of the evolution of char structure during the pyrolysis of a Victorian brown coal. *Fuel* **2006,** 85, (12–13), 1700-1707.

179. Fu, P.; Hu, S.; Sun, L.; Xiang, J.; Yang, T.; Zhang, A.; Zhang, J., Structural evolution of maize stalk/char particles during pyrolysis. *Bioresource Technology* **2009,** 100, (20), 4877-4883.

180. Antal, M. J.; Mok, W. S. L.; Varhegyi, G.; Szekely, T., Review of methods for improving the yield of charcoal from biomass. *Energy & Fuels* **1990,** 4, (3), 221-225.

181. Bridgwater, A. V.; Peacocke, G. V. C., Fast pyrolysis processes for biomass. *Renewable and Sustainable Energy Reviews* **2000,** 4, (1), 1-73.

182. Antal, M. J.; Mochidzuki, K.; Paredes, L. S., Flash Carbonization of Biomass. *Industrial & Engineering Chemistry Research* **2003,** 42, (16), 3690-3699.

183. Zeriouh, A.; Belkbir, L., Thermal decomposition of a Moroccan wood under a nitrogen atmosphere. *Thermochimica Acta* **1995,** 258, (0), 243-248.

184. Antal, M. J., Jr.; Varhegyi, G., Cellulose Pyrolysis Kinetics: The Current State of Knowledge. *Industrial & Engineering Chemistry Research* **1995,** 34, (3), 703-717.

185. Evans, R. J.; Milne, T. A., Molecular characterization of the pyrolysis of biomass. 2. Applications. *Energy & Fuels* **1987,** 1, (4), 311-319.

186. Lua, A. C.; Yang, T.; Guo, J., Effects of pyrolysis conditions on the properties of activated carbons prepared from pistachio-nut shells. *Journal of Analytical and Applied Pyrolysis* **2004,** 72, (2), 279-287.

187. Kastanaki, E.; Vamvuka, D.; Grammelis, P.; Kakaras, E., Thermogravimetric studies of the behavior of lignite–biomass blends during devolatilization. *Fuel Processing Technology* **2002,** 77–78,

(0), 159-166.

188. Vamvuka, D.; Troulinos, S.; Kastanaki, E., The effect of mineral matter on the physical and chemical activation of low rank coal and biomass materials. *Fuel* **2006,** 85, (12–13), 1763-1771.

189. Ashu, J. T., Enhancement of char reactivity by rapid heating of precursor coal. *Fuel* **1978,** 57, (4), 250-251.

190. Rodríguez-Mirasol, J. J.; Cordero, T.; Rodriguez, J. J., CO2-reactivity of eucalyptus kraft lignin chars. *Carbon* **1993,** 31, (1), 53-61.

191. Raveendran, K.; Ganesh, A., Adsorption characteristics and pore-development of biomass-pyrolysis char. *Fuel* **1998,** 77, (7), 769-781.

192. Pastor-Villegas, J.; Durán-Valle, C. J., Pore structure of chars and activated carbons prepared using carbon dioxide at different temperatures from extracted rockrose. *Journal of Analytical and Applied Pyrolysis* **2001,** 57, (1), 1-13.

193. Coates, J., Interpretation of infrared spectra, a practical approach
In *Encyclopedia of Analytical Chemistry*, John Wiley & Sons, Ltd: 2006.

194. Gomez-Serrano, V.; Pastor-Villegas, J.; Perez-Florindo, A.; Duran-Valle, C.; Valenzuela-Calahorro, C., FT-IR study of rockrose and of char and activated carbon. *Journal of Analytical and Applied Pyrolysis* **1996,** 36, (1), 71-80.

195. Pastor-Villegas, J.; Gómez-Serrano, V.; Durán-Valle, C. J.; Higes-Rolando, F. J., Chemical study of extracted rockrose and of chars and activated carbons prepared at different temperatures. *Journal of Analytical and Applied Pyrolysis* **1999,** 50, (1), 1-16.

196. Whalley, W. R.; Clark, L. J.; Gowing, D. J. G.; Cope, R. E.; Lodge, R. J.; Leeds-Harrison, P. B., Does Soil Strength Play a Role in Wheat Yield Losses Caused by Soil Drying? *Plant and soil* **2006,** 280, (1-2), 279-290.

197. J. Leifeld ; Fenner, S.; Müller, M., Mobility of black carbon in drained peatland soils. *Biogeosciences* **2007,** 4, (3), 425-432.

198. MAJOR J, S. C., DOWNIE A, Biochar effects on nutrient leaching. In *Biochar for Environ-mental Management Science and Technology*, LEHMANN J, J., Ed. London Earthscan, 2009; pp 271-287.

199. Cornelissen, G.; Gustafsson, Ö.; Bucheli, T. D.; Jonker, M. T. O.; Koelmans, A. A.; van Noort, P. C. M., Extensive Sorption of Organic Compounds to Black Carbon, Coal, and Kerogen in Sediments and Soils: Mechanisms and Consequences for Distribution, Bioaccumulation, and Biodegradation. *Environmental Science & Technology* **2005,** 39, (18), 6881-6895.

200. Quénéa, K.; Derenne, S.; Rumpel, C.; Rouzaud, J. N.; Gustafsson, O.; Carcaillet, C.; Mariotti, A.; Largeau, C., Black carbon yields and types in forest and cultivated sandy soils (Landes de Gascogne, France) as determined with different methods: Influence of change in land use. *Organic Geochemistry* **2006,** 37, (9), 1185-1189.

201. Cheng, C.-H.; Lehmann, J.; Thies, J. E.; Burton, S. D.; Engelhard, M. H., Oxidation of black carbon by biotic and abiotic processes. *Organic Geochemistry* **2006,** 37, (11), 1477-1488.

202. Hamer, U.; Marschner, B.; Brodowski, S.; Amelung, W., Interactive priming of black carbon and glucose mineralisation. *Organic Geochemistry* **2004,** 35, (7), 823-830.

203. Lee, J. W.; Kidder, M.; Evans, B. R.; Paik, S.; Buchanan Iii, A. C.; Garten, C. T.; Brown, R. C., Characterization of Biochars Produced from Cornstovers for Soil Amendment. *Environmental Science & Technology* **2010,** 44, (20), 7970-7974.

204. Uchimiya, M.; Lima, I. M.; Thomas Klasson, K.; Chang, S.; Wartelle, L. H.; Rodgers, J. E.,

Immobilization of Heavy Metal Ions (CuII, CdII, NiII, and PbII) by Broiler Litter-Derived Biochars in Water and Soil. *Journal of Agricultural and Food Chemistry* **2010,** 58, (9), 5538-5544.

205. Sheng, G.; Yang, Y.; Huang, M.; Yang, K., Influence of pH on pesticide sorption by soil containing wheat residue-derived char. *Environmental Pollution* **2005,** 134, (3), 457-463.

206. Bhupinder Pal, S.; Blake, J. H.; Balwant, S.; Annette, L. C.; Amrit, K., Influence of Biochars on Nitrous Oxide Emission and Nitrogen Leaching from Two Contrasting Soils. *Journal of Environmental Quality* **2010,** 39, (4), 1224-1235.

207. Samaras, P.; Diamadopoulos, E.; Sakellaropoulos, G. P., The effect of mineral matter and pyrolysis conditions on the gasification of Greek lignite by carbon dioxide. *Fuel* **1996,** 75, (9), 1108-1114.

208. Molina Sabio, M., Adsorption of CO2 and SO2 on activated carbons with a wide range of micropore size distribution. *Carbon* **1995,** 33, (12), 1777.

209. Román, S.; González, J. F.; González-García, C. M.; Zamora, F., Control of pore development during CO2 and steam activation of olive stones. *Fuel Processing Technology* **2008,** 89, (8), 715-720.

210. Rios, R. V. R. A., Kinetic restrictions in the characterization of narrow microporosity in carbon materials. *The journal of physical chemistry. C* **2007,** 111, (10), 3803-3805.

211. Rodriguez Reinoso, F., Activated carbons from lignocellulosic materials by chemical and/or physical activation: an overview. *Carbon* **1992,** 30, (7), 1111.

212. Neimark, A. V.; Ravikovitch, P. I., Capillary condensation in MMS and pore structure characterization. *Microporous and Mesoporous Materials* **2001,** 44–45, (0), 697-707.

213. Skodras, G.; Orfanoudaki, T.; Kakaras, E.; Sakellaropoulos, G. P., Production of special activated carbon from lignite for environmental purposes. *Fuel Processing Technology* **2002,** 77-78, (0), 75-87.

214. Kannan, M. P.; Richards, G. N., Gasification of biomass chars in carbon dioxide: dependence of gasification rate on the indigenous metal content. *Fuel* **1990,** 69, (6), 747-753.

215. Van Heek, K. H.; Mühlen, H.-J., Aspects of coal properties and constitution important for gasification. *Fuel* **1985,** 64, (10), 1405-1414.

216. Miura, K.; Hashimoto, K.; Silveston, P. L., Factors affecting the reactivity of coal chars during gasification, and indices representing reactivity. *Fuel* **1989,** 68, (11), 1461-1475.

217. Kumar, M.; Gupta, R. C., Influence of carbonization conditions on the gasification of acacia and eucalyptus wood chars by carbon dioxide. *Fuel* **1994,** 73, (12), 1922-1925.

218. Mermoud, F.; Salvador, S.; Van de Steene, L.; Golfier, F., Influence of the pyrolysis heating rate on the steam gasification rate of large wood char particles. *Fuel* 85, (10-11), 1473-1482.

219. Fushimi, C.; Araki, K.; Yamaguchi, Y.; Tsutsumi, A., Effect of Heating Rate on Steam Gasification of Biomass. 1. Reactivity of Char. *Industrial & Engineering Chemistry Research* **2003,** 42, (17), 3922-3928.

220. Hurt, R. H.; Sarofim, A. F.; Longwell, J. P., The role of microporous surface area in the gasification of chars from a sub-bituminous coal. *Fuel* **1991,** 70, (9), 1079-1082.

221. Roberts, D. G.; Harris, D. J.; Wall, T. F., Total pressure effects on chemical reaction rates of chars with O2, CO2 and H2O. *Fuel* **2000,** 79, (15), 1997-1998.

222. Roberts, D. G.; Harris, D. J., Char Gasification with O2, CO2, and H2O: Effects of Pressure on Intrinsic Reaction Kinetics. *Energy & Fuels* **2000,** 14, (2), 483-489.

223. Roberts, D. G.; Harris, D. J.; Wall, T. F., On the Effects of High Pressure and Heating Rate during Coal Pyrolysis on Char Gasification Reactivity. *Energy & Fuels* **2003,** 17, (4), 887-895.

224. Roberts, D. G.; Harris, D. J., A Kinetic Analysis of Coal Char Gasification Reactions at High

Pressures. *Energy & Fuels* **2006,** 20, (6), 2314-2320.

225. WU, M., *Plant Fiber Chemistry*. Light Industry Press: China, 1991.

226. Müller-Hagedorn, M.; Bockhorn, H.; Krebs, L.; Müller, U., A comparative kinetic study on the pyrolysis of three different wood species. *Journal of Analytical and Applied Pyrolysis* **2003,** 68–69, (0), 231-249.

227. Amen-Chen, C.; Pakdel, H.; Roy, C., Production of monomeric phenols by thermochemical conversion of biomass: a review. *Bioresource Technology* **2001,** 79, (3), 277-299.

228. Bin Zhang; Binshu Wu; Xiuli Yin; Chuangzhi Wu; Zejin Qiu; Ma, L., Structure and Pyrolysis Products Analysis of Acid Hydrolysis Lignin. *ACTA ENERGIAE SOLARIS SINICA* **2011,** 32, (1), 19-24.

229. Gutiérrez, A.; Rencoret, J.; Cadena, E. M.; Rico, A.; Barth, D.; del Río, J. C.; Martínez, Á. T., Demonstration of laccase-based removal of lignin from wood and non-wood plant feedstocks. *Bioresource Technology* **2012,** 119, (0), 114-122.

230. Irfan, M. F.; Usman, M. R.; Kusakabe, K., Coal gasification in CO2 atmosphere and its kinetics since 1948: A brief review. *Energy* **2011,** 36, (1), 12-40.

231. Von Fredersdorff, C., *Reactions of carbon with carbon dioxide and with steam*. 1955.

232. Çakal, G. Ö.; Yücel, H.; Gürüz, A. G., Physical and chemical properties of selected Turkish lignites and their pyrolysis and gasification rates determined by thermogravimetric analysis. *Journal of Analytical and Applied Pyrolysis* **2007,** 80, (1), 262-268.

233. Littlewood, K., Gasification: Theory and application. *Progress in Energy and Combustion Science* **1977,** 3, (1), 35-71.

234. F. Rodríguez-Reinoso; Molina-Sabio, M.; GonzálezRodr, M. T., The use of steam and CO2 as activating agents in the preparation of activated carbons. *Carbon* **1995,** 33, (1), 15-23.

235. Vamvuka, D.; Karouki, E.; Sfakiotakis, S., Gasification of waste biomass chars by carbon dioxide via thermogravimetry. Part I: Effect of mineral matter. *Fuel* 90, (3), 1120-1127.

236. Sha, X.-Z.; Chen, Y.-G.; Cao, J.; Yang, Y.-M.; Ren, D.-Q., Effects of operating pressure on coal gasification. *Fuel* **1990,** 69, (5), 656-659.

237. Shufen, L.; Ruizheng, S., Kinetic studies of a lignite char pressurized gasification with CO2, H2 and steam. *Fuel* **1994,** 73, (3), 413-416.

238. Liu, G.-s.; Tate, A. G.; Bryant, G. W.; Wall, T. F., Mathematical modeling of coal char reactivity with CO2 at high pressures and temperatures. *Fuel* **2000,** 79, (10), 1145-1154.

239. Ergun, S., Kinetics of the reaction of carbon with carbon dioxide. *Journal of physical chemistry* **1956,** 60, (4), 480-485.

240. Feng, B.; Bhatia, S. K., On the validity of thermogravimetric determination of carbon gasification kinetics. *Chemical Engineering Science* **2002,** 57, (15), 2907-2920.

241. Zhongsuo Liu; Qi Wang; Zongshu Zou; Tan, G., Reaction Mechanism of Carbon Gasification Reaction. *Journal of Materials and Metallurgy* **2010**, (1), 68-71.

242. Chen, S. G.; Yang, R. T.; Kapteijn, F.; Moulijn, J. A., A new surface oxygen complex on carbon: Toward a unified mechanism for carbon gasification reactions. *Industrial and Engineering Chemistry Research* **1993,** 32, (11), 2835-2840.

243. Nabais, J. V.; Carrott, P.; Ribeiro Carrott, M. M. L.; Luz, V.; Ortiz, A. L., Influence of preparation conditions in the textural and chemical properties of activated carbons from a novel biomass precursor: The coffee endocarp. *Bioresource Technology* **2008,** 99, (15), 7224-7231.

244. RadovićR.Ljubiša, R.; Walker Jr, P. L.; Jenkins, R. G., Importance of carbon active sites in the

gasification of coal chars. *Fuel* **1983,** 62, (7), 849-856.

245. Jones, L. E.; Thrower, P. A.; Walker Jr, P. L., Reactivity and related microstructure of 3d carbon/carbon composites. *Carbon* **1986,** 24, (1), 51-59.

246. Lizzio, A. A.; Jiang, H.; Radovic, L. R., On the kinetics of carbon (Char) gasification: Reconciling models with experiments. *Carbon* **1990,** 28, (1), 7-19.

247. Walker Jr, P. L.; Taylor, R. L.; Ranish, J. M., An update on the carbon-oxygen reaction. *Carbon* **1991,** 29, (3), 411-421.

248. Tsachi Livneh; Ezra Bar-ziv; Senneca, O.; Salatino, P., Evolution of Reactivity of Highly Porous Chars from Raman Microscopy. *Combustion Science and Technology* **2000,** 153, (1), 65-82.

249. Rodríguez-Reinoso, F.; Molina-Sabio, M.; González, M. T., The use of steam and CO2 as activating agents in the preparation of activated carbons. *Carbon* **1995,** 33, (1), 15-23.

250. Mahajan, O. P., Physical characterization of coal. *Powder Technology* **1984,** 40, (1–3), 1-15.

251. Chattopadhyaya, G.; Macdonald, D. G.; Bakhshi, N. N.; Soltan Mohammadzadeh, J. S.; Dalai, A. K., Preparation and characterization of chars and activated carbons from Saskatchewan lignite. *Fuel Processing Technology* **2006,** 87, (11), 997-1006.

252. Kühl, H.; Kashani-Motlagh, M. M.; Mühlen, H. J.; van Heek, K. H., Controlled gasification of different carbon materials and development of pore structure. *Fuel* **1992,** 71, (8), 879-882.

253. Pastor-Villegas, J.; Durán-Valle, C. J., Pore structure of activated carbons prepared by carbon dioxide and steam activation at different temperatures from extracted rockrose. *Carbon* **2002,** 40, (3), 397-402.

254. Walker Jr, P. L.; Almagro, A., Activation of pre-chlorinated anthracite in carbon dioxide and steam. *Carbon* **1995,** 33, (2), 239-241.

Every reasonable effort has been made to acknowledge the owners of copyright material. I would be pleased to hear from any copyright owner who has been omitted or incorrectly acknowledged.